รายงานวิจัยฉบับสมบูรณ์

โครงการความหลากหลายทางโครงสร้าง โครงสร้างเชิงพลวัติ และสมบัติทางแม่เหล็กของโครงข่ายโลหะ-อินทรีย์ที่ประกอบด้วยสะพานไซยาโนอะซิเตตและตัวเชื่อมอินทรีย์ชนิด *N,N´*-ditopic

โดย ดร.เจ้าทรัพย์ บุญมาก และคณะ

พฤษภาคม 2559

สัญญาเลขที่ TRG5780003

รายงานวิจัยฉบับสมบูรณ์

โครงการความหลากหลายทางโครงสร้าง โครงสร้างเชิงพลวัติ และสมบัติทางแม่เหล็กของโครงข่ายโลหะ-อินทรีย์ที่ประกอบด้วยสะพานไซยาโนอะซิเตตและตัวเชื่อมอินทรีย์ชนิด *N,N´*-ditopic

คณะผู้วิจัย	**สังกัด**
1. ดร.เจ้าทรัพย์ บุญมาก	มหาวิทยาลัยขอนแก่น
2. ศ.ดร.สุจิตรา ยังมี	มหาวิทยาลัยขอนแก่น
3. Prof. Keith S. Murray	Monash University, Australia

สนับสนุนโดยสำนักงานกองทุนสนับสนุนการวิจัยและมหาวิทยาลัยขอนแก่น

สัญญาเลขที่ TRG5780003

โครงการความหลากหลายทางโครงสร้าง โครงสร้างเชิงพลวัติ และสมบัติทางแม่เหล็กของโครงข่ายโลหะ-อินทรีย์ที่ประกอบด้วยสะพานไซยาโนอะซิเตต และตัวเชื่อมอินทรีย์ชนิด *N,N´*-ditopic

Abstract

The crystal design of new coordination polymers containing cyanoacetato ligand (cna) with various *N,N'*-organic bridges are presented. Novel twelve coordination polymers were systematically designed, synthesized and structurally characterized as following: a series of five Cu^{II} coordination polymers, $[Cu(cna)_2(pyz)]_n$ (**1**), $[Cu(cna)_2(bpy)(H_2O)_2]_n$ **(2)**, $[Cu(cna)_2(dpe)]_n$ (**3**), $[Cu(cna)_2(dpe)]_n(H_2O)_n$ (**4**) and $[Cu(cna)_2(bpa)]_n$ (**5**); secondly, a series of seven Zn^{II}/Cd^{II} coordination polymers, $[Zn(cna)_2(dpe)]_n$ **(II-1)**, $[Zn(cna)_2(dpe)]_n$ **(II-2)**, $[Cd(cna)_2(dpe)]_n$ **(II-3)** $[Zn(cna)_2(bpy)(H_2O)_2]_n$ **(II-4)** and $[Cd_3(cna)_6(bpy)_3]_n$ **(II-5)**, $[Zn(cna)_2(bpa)]_n$ **(II-6)** and $[Cd(cna)_2(bpa)]_n$ **(II-7)** (when pyz = pyrazine, bpy = 4,4'-bipyridyl, dpe = 1,2-di(4-pyridyl)ethylene and bpa = 1,2-di(4-pyridyl)ethane). All compounds exhibit low-dimensional coordination polymers with diverse topologies. Weak interactions such as hydrogen bonding and N···π and/or C–H···π interactions join the adjacent layers or polymeric chains to stabilize overall supramolecular networks. The thermal stabilities of **1**-**5** were investigated. Compound **2** reveals a robust supramolecular framework during thermal dehydration and rehydration processes. Moreover, this behavior is not observed in the isomorphous series containing Co(II) and Ni(II) ions. The magnetic properties of **1** and **3** exhibit very weak antiferromagnetic interaction. Moreover, the solid-state luminescent properties for **II-1**-**3** and **II-6**-**7** have been demonstrated.

Keywords: coordination polymers**,** cyanoacetic acid, luminescent properties, magnetic properties

สัญญาเลขที่ TRG5780003

โครงการความหลากหลายทางโครงสร้าง โครงสร้างเชิงพลวัติ และสมบัติทางแม่เหล็กของโครงข่ายโลหะ-อินทรีย์ที่ประกอบด้วยสะพานไซยาโนอะซิเตต และตัวเชื่อมอินทรีย์ชนิด *N,N′*-ditopic

บทคัดย่อ

งานวิจัยนี้เป็นการออกแบบ สังเคราะห์ พิสูจน์เอกลักษณ์ทางสเปกโทรสโกปีและวิเคราะห์โครงสร้างผลึกของไซยาโนอะซิเตโตโคออร์ดิเนชันพอลิเมอร์ร่วมกับสะพานอินทรีย์แบบเอ็นดอเนอร์ (*N,N′*) ทำให้ได้ โคออร์ดิเนชันพอลิเมอร์ชนิดใหม่ จำนวน 12 สาร ดังต่อไปนี้ กลุ่มแรกคือโคออร์ดิเนชันพอลิเมอร์ของคอปเปอร์(II) จำนวน 5 สาร ได้แก่ $[Cu(cna)_2(pyz)]_n$ (**1**), $[Cu(cna)_2(bpy)(H_2O)_2]_n$ **(2)**, $[Cu(cna)_2(dpe)]_n$ (**3**),$[Cu(cna)_2(dpe)]_n(H_2O)_n$ (**4**) และ $[Cu(cna)_2(bpa)]_n$ (**5**) และกลุ่มที่สอง คือโคออร์ดิเนชันพอลิเมอร์ของสังกะสี(II) และแคดเมียม(II) จำนวน 7 สาร ได้แก่ $[Zn(cna)_2(dpe)]_n$ **(II-1),** $[Zn(cna)_2(dpe)]_n$ **(II-2)**, $[Cd(cna)_2(dpe)]_n$ **(II-3)**, $[Zn(cna)_2(bpy)(H_2O)_2]_n$ **(II-4)**, $[Cd_3(cna)_6(bpy)_3]_n$ **(II-5)**, $[Zn(cna)_2(bpa)]_n$ **(II-6)** และ $[Cd(cna)_2(bpa)]_n$ **(II-7)** (เมื่อ pyz = pyrazine, bpy = 4,4'-bipyridyl, dpe = 1,2-di(4-pyridyl)ethylene และ bpa = 1,2-di(4-pyridyl)ethane) สารประกอบทั้งหมดเป็นโคออร์ดิเนชันพอลิเมอร์ที่มีมิติต่ำ โดยแสดงโทโพโลยีที่หลากหลาย นอกจากนี้ยังมีอันตรกิริยาอ่อนๆระหว่างโมเลกุล ได้แก่ พันธะไฮโดรเจน และอันตรกิริยาชนิด N···**π** หรือ C—H···**π** เชื่อมระหว่างชั้นหรือสายโซ่ข้างเคียงทำให้เกิดความเสถียรต่อโครงข่ายซุปราโมเลกุลโดยรวม จากนั้นทำการศึกษาความเสถียรทางความร้อนของสาร **1-5** นอกจากนี้พบว่า **2** เป็นโครงข่ายซุปราโมเลกุลแบบแข็งแกร่งในระหว่างกระบวนการสูญเสียและดูดกลับของโมเลกุลน้ำ ซึ่งพฤติกรรมนี้ไม่พบในโครงสร้างที่คล้ายกัน(สมสัณฐาน)ของไอออน Co(II) และ Ni(II) จากการศึกษาสมบัติทางแม่เหล็กของ **1** และ **3** พบว่าแสดงอันตรกิริยาชนิดแอนไทเฟอร์โรแมกเนติกแบบอ่อน และนอกจากนี้ได้ทำการศึกษาสมบัติเชิงแสงของสาร **II-1-3** และ **II-6-7**

คำสำคัญ: โคออร์ดิเนชันพอลิเมอร์ ไซยาโนอะซิติก สมบัติเชิงแสง สมบัติทางแม่เหล็ก

สัญญาเลขที่ TRG5780003

โครงการความหลากหลายทางโครงสร้าง โครงสร้างเชิงพลวัติ และสมบัติทางแม่เหล็กของโครงข่ายโลหะ-อินทรีย์ที่ประกอบด้วยสะพานไซยาโนอะซิเตต และตัวเชื่อมอินทรีย์ชนิด *N,N′*-ditopic

Executive Summary

The design and construction of coordination polymers has received much attention and become an interesting research area of chemistry in recent decades due to their potential applications in gas storage, catalysis, luminescence, ion exchange and magnetism. Generally, the structural diversity and the construction of such promising materials strongly depend on the chemical nature of the main or ancillary ligands and the coordination geometries of metal ions. It is well known that the coordination polymers containing carboxylates shows various dimensional networks with interesting properties. This diversity results from the fact that the carboxylate groups can bind metal centers in various ways and may account for the possible intermolecular hydrogen bonds spreading low dimensional materials to higher dimensional supramolecular frameworks. Besides the structural aspect, the carboxylate bridges provide an efficient pathways for transmitting magnetic information between paramagnetic centers. Different coordination modes contribute different forms of cooperative coupling which can be principally used to modulate the overall magnetic behavior in coordination network.

In the present studies, the cyanoacetate anion (cna) is used as a ligand for binding more than one metal ion through carboxylate bridge. The cyanoacetate ($NC_2H_2CO_2^-$) is a mono-carboxylate with many interaction sites. It contains both nitrile (–C≡N) and carboxylic groups which not only well provides coordination sites but also effectively serves as hydrogen accepter site at cyano group as well as fabricating the intermolecular N···π interaction toward neighboring electron-deficient aromatic moieties. In general, the intermolecular noncovalent interactions are useful tools for the construction of a soft supramolecular framework with low dimensional molecular building blocks that can show a variety of structural dynamic behaviors, such as reversible single-crystal-to-single-crystal, reversible single crystal to amorphous and also nonreversible transformations. Therefore, these versatile connection sites allow the cyanoacetate to be a promising candidate for constructing the flexible but robust coordination frameworks. However, the chemistry of coordination complexes containing cyanoacetate has been rarely explored to date. Apart from carboxylate linkers, the *N,N′*-ditopic spacers are frequently used as ancillary ligands for dimensional extension. Their length, rigidity and functional groups have consequential effects on the final structures of coordination networks. Therefore, the development of synthetic routes to novel coordination polymers by mixed bridging ligands remains much to be explored.

In order to study the effect of different *N,N'*-ditopic spacers on the self-assembly process of CPs, we have herein taken cyanoacetate and different pyridine-based neutral coligands, pyrazine (pyz), 4,4'-bipyridyl (bpy), 1,2-di(4-pyridyl)ethylene (dpe) and 1,2-di(4-pyridyl)ethane (bpa) in Cu(II) and Zn(II)/Cd(II) systems. The new series of coordination polymers were successfully synthesized by solvent evaporation method and layered diffusion method. The characterizations have been done through X-ray crystallography, infrared spectroscopy (IR), solid-state (diffuse reflectance) electronic spectra (UV-vis), elemental analyses and X-ray powder diffraction (XRPD). Thus, this research can be separated into two parts:

Part I: Five novel copper(II) coordination polymers containing cyanoacetate (cna) anion with various *N,N'*-ditopic spacers $[Cu(cna)_2(pyz)]_n$ (**1**), $[Cu(cna)_2(bpy)(H_2O)_2]_n$ **(2)**, $[Cu(cna)_2(dpe)]_n$ (**3**), $[Cu(cna)_2(dpe)]_n(H_2O)_n$ (**4**) and $[Cu(cna)_2(bpa)]_n$ (**5**) were structurally and spectroscopically characterized. Compound **1** shows 2D sheet structure constructed from μ_2-1,3(*syn,anti*) coordinative mode of cyanoacetate and μ_2-pyz linking adjacent Cu(II) centers. Compound **2** exhibits 1D polymeric chain which is formed by μ_2-bpy bridging between $[Cu(cna)_2(H_2O)_2]$ units. Whereas compounds **3-5** reveal 1D ladder-like structures which are built from double-μ_2-dpe/bpa spacers connecting neighboring Cu(II) cyanoacetate dimers. Weak interactions such as hydrogen bonding and N···π and/or C–H···π interactions join the adjacent layers of **1** or polymeric chains of **2-5** to stabilize overall supramolecular networks. The thermal stabilities of **1-5** were investigated. Interestingly, compound **2** reveals a robust supramolecular framework constructed by 1D polymeric chains during thermal dehydration and rehydration processes, that has been further verified by spectroscopic techniques, elemental analyses, TGA, and XRPD. Moreover, this behavior is not observed in the isomorphous series containing Co(II) and Ni(II) ions. The magnetic properties of **1** and **3** exhibit very weak antiferromagnetic interactions between Cu(II) centers.

Part II: A series of seven Zn^{II}/Cd^{II} coordination polymers, $[Zn(cna)_2(dpe)]_n$ **(II-1)**, $[Zn(cna)_2(dpe)]_n$ **(II-2)**, $[Cd(cna)_2(dpe)]_n$ **(II-3)** $[Zn(cna)_2(bpy)(H_2O)_2]_n$ **(II-4)** and $[Cd_3(cna)_6(bpy)_3]_n$ **(II-5)**, $[Zn(cna)_2(bpa)]_n$ **(II-6)** and $[Cd(cna)_2(bpa)]_n$ **(II-7)** were synthesized and structurally characterized. Compound **II-1** exhibits a 1D zigzag polymeric chain, while compounds **II-2** and **II-3** are isostructural exhibiting 1D-ladder chain structures built from double-μ_2-dpe connecting between $[M_2(\mu_{1,3}\text{-}cna)_2(cna)_2]$ secondary building units. Compound **II-4** reveals a linear chain structure which is formed by μ_2-bpy bridging between $[Zn(cna)_2(H_2O)_2]_n$ units. Compound **II-5** shows a triple-stranded chain consisting of six- and seven-coordinated Cd(II) centers. Compound **II-6** exhibits a zigzag chain coordination polymer containing μ_2-bpa spacers bridging between tetrahedral Zn(II) ions. Whereas **II-7** shows a ladder-like structure which is built from double μ_2-bpa spacers connecting between Cd(II) cyanoacetate dimeric units. All compounds are further extended into a 3D supramolecular architectures through non-

covalent weak hydrogen bonds and N···π and/or C–H···π interactions. The divergence of structural motifs between **II-1** and isostructures **II-2** and **II-3** strongly influences on their solid-state photoluminescent properties at room temperature. Compound **II-1** exhibits intense photoluminescence, whereas this is quenched in compounds **II-2** and **II-3**. The free bpa ligand exhibits very weak photoluminescence in the solid state, while this property is significantly enhanced in **II-6** and **II-7**.

Output: The research outcome includes three international publication papers.

1) P. Suvanvapee, J. Boonmak*, F. Klongdee, C. Pakawatchai, B. Moubaraki, K.S. Murray, S. Youngme, A Series of cyanoacetato copper(II) coordination polymers with various *N*,*N*'-ditopic spacers: Structural diversity, supramolecular robustness and magnetic properties. *Crystal Growth & Design*, **2015**, 15(8), 3804. (IF 2014 = 4.89)

2) P. Suvanvapee, J. Boonmak*, S. Youngme, Structural diversity and luminescent properties of cyanoacetato zinc/cadmium coordination polymers with *N*,*N*'-ditopic auxiliary ligands**.** *Polyhedron,* **2015**, 102, 693. (IF 2014 = 2.01)

3) P. Suvanvapee, J. Boonmak*, S. Youngme, Synthesis, crystal structure and luminescent properties of three new zinc/cadmium coordination polymers containing cyanoacetate and 1,2-di(4-pyridyl)ethylene. *Inorganica Chimica Acta*, **2015**, 437, 11. (IF 2014 = 2.05)

TABLE OF CONTENTS

PART I
A SERIES OF CYANOACETATO COPPER(II) COORDINATION POLYMERS WITH VARIOUS *N,N′*-DITOPIC SPACERS: STRUCTURAL DIVERSITY, SUPRAMOLECULAR ROBUSTNESS AND MAGNETIC PROPERTIES

Introduction

Design and construction of coordination polymers has received much attention and become an interesting research area of chemistry in recent decades due to their potential applications in gas storage, catalysis, luminescence, ion exchange and magnetism.[1-9] Generally, the structural diversity and the construction of such promising materials strongly depend on the chemical nature of the main or ancillary ligands and the coordination geometries of metal ions. It is well known that the coordination polymers containing carboxylates shows various dimensional networks with interesting properties.[10-18] This diversity results from the fact that the carboxylate groups can bind metal centers in various ways and may account for the possible intermolecular hydrogen bonds spreading low dimensional materials to higher dimensional supramolecular frameworks.[1,6,13-19] Besides the structural aspect, the carboxylate bridges provide an efficient pathways for transmitting magnetic information between paramagnetic centers. Different coordination modes contribute different forms of cooperative coupling which can be principally used to modulate the overall magnetic behavior in coordination network.[17,18,20,21] In the present studies, the cyanoacetate anion (cna) is used as a ligand for binding more than one metal ion through carboxylate bridge. The cyanoacetate ($NC_2H_2CO_2^-$) is a mono-carboxylate with many interaction sites. It contains both nitrile (−C≡N) and carboxylic groups which not only well provides coordination sites but also effectively serves as hydrogen accepter site at cyano group as well as fabricating the intermolecular N···π interaction toward neighboring electron-deficient aromatic moieties.[22-29] In general, the intermolecular noncovalent interactions are useful tools for the construction of a soft supramolecular framework[3,5,30,31] with low dimensional molecular building blocks that can show a variety of structural dynamic behaviors, such as reversible single-crystal-to-single-crystal, reversible single crystal to amorphous and also nonreversible transformations.[3,5,31-40] Therefore, these versatile connection sites allow the cyanoacetate to be a promising candidate for constructing the flexible but robust coordination frameworks. However, the chemistry of coordination complexes containing cyanoacetate has been rarely explored to date.[22-29] Apart from carboxylate linkers, the *N,N′*-ditopic spacers are frequently used as ancillary ligands for dimensional extension. Their length, rigidity and functional groups have consequential effects on the final structures of coordination networks. Therefore, the development of synthetic routes to novel coordination polymers by mixed bridging ligands remains much to be explored.[10,41-50]

Consequently, in our efforts toward rational design and systematic synthesis of coordination polymers, the use of *N,N′*-ditopic spacers acting as coligands, *i.e.* pyrazine (pyz), 4,4'-bipyridyl (bpy), 1,2-di(4-pyridyl)ethylene (dpe) and 1,2-di(4-pyridyl)ethane (bpa) in combination with cyanoacetate in Cu(II) system have been used to construct a variety of new coordination polymers. We found that cyanoacetate can bind Cu(II) ions through diverse coordination modes of carboxylate to generate Cu(II) dinuclear unit and 1D coordination polymeric chain. To connect these segments, ancillary *N,N′*-ditopic spacer has been fulfilled. Herein, we report the syntheses and characterizations of a novel series of Cu(II) coordination polymers, namely, $[Cu(cna)_2(pyz)]_n$ (**1**), $[Cu(cna)_2(bpy)(H_2O)_2]_n$ **(2)**, $[Cu(cna)_2(dpe)]_n$ (**3**), $[Cu(cna)_2(dpe)]_n(H_2O)_n$ (**4**) and $[Cu(cna)_2(bpa)]_n$ (**5**) (Figure 1). The resulted coordination networks exhibit a variation of architectures from 1D polymeric chain, 1D-ladder chain to 2D

layer depending upon the length and rigidity of the spacers and diverse coordination modes of carboxylates. The nitrile functional group in cyanoacetate plays a key role on 3D packing motifs *via* intermolecular hydrogen bonding and N···π interactions. Furthermore, we found that compound **2** reveals a robust supramolecular framework during dehydration and rehydration processes which is not observed in the Co(II) and Ni(II) analogues. This behavior is not common for low dimensional coordination polymer because the noncovalent supramolecular motif easily collapses upon removal of the coordination water molecules.[36,38] The result demonstrates the significant role of various weak intermolecular interactions among interlaced covalently bonded chain in **2** and the influence of Jahn-Teller distortion in octahedral Cu(II) system to preserve the crystalline phase of anhydrous frameworks of **2**. The magnetic properties of **1** and **3** have also been investigated.

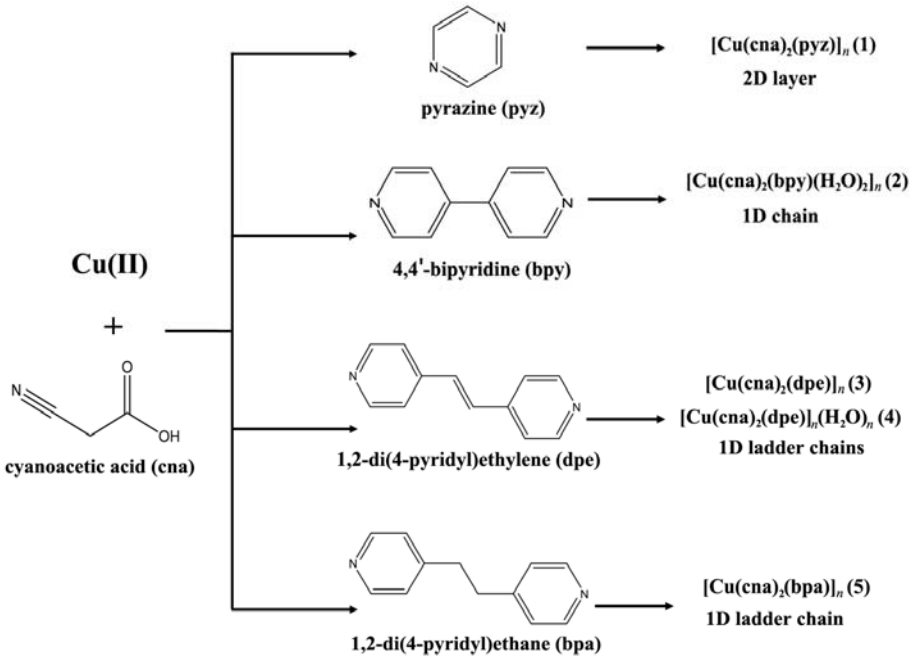

Figure 1 A series of Cu(II) coordination polymers **1-5**

The resulted coordination networks exhibit a variation of architectures from 1D polymeric chain, 1D-ladder chain to 2D layer depending upon the length and rigidity of the spacers and diverse coordination modes of carboxylates. The nitrile functional group in cyanoacetate plays a key role on 3D packing motifs *via* intermolecular hydrogen bonding and N···π interactions. Furthermore, we found that compound **2** reveals a robust supramolecular framework during dehydration and rehydration processes which is not observed in the Co(II) and Ni(II) analogues. This behavior is not common for low dimensional coordination polymer because the noncovalent supramolecular motif easily collapses upon removal of the coordination water molecules.[36,38] The result demonstrates the significant role of various weak intermolecular interactions among interlaced covalently bonded chain in **2** and the influence of Jahn-Teller distortion in octahedral Cu(II) system to preserve the crystalline phase of anhydrous frameworks of **2**. The magnetic properties of **1** and **3** have also been investigated.

Experimental section

General. All chemical were obtained from commercial sources and were used without further purification. Elemental analyses (C, H, N) were carried out with a Perkin-Elmer PE

2400CHNS analyzer. FT-IR spectra were obtained in KBr disks on a Perkin-Elmer Spectrum One FT-IR spectrophotometer in 4000-450 cm^{-1} spectral range. Solid-state (diffuse reflectance) electronic spectra were measured as polycrystalline samples on a Perkin-Elmer Lambda2S spectrophotometer, within the range 400-1100 nm. The X-ray powder diffraction (XRPD) data were collected on a Bruker D8 ADVANCE diffractometer using monochromatic Cu*K*α radiation, and the recording speed was 0.5 s/step over the 2θ range of 5-40° at room temperature. Thermogravimetric analyses (TGA) were performed using a TG-DTA 2010S MAC apparatus between 30-500 °C in N_2 atmosphere with heating rate of 10 °C min^{-1}. Magnetic susceptibility measurements (2-300 K) were carried out using a Quantum design MPMS-5S SQUID magnetometer. Measurements carried out using a 1 kOe dc field. Accurately weighed samples of ~25 mg were contained in a gel capsule that was held in the centre of a soda straw that was attached to the end of the sample rod. Data were corrected for magnetization of the sample holder and for diamagnetic contributions, which were estimated from Pascal constants.

Syntheses. $[Cu(cna)_2(pyz)]_n$ (1). The aqueous solution (4 mL) of $Cu(NO_3)_2{\cdot}3H_2O$ (120 mg, 0.5 mmol) and cyanoacetic acid (85 mg, 1 mmol) was mixed with pyrazine (40 mg, 0.5 mmol) in dimethylformamide (2 mL). This mixture solution was allowed to stand undisturbed at room temperature, yielding blue crystals of **1** after two days. Yield: 97 mg (62%) based on copper salt. Anal. Calcd for $CuC_{10}H_8N_4O_4$: C, 38.53; H, 2.59; N, 17.93%. Found: C, 37.65; H, 2.62; N, 18.03%. IR (KBr, cm^{-1}): 3096(w), 3045(w), 2255(w), 1645(s), 1600(s), 1440(m), 1365(s), 1253(m), 1160(m), 1126(m), 1075(m), 923(m), 838(m), 718(w), 574(w), 506(m). UV-vis (diffuse reflectance, cm^{-1}): 15450.

$[Cu(cna)_2(bpy)(H_2O)_2]_n$ (2). The mixture solution of $Cu(NO_3)_2{\cdot}3H_2O$ (120 mg, 0.5 mmol) and 4,4'-bipyridyl (78 mg, 0.5 mmol) in aqueous media (4 mL) was carefully layered on cyanoacetic acid (85 mg, 1 mmol) in dimethylformamide (2 mL) in 15 mL of glass vial. The vial was sealed and allowed to stand undisturbed at room temperature. After two days, blue crystals of **2** were obtained. Yield: 100 mg (47%) based on copper salt. Anal. Calcd for $CuC_{16}H_{16}N_4O_6$: C, 45.34; H, 3.80; N, 13.22%. Found: C, 44.55; H, 3.53; N, 12.40%. IR (KBr, cm^{-1}): 3544(br), 3199(w), 3007(w), 2923(w), 2259(w), 1610(s), 1373(s), 1276(m), 1218(m), 1075(m), 942(w), 818(m), 714(m), 645(w), 596(w), 491(w). UV-vis (diffuse reflectance, cm^{-1}): 15470.

$[Cu(cna)_2(dpe)]_n$ (3) and **$[Cu(cna)_2(dpe)]_n(H_2O)_n$ (4).** A mixture solution of ethanol and water (4 mL, 1:1 v/v) was carefully layered on an aqueous solution (4 mL) containing $Cu(BF_4)_2{\cdot}nH_2O$ (118 mg, 0.5 mmol) and cyanoacetic acid (85 mg, 1 mmol) in 15 mL of glass vial. Then an ethanolic solution (2 mL) of 1,2-di(4-pyridyl)ethylene (90 mg, 0.5 mmol) was layered over the mixture layer. Then, the vial was sealed and allowed to stand undisturbed at room temperature. After two days, greenish-blue block-shaped crystals of **3** and blue polygonal crystals of **4** were obtained. These crystals were manually separated, washed with water and dried in air. Yield for **3**: 49 mg (24%) based on copper salt. Anal. Calcd for $CuC_{18}H_{14}N_4O_4$: C, 52.24; H, 3.41; N, 13.54%. Found: C, 51.82; H, 3.41; N, 13.27%. IR (KBr, cm^{-1}): 3088(w), 2258(w), 1633(s), 1613(s), 1496(m), 1385(s), 1266(m), 1207(m), 1073(m), 816(m), 720(w), 643(w). UV-vis (diffuse reflectance, cm^{-1}): 13770. Yield for **4**: 11 mg (5%) based on copper salt. Anal. Calcd for $CuC_{18}H_{16}N_4O_5$: C, 50.06; H, 3.73; N, 12.97%. Found: C, 50.92; H, 3.40; N, 13.07%. IR (KBr,cm^{-1}): 3419(br), 3060(w), 2933(w), 2258(w), 1626(s), 1463(s), 1372(s), 1286(s), 1080(m), 1030(m), 903(w), 844(s), 727(m), 549(m). UV-vis (diffuse reflectance, cm^{-1}): 16860. The single-crystals of **4** were synthesized in a similar manner but using dimethylformamide instead of ethanol. After one week, the suitable single-

crystals of **4** for X-ray diffraction study were obtained. The low yields of **3** and **4** are owing to the tiny crystals of the mixed products which are difficult to separate manually.

$[Cu(cna)_2(bpa)]_n$ (5). The solution containing $Cu(BF_4)_2{\cdot}nH_2O$ (118 mg, 0.5 mmol) and cyanoacetic acid (85 mg, 1 mmol) in water and ethanol (4 mL, 1:1 v/v) was mixed with 1,2-di(4-pyridyl)ethane (90 mg, 0.5 mmol) in dimethylformamide (2 mL). This mixture solution was allowed to stand undisturbed at room temperature. After two days, greenish-blue crystals of **5** were obtained. Yield: 86 mg (41%) based on copper salt. Anal. Calcd for $CuC_{18}H_{16}N_4O_4$: C, 51.98; H, 3.88; N, 13.47%. Found: C, 51.73; H, 3.78; N, 13.36%. IR (KBr, cm^{-1}): 3432(br), 2258(w), 1627(s), 1367(s), 1255(m), 1073(w), 1030(w), 901(w), 849(m), 719(w), 555(w). UV-vis (diffuse reflectance, cm^{-1}): 13770.

X-ray Crystallography. The reflection data of **1-4** and **2-Co** were collected on a 1 K Bruker SMART CCD area-detector diffractometer with graphite-monochromated Mo*K*α radiation (λ = 0.71073 Å) using the SMART program.[51] The reflection data of **5** was collected on a Bruker D8 Quest PHOTON100 CMOS detector with graphite-monochromated Mo*K*α radiation using the APEX2 program.[52] Raw data frame integration was performed with SAINT[53], which also applied correction for Lorentz and polarization effects. An empirical absorption correction by using the SADABS program[54] was applied. The structure was solved by direct methods and refined by full-matrix least-squares method on F^2 with anisotropic thermal parameters for all non-hydrogen atoms using the SHELXTL software package.[55] All hydrogen atoms were placed in calculated positions and refined isotropically, with the exception of the hydrogen atoms of all coordination water molecules in **2** were found *via* difference Fourier maps, then restrained at fixed positions and refined isotropically whereas hydrogen atoms on the disordered lattice water molecule in **4** could not be located. The nitrile groups of μ-cna for **4** and those of terminal cna for **5** are disordered, so the occupancies of conformations A and B refined to 0.8 and 0.2 (for **4**) and 0.7 and 0.3 (for **5**), respectively. Therefore, there are hydrogen bonding networks and N···π interactions present *via* the disordered nitrile N3 atom for **4** and both are symmetry related in which changing one interaction has a knock-on effect.

Results and Discussion

General observations and spectroscopic characterizations

The solid-state IR spectra of **1-5** in the region 4000-450 cm^{-1} are displayed in Figure 2. The IR spectra of all compounds exhibit the vibrations of the pyridyl rings for *N,N′*-ditopic spacers in the region 1650-1600 cm^{-1} overlapping the ν_{as}(OCO) bands around ~1630-1570 cm^{-1}. The strong bands in the region 1430-1360 cm^{-1} are attributed to the ν_s(OCO). The splitting of ν(OCO) reflects that the carboxylate groups of cyanoacetate adopt a variety of coordination modes. The $\Delta\ \nu_{asym-sym}$ values are in range of 200-260 cm^{-1} which are consistent with monodentate and bridging coordination by the carboxylato group.[10,26,41,56] The medium sharp band at 2258 cm^{-1} can be assigned to the ν(C≡N) from cyanoacetate.[22,26,29] Compounds **2** and **4** show broad bands in the region 3200-3460 cm^{-1} due to the ν(O–H) of water molecules.

The electronic spectra of **1-5** were studied in solid state at room temperature (Figure 3). Compounds **1, 2** and **4** show a broad absorption band at higher energy around 16860-15450 cm^{-1}, corresponding to the ^2E_g to $^2T_{2g}$ (parent) transition in the distorted octahedral geometry of **2** and this feature is also consistent with the elongated octahedral geometry with the sixth off-the-axis weakly interacting to Cu center for **1** and **4**.[18,57] While, compounds **3** and **5** exhibit the single broad band in much lower transition energy around 13770 cm^{-1} which is in agreement with the distorted square pyramidal geometry with high τ values.[58-60]

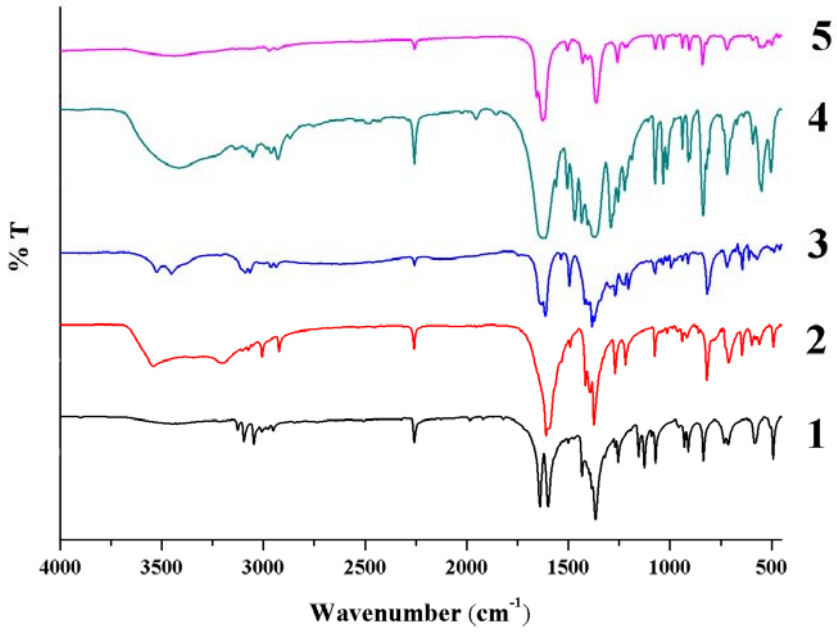

Figure 2 IR spectra of compounds **1-5**

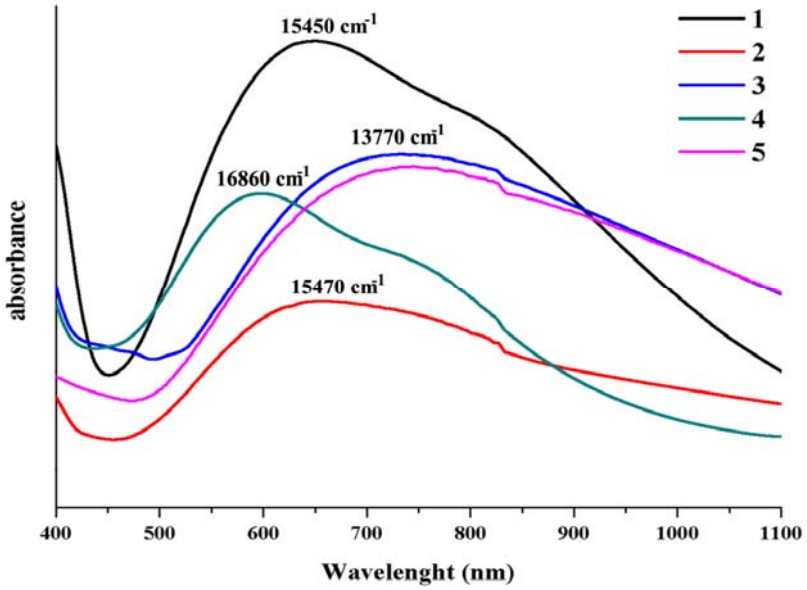

Figure 3 The electronic spectra of **1-5**

Description of the structures

[Cu(cna)$_2$(pyz)]$_n$ (1). Single-crystal structure analysis reveals that **1** crystallizes in the monoclinic system $P2_1/c$ space group. The coordination environment of the Cu(II) center is shown in Figure 4a. Each Cu(II) ion is five-coordinated showing a distorted square pyramidal CuN_2O_3 chromophore with a τ value of 0.24 (Addison's parameter τ[61] = 0 for square pyramid and τ = 1 for trigonal bipyramid). The equatorial plane around the copper atom is composed of two carboxylic oxygen atoms (O1 and O2) from two different

cyanoacetate groups and two nitrogen atoms from μ_2-pyz with average Cu−O and Cu−N distances of 1.959(2) and 2.030(2) Å, respectively.

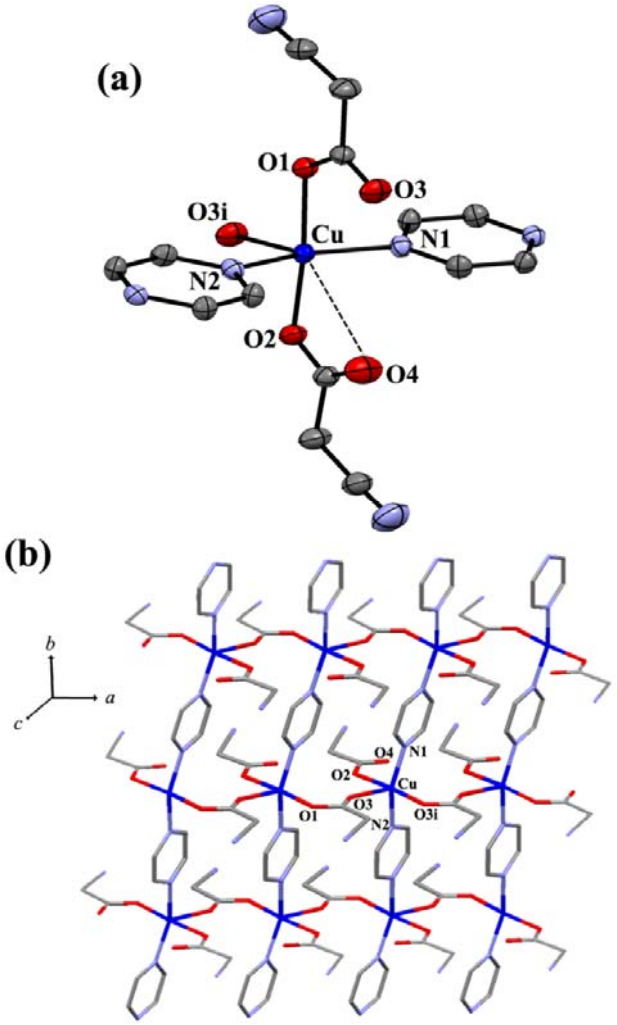

Figure 4 (a) Asymmetric unit and atom labeling scheme of **1**. The ellipsoids are shown at 50% probability level. All hydrogen atoms are omitted for clarity. The dashed line represents weak interaction in the off-the-axis position. (i) = 1+*x*, *y*, *z*. (b) Two-dimensional sheet structure of **1**

The apical position is occupied by oxygen (O3) atom from μ_2-cyanoacetate with the Cu−O3 distance of 2.283(2) Å. The CuN_2O_2 square base is not perfectly planar with tetrahedral twists between the N2−Cu−O2 and N1−Cu−O1 planes of 24.53°. The copper atom is slightly shifted by 0.087 Å from the mean basal plane toward the apical position, which is attributed to semi-coordinated O4 atom from the terminal cyanoacetate weakly interacting to copper center in off-the-axis position of an elongated octahedral geometry with the longest Cu···O4 distance of 2.970 Å.[18,62] The cyanoacetate acts as bridging and terminal ligands. The μ_2-cyanoacetate exhibits a *syn*,*anti*-η^1:η^3:μ_2 coordinative mode of carboxylate bridging between adjacent Cu(II) centers along the *a* axis with Cu···Cu separation of 4.896(5) Å, resulting a zigzag polymeric chain structure of **1**. Moreover, each cyanoacetato Cu(II) wavy chain is connected by μ_2-pyz along *b* axis giving rise to 2D sheet structure of **1** with Cu···Cu

separation of 6.832 Å *via* pyz (Figure 4b). The packing motif of **1** is stabilized by weak hydrogen bonding and N···π interactions between the layers (Figure 5).

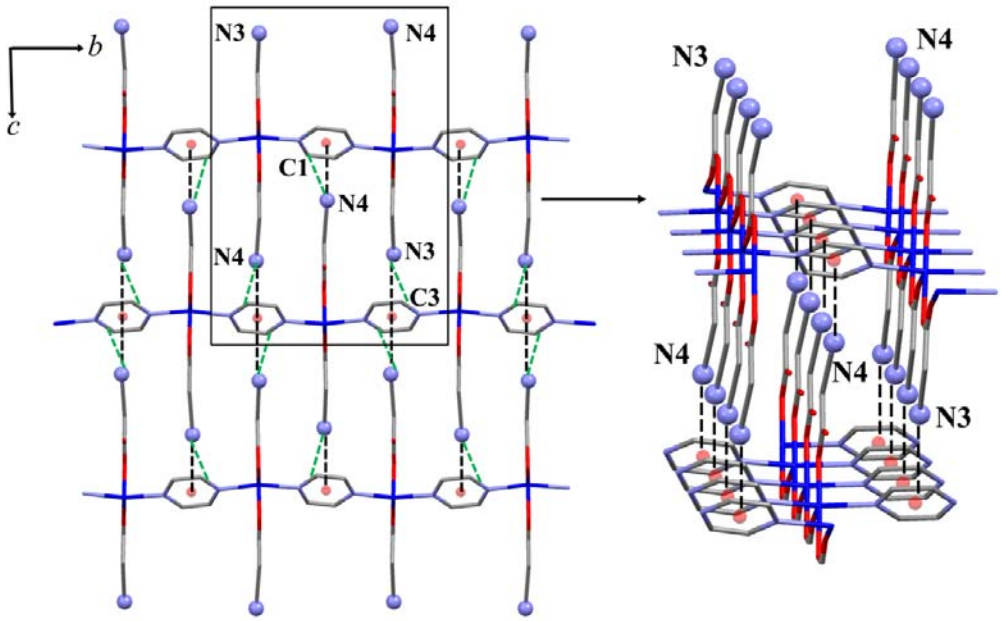

Figure 5 The packing motif of **1** in the *bc* plane; the inset presents the interlayered N···π(pyz) interactions. The green broken lines present weak hydrogen bonding between layers of **1**

The interlayer weak hydrogen bonding are constructed from the C−H on pyrazine ring and the nitrogen atom of nitrile group from the terminal and bridging cyanoacetates [C3H···N3^{i}= 2.61 Å (147°), C3···N3^{i}= 3.4290(6) Å, (i) = 3-*x*, 1-*y*, 1-*z*; C1H···N4^{ii}= 2.49 Å (147°), C1···N4^{ii}= 3.3091(4) Å, (ii) = 1+*x*, 1/2-*y*, 1/2+*z*]. Moreover, the nitrile N atoms from the terminal and μ_2-cyanoacetate can interact with the electron-deficient μ_2-pyz ring with N···centroid(pyz) distance of 3.420 Å for N3···π and 3.169 Å for N4···π, stabilizing 3D supramolecular framework of **1**, as shown in Figure 5. The distance between a R≡N donor and a centroid of six-membered heteroaromatic rings is found to be in the usual range of 3.00-3.40 Å.[63]

$[Cu(cna)_2(bpy)(H_2O)_2]_n$ (2). Single-crystal structure determination of **2** reveals 1D chain structure that crystallizes in orthorhombic *Pccn* space group. The crystal structure of **2** consists of neutral $[Cu(cna)_2(H_2O)_2]$ unit bridged *via* μ_2-bpy with the Cu···Cu separation of 11.018(8) Å. The cyanoacetate behaves as a monodentate ligand. Each Cu(II) ion is six-coordinated showing a distorted octahedral CuN_2O_4 chromophore (Figure 6a). The two nitrogen atoms from two μ_2-bpy spacers and two oxygen atoms from two terminal cyanoacetates reside in equatorial plane with Cu−N1 and Cu−O2 distances of 2.023(1) and 1.990(1) Å, respectively. Two oxygen atoms from two coordination water molecules are located in the axial positions with Cu−O1 distances of 2.500(1) Å. The adjacent Cu(II) centers are connected by μ_2-bpy forming a 1D chain coordination polymers, as shown in Figure 6b. The two pyridine rings of bipyridyl moieties are not coplanar with the dihedral angle between the two planar pyridine rings of 24.15°. The structure of **2** is isomorphous with previously reported Mn^{II} complex, $[Mn(cna)_2(bpy)(H_2O)_2]_n$.[23] However, the overall packing motif has not been entirely investigated. Each 1D chain of **2** is interlaced by 1D interchain

weak hydrogen bonding array between terminal cyanoacetate ligands along *c* axis (C7H···N2) (Figure 7) and the intermolecular hydrogen bonding between unbound O atom from cyanoacetate and H atom from coordination water molecules (O1H···O3), additionally, weak hydrogen bonding between the pyridyl H atom from μ_2-bpy and coordination water molecules (C2H···O3). Moreover, the C2–H···π interaction is observed among the adjacent μ_2-bpy moieties along *c* axis with the separation of 3.372 Å (Figure 7). These weak interactions complete the overall 3D supramolecular motif of **2** with the closest interchain Cu···Cu separation of 7.4363(7) Å. [C2H···O3^{i}= 2.59 Å (145°), C2···O3^{i}= 3.391(2) Å, (i) = 1/2+*x*, 1-*y*, 1/2-*z*; C7H···N2^{ii}= 2.59 Å (122°), C7···N2^{ii}= 3.213(3) Å, (ii) = *x*, 1/2-*y*, 1/2+*z*; O1H···O3^{iii}= 2.26 Å (147°), O1···O3^{iii}= 3.097(2) Å, (iii) = 1-*x*, 1-*y*, 1-*z*].

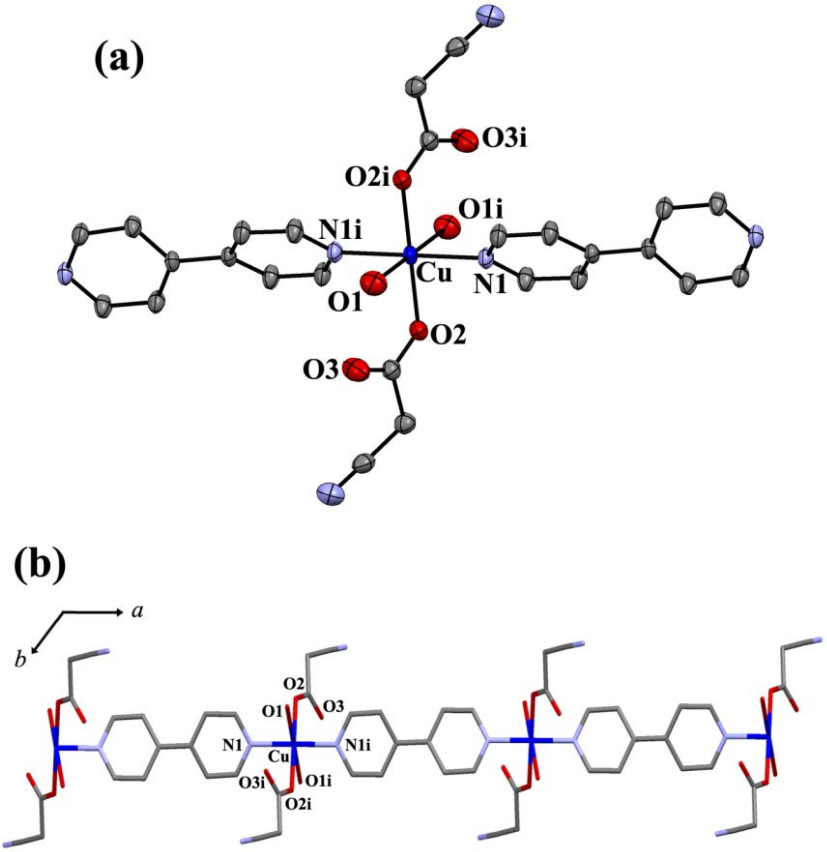

Figure 6 (a) Asymmetric unit and atom labeling scheme of **2**. The ellipsoids are shown at 50% probability level. All hydrogen atoms are omitted for clarity (i) = 1–*x*, 1–*y*, –*z*. (b) 1D chain structure of **2** along *a* axis

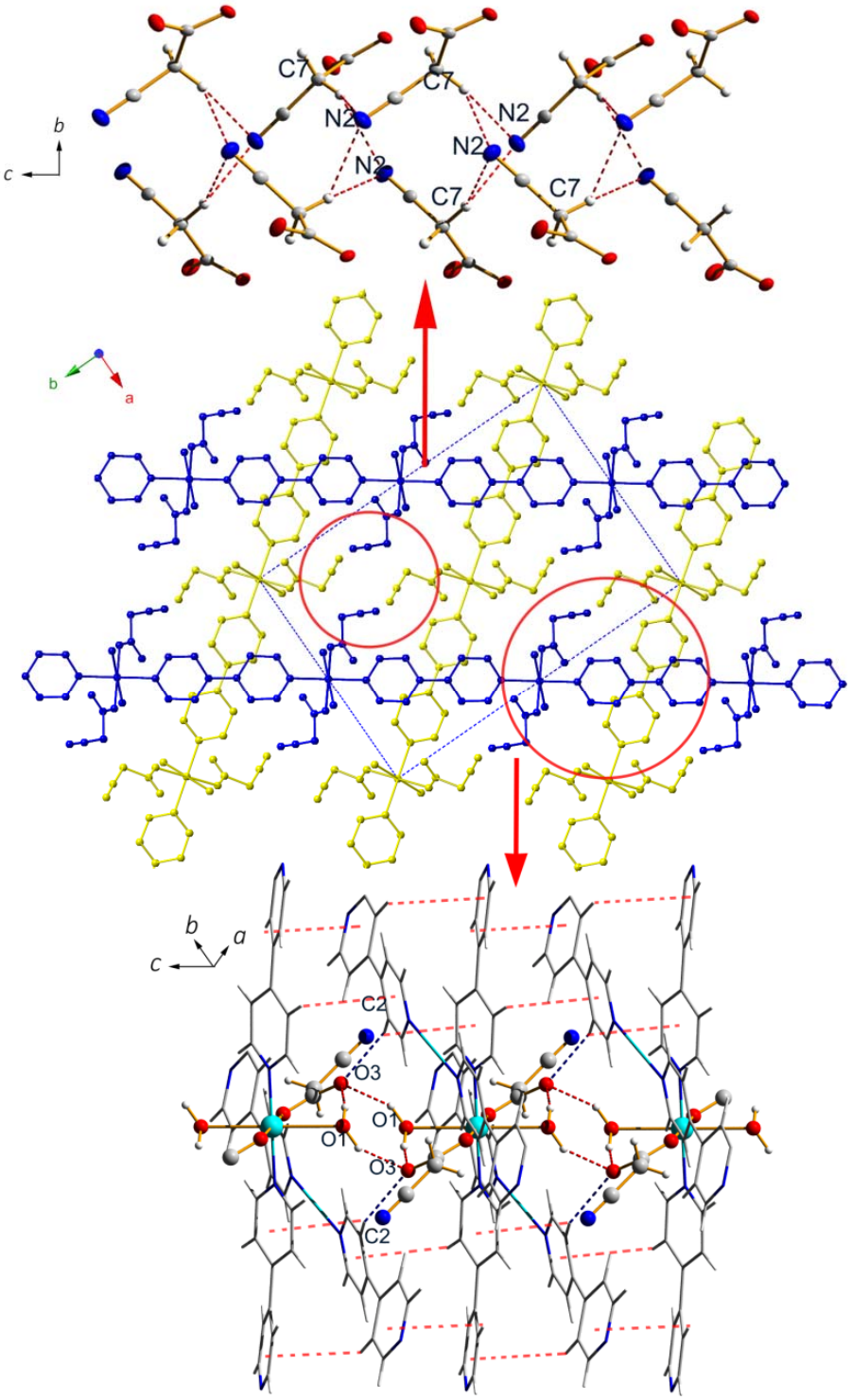

Figure 7 The interlaced chain structure of **2** in *ab* plane formed by 1D intermolecular weak hydrogen bonding array between terminal cyanoacetates along *c* axis (top). The hydrogen bonding between unbound O3-cyanoacetate and coordination water represents in red dotted lines (bottom). The blue dotted lines represent the C2H···O3 weak hydrogen bonding and the red broken lines represent C–H···π interaction

$[Cu(cna)_2(dpe)]_n$ (3), $[Cu(cna)_2(dpe)]_n(H_2O)_n$ (4) and $[Cu(cna)_2(bpa)]_n$ (5). Compounds **3-5** exhibit 1D ladder chain structures as shown in Figure 8. Single-crystal structure analysis reveals that **3** and **5** are isostructures crystallizing in the triclinic system $P\bar{1}$ space group whereas compound **4** crystallizes in the monoclinic *C2/c* space group. All Cu(II) ions are five-coordination showing distorted square pyramidal geometry CuN_2O_3 chromophore with τ values of 0.42, 0.04 and 0.46 for **3-5**, respectively. Each Cu(II) center is surrounded by two carboxylate oxygen atoms from two different cyanoacetates and two nitrogen atoms from two μ_2-dpe (for **3** and **4**) or μ_2-bpa (for **5**) living in an equatorial site with average Cu−O distances of 2.000(2), 1.968(1) and 1.990(2) Å and Cu−N distances of 2.016(2), 2.010(1) and 2.014(2) Å for **3-5**, respectively. The leaving one apical position is occupied by carboxylate oxygen atom from bridging cyanoacetate with the distances of Cu−O4 = 2.282(2), Cu−O1 = 2.446(1) and Cu−O2 = 2.264(2) Å for **3-5**, respectively. The CuN_2O_2 square base is not completely planar with tetrahedral twists between the planes of 26.61°, 14.45° and 29.06° for **3-5**, respectively. The copper atoms are shifted by 0.303, 0.056 and 0.270 Å from the mean basal planes toward the apical positions for **3-5**, respectively. Those of slightly shifted value of **4** results from semi-coordinated O4 atom from terminal cyanoacetate weakly interacting to copper center in off-the-axis position of an elongated octahedral geometry with the longest Cu···O4 distance of 2.828(2) Å. The carboxylic bridges for μ_2-cyanoacetate of **3** and **5** exhibit a double-*syn*,*anti*-η^1:η^3:μ_2 coordinative mode connecting between Cu(II) ions, generating the dinuclear Cu(II) units with Cu···Cu separation of 4.278(3) Å for **3** and 4.352(4) Å for **5**, whereas those of **4** exhibit a double-μ_2-1,1-monoatomic bridging mode with the shorter Cu···Cu separation of 3.433(4) Å. The carboxyl-bridged dinuclear Cu(II) units are extended along the particular direction by paired μ_2-dpe (for **3** and **4**) or μ_2-bpa spacers (for **5**) to create the infinite 1D ladder-like structures. The Cu···Cu separations across μ_2-dpe (for **3** and **4**) are 13.407(8), 13.349(6) Å and μ_2-bpa (for **5**) 13.288(5) Å, respectively. The two pyridine rings of bipyridyl moieties are not coplanar with the dihedral angles between the two planar pyridine rings of 9.24º, 11.59º and 18.64º for **3-5**, respectively. The conformations of μ_2-dpe and μ_2-bpa ligands are *anti* with C−CH=CH−C torsion angles of 177.30º (for **3**) and 179.03º (for **4**), and C−CH_2−CH_2−C torsion angle of 179.91º (for **5**). The supramolecular structures of **3** and **5** (Figure 9) are stabilized by weak interchain hydrogen bonding with the closest Cu···Cu distances of 6.7787(7) Å for **3** and 6.5672(5) Å for **5**. [for **3**, C15H···O2^{i}= 2.46 Å (126°), C15···O2^{i} = 3.099(4) Å, (i) = -*x*, 2-*y*, 1-*z*; C16H···O2^{i}= 2.60 Å (121°), C16···O2^{i} = 3.147(4) Å; for **5**, C2H···O4^{i}= 2.52 Å (152°), C2···O4^{i} = 3.373(4) Å, (i) = -*x*, -*y*,-*z*; C17H···N4^{ii} = 2.54 Å (161°), C17···N4^{ii} = 3.170(1) Å, (ii) = -*x*, 1-*y*,1-*z*]. Moreover, the nitrile N atoms from the terminal and bridging cyanoacetates interact with the adjacent electron-deficient μ_2-dpe rings with N···centroid distances of 3.665 Å (for N3···π) and 3.274 Å (for N4···π), stabilizing the overall packing structure of **3**. The N···π(bpa) interactions in **5** is not observed because two bipyridyl moieties in a flexible μ_2-bpa spacer are notably twisted with the highest dihedral angle compared with those of **3** and **4**.

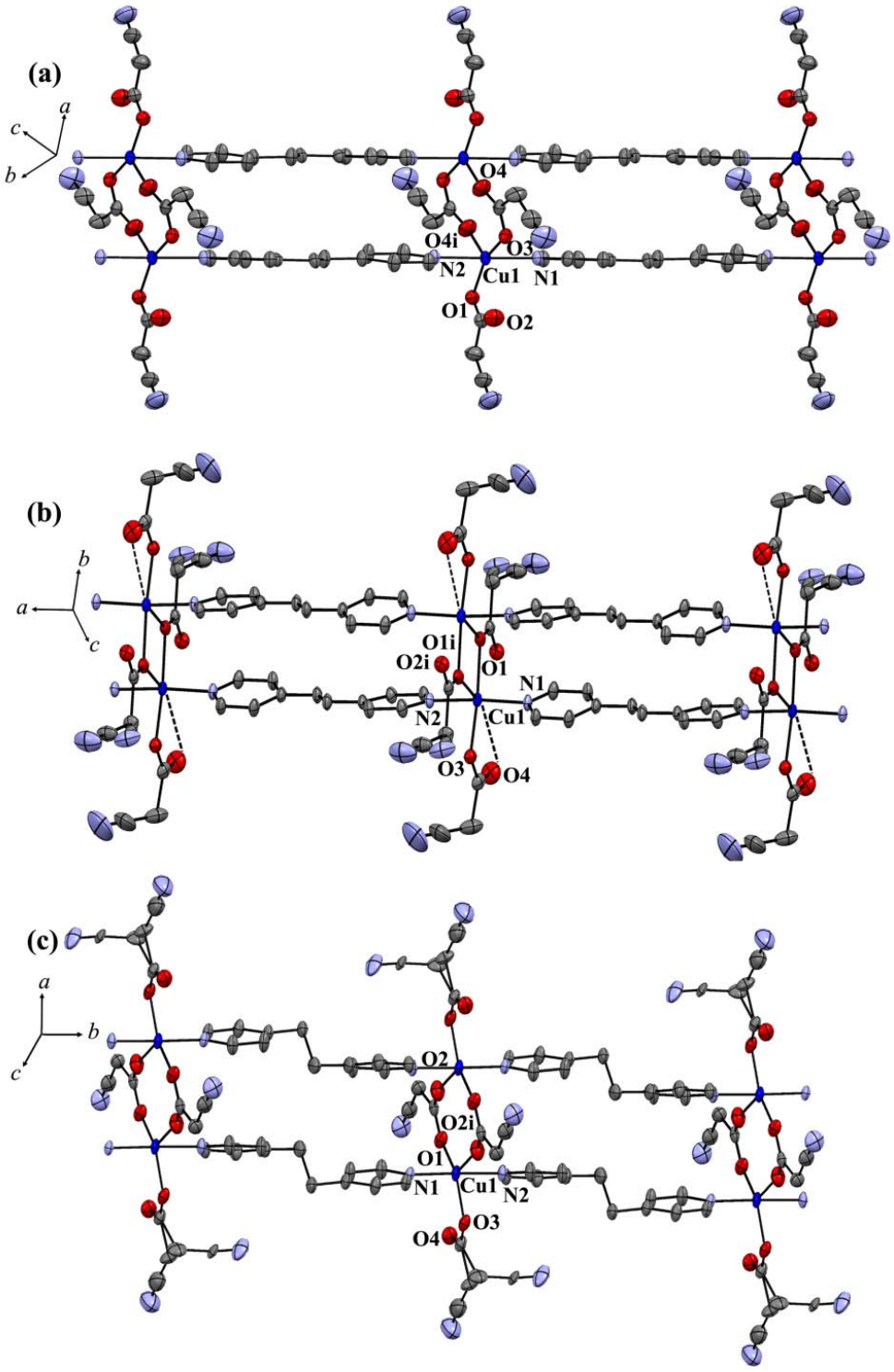

Figure 8 Part of 1D ladder chain structures of **3**(a), **4**(b) and **5**(c) with used atom labeling. The ellipsoids are shown at 35% probability level. The lattice water molecules for **4** and all hydrogen atoms are omitted for clarity. Both disordered nitrile groups of μ_2-cna for **4** and those of terminal cna for **5** are shown

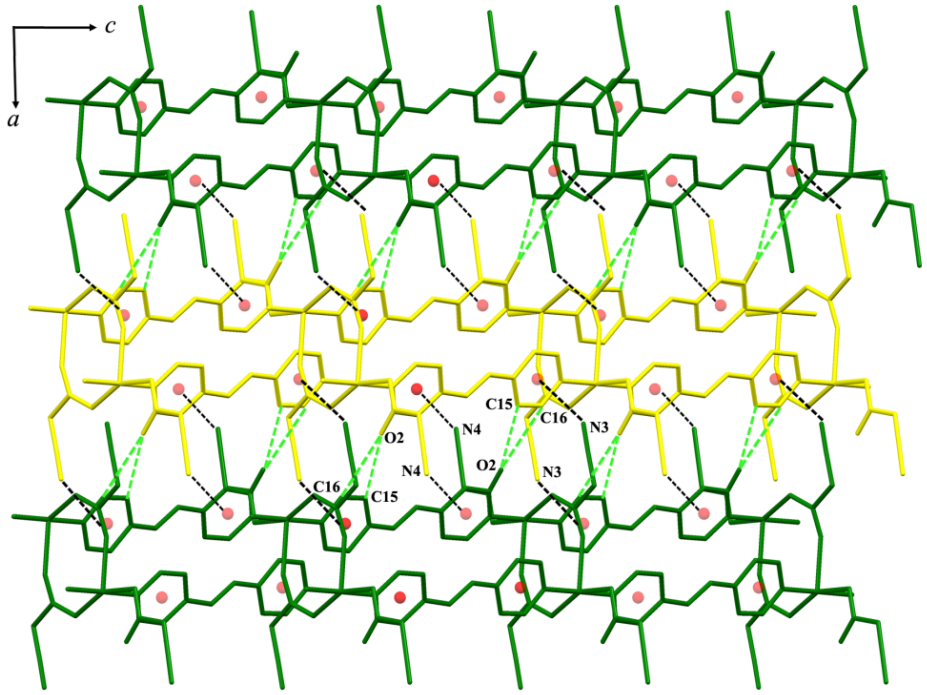

Figure 9 2D packing structure of ladder chains in **3** in *ac* plane showing weak hydrogen bonding (green broken lines) and N···π interactions between the ladder chains (black broken lines)

In contrast, the ladder chains of **4** are crossed by the hydrogen bonding between the nitrile N atoms from the terminal and bridging cyanoacetates and oxygen atoms from lattice water molecules with N4···O5 = 2.819 Å and N3···O5 = 3.194 Å, as well as, the hydrogen bonding between lattice water molecules with O5···O5i separation of 2.762 Å. In addition, the N3···centroid(pyridyl) is observed with the distance of 3.328 Å and the weak hydrogen bonding among the carboxylate oxygen of cyanoacetate and pyridyl hydrogen of μ_2-dpe cooperatively stabilizes the entire 3D packing motif of **4** with the closest Cu···Cu interchain distance of 7.2746(5) Å [C5H···N3^{i} = 2.51 Å (170°), C5···N3^{i} = 3.433(5) Å, (i) = 1/2-*x*, 5/2-*y*,-*z*; C7H···O4^{ii} = 2.56 Å (127°), C7···O4^{ii} = 3.212(3) Å, (ii) = 1/2-*x*, -1/2+*y*, 1/2-*z*; C14H···O4^{iii} = 2.50 Å (156°), C14···O4^{iii} = 3.289(4) Å, (iii) = *x*, 2-*y*, 1/2-*z*; C17H···O2^{ii} = 2.30 Å (153°), C17···O2^{ii} = 3.191(4) Å] (Figure10).

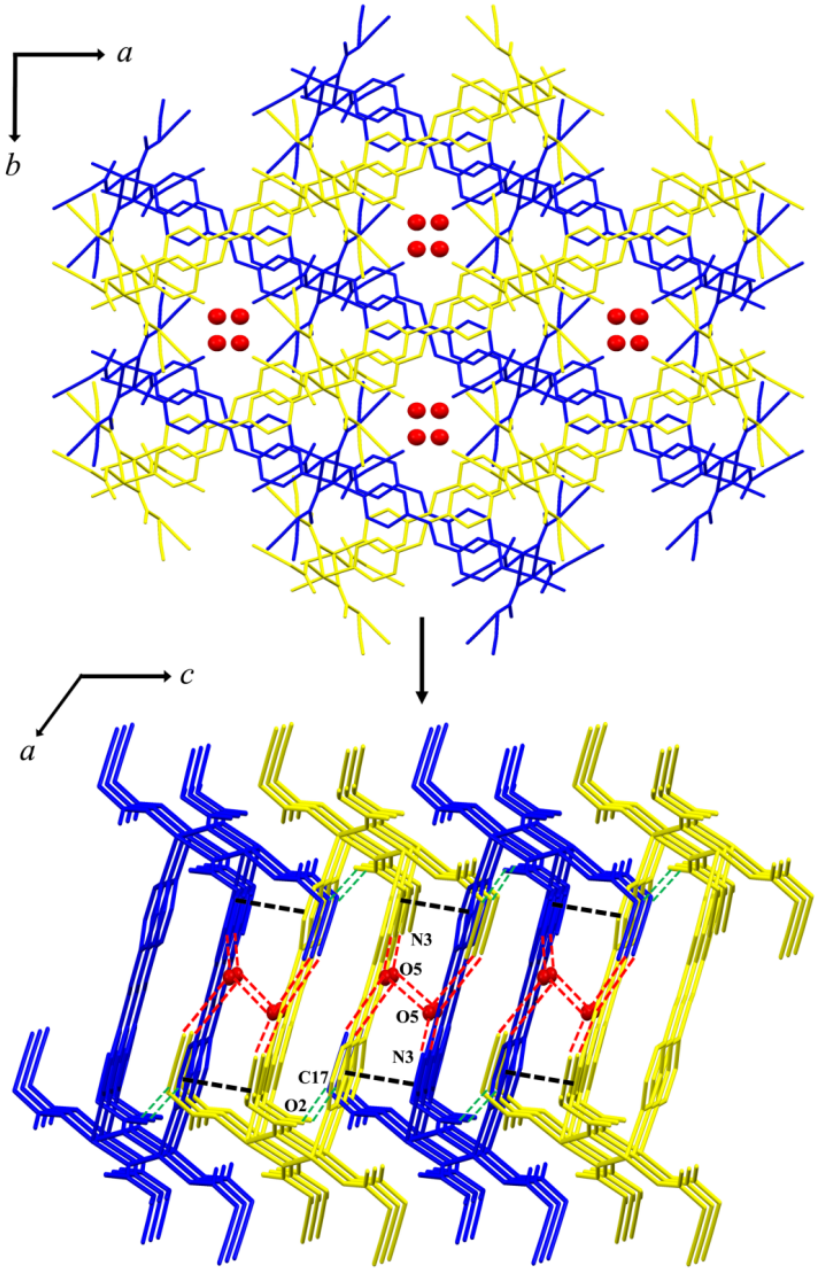

Figure10 The packing diagram of ladder chains **4** in *ab* and *ac* planes showing hydrogen bonding (red broken lines) between lattice water molecules and cyanoacetates. The weak C–H···O bond presents in green broken lines and N···π interaction presents in black broken line

Table 1 Crystallographic data for compounds **1-5**

	1	**2**	**3**	**4**	**5**
Formula	Cu	Cu	Cu	Cu	Cu
	$C_{10}H_8N_4O_4$	$C_{16}H_{16}N_4O_6$	$C_{18}H_{14}N_4O_4$	$C_{18}H_{16}N_4O_5$	$C_{18}H_{16}N_4O_4$
MW	311.74	423.87	413.87	431.87	415.90
T (K)	293(2)	293(2)	293(2)	293(2)	293(2)
Crystal system	monoclinic	orthorhombic	triclinic	monoclinic	triclinic
Space group	$P2_1/c$	$Pccn$	$P\bar{1}$	$C2/c$	$P\bar{1}$
a (Å)	4.8966(1)	12.7963(12)	9.6394(7)	23.9507(12)	8.1148(3)
b (Å)	13.3780(4)	18.0945(17)	10.0132(7)	11.7986(6)	10.2084(3)
c (Å)	17.6679(5)	7.4363(7)	10.2337(7)	14.5996(8)	12.3390(4)
α (deg)	90.00	90.00	97.073(2)	90.00	105.745(1)
β (deg)	101.794(1)	90.00	91.002(2)	110.044(1)	95.226(1)
γ (deg)	90.00	90.00	117.107(1)	90.00	110.908(1)
V (Å^3)	1132.93(5)	1721.8(3)	869.54(11)	3875.7(3)	898.72(5)
Z	4	4	2	8	2
ρ_{calcd} (g cm^{-3})	1.828	1.635	1.581	1.473	1.537
μ (Mo Kα) (mm^{-1})	1.945	1.312	1.289	1.163	1.247
Data collected	3028	2075	4324	3988	3670
Unique	2239	1796	3493	3451	3177
data (*R*int)	(0.0320)	(0.0192)	(0.0463)	(0.0219)	(0.0182)
$R_1{}^a/wR_2{}^b$	0.0567/	0.0347/	0.0467/	0.0322/	0.0331/
[$I > 2\sigma(I)$]	0.1378	0.0921	0.1001	0.0820	0.0837
$R_1{}^a/wR_2{}^b$	0.0731/	0.0395/	0.0625/	0.0405/	0.0420/
[all data]	0.1488	0.0958	0.1064	0.0864	0.0882
GOF	0.996	1.091	1.072	1.055	1.056
Max/min	0.469/	0.332/	0.584/	0.354/	0.542/
electron density	-0.775	-1.238	-0.250	-0.264	-0.217
(e Å^{-3})					

$^aR = \sum||F_o|-|F_c||/\sum|F_o|$. $^bR_w = \{ \sum[w(|F_o|-|F_c|)]^2/\sum[w|F_o|^2] \}^{1/2}$

Table 2 Selected bond lengths (Å) and angles (°) for compounds **1-5**

	Compound **1**[a]		
Cu1–O2	1.949(2)	Cu1–N1	2.031(2)
Cu1–O1	1.969(2)	Cu1–O3^{i}	2.283(2)
Cu1–N2	2.030(2)	Cu1···O4	2.970(28)
O1–Cu1–N1	90.73(9)	N2–Cu1–N1	156.83(12)
O2–Cu1–O1	171.54(9)	O2–Cu1–O3^{i}	80.59(9)
O2–Cu1–N2	91.43(9)	O1–Cu1–O3^{i}	90.95(9)
O1–Cu1–N2	90.15(9)	N2–Cu1–O3^{i}	101.86(10)
O2–Cu1–N1	91.08(9)	N1–Cu1–O3^{i}	101.28(10)
	Compound **2**[b]		
Cu1–O2^{i}	1.9807(12)	Cu1–N1	2.0228(13)
Cu1–O2	1.9807(12)	Cu1–N1^{i}	2.0228(13)
Cu1–O1	2.4998(15)	Cu1–O1^{i}	2.4998(15)
O2^{i}–Cu1–O2	180.00	O1^{i}–Cu1–O1	180.00
O2^{i}–Cu1–N1	91.14(5)	N1–Cu1–N1^{i}	180.00
O2–Cu1–N1	88.86(5)	O2^{i}–Cu1–O1	86.75(5)
O2^{i}–Cu1–N1^{i}	88.86(5)	O2–Cu1–O1	93.25(5)
O2–Cu1–N1^{i}	91.14(5)	N1–Cu1–O1	91.00(6)
N1^{i}–Cu1–O1	89.00(6)		
	Compound **3**[c]		
Cu1–O1	2.0138(19)	Cu1–N2	2.010(2)
Cu1–O3	1.9667(18)	Cu1–O4^{i}	2.282(2)
Cu1–N1	2.023(2)	O4i–Cu1–O2	142.13(8)
O3–Cu1–N2	90.25(8)	O3–Cu1–O1	153.34(8)
N2–Cu1–O1	90.74(8)	O3–Cu1–N1	88.79(8)
N2–Cu1–N1	178.99(9)	O1–Cu1–N1	90.26(8)
O3–Cu1–O4^{i}	119.06(8)	N2–Cu1–O4^{i}	92.86(8)
O1–Cu1–O4^{i}	87.49(8)	N1–Cu1–O4^{i}	87.35(8)
O3–Cu1–O2	98.69(7)		
	Compound **4**[d]		
Cu1–O1	1.9866(13)	Cu1–N2	2.0082(15)
Cu1–O3	1.9493(14)	Cu1···O4	2.8283(23)
Cu1–N1	2.0136(15)	Cu1–O1^{i}	2.4459(14)
N2–Cu1–N1	170.77(7)	O3–Cu1–O1	168.51(6)
O3–Cu1–N2	90.76(6)	O1–Cu1–N2	91.27(6)
O3–Cu1–N1	88.31(6)	O1–Cu1–N1	91.46(6)
	Compound **5**[e]		
Cu1–O1	1.9743(16)	Cu1–O3	1.9998(16)
Cu1–N2	2.0139(17)	Cu1–N1	2.0158(16)
Cu1–O2^{i}	2.2642(19)	N1–Cu1–O2^{i}	90.03(7)
O1–Cu1–O3	150.86(7)	O1–Cu1–N2	89.41(7)
O3–Cu1–N2	88.54(7)	O1–Cu1–N1	91.83(7)
O3–Cu1–N1	90.11(7)	N2–Cu1–N1	178.65(7)
O1–Cu1–O2^{i}	117.27(8)	O3–Cu1–O2^{i}	91.80(8)
N2–Cu1–O2^{i}	89.88(8)		

[a] Symmetry codes for **1**: (i) 1+*x*, *y*, *z*. [b]For **2**: (i) 1–*x*, 1–*y*, –*z*.

[c] For **3**: (i) 1–*x*, 2–*y*, 1–*z*.[d] For **4**: (i) 0.5+*x*, 0.5+*y*, *z*.

[e] For **5**: (i) 1–*x*, 1–*y*, –*z*.

Supramolecular robustness in 2

To examine the thermal stabilities of compounds **1**-**5**, thermogravimetric analyses (TGA) were performed in the temperature range 30-500°C in N_2 atmosphere (Figure11). Compounds **1**, **3**, **4** and **5** show no weight loss and stable up to ~140, 120, 110, 100°C, respectively. Then the structures gradually decompose corresponding to the removal of lattice water molecule, cyanoacetate and organic coligands, finally giving a mixture of the CuO and Cu_2O as main products.[64] The TGA curve of **2** reveals the release of two coordination water molecules at the first step of weight loss in the temperature range 50-92°C (found, 8.33%; Calcd, 8.50%) resulting to the dehydrated form of $[Cu(cna)_2(bpy)]_n$ (**2-A**), which is stable up to ~107°C and then the structure gradually collapses.

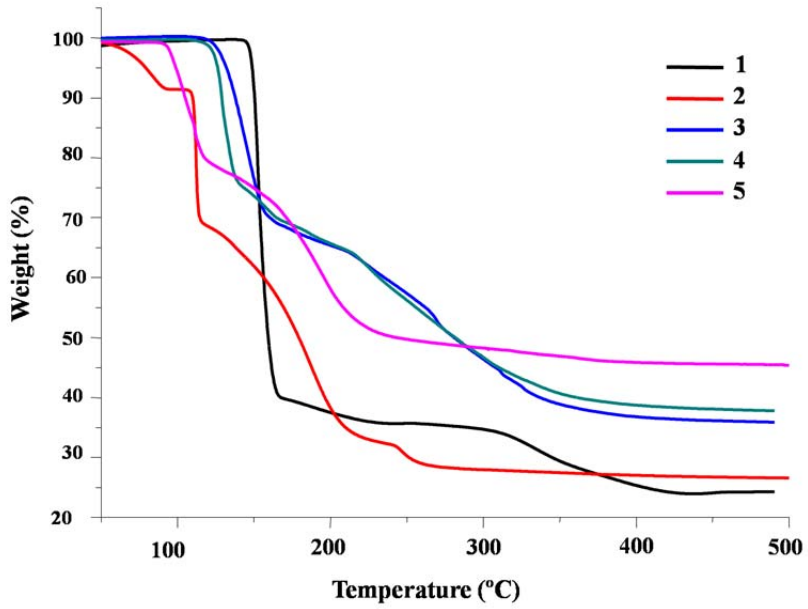

Figure11 TGA curves of compounds **1**-**5**

Aforementioned compound **2** contains two coordination water molecules and its anhydrous phase remaining stable up to 107°C, as evidenced by TGA profile. This inspired us to examine the dynamic structures of **2** during the dehydration and rehydration processes by elemental analyses, XRPD, and spectroscopic techniques. Consequently, the dehydrated form, $[Cu(cna)_2(bpy)]_n$ (**2-A**) was obtained by heating the polycrystalline samples of **2** at 105ºC for 20 min and the color changed from blue to deep blue. Furthermore, the rehydrated form of **2-A'** was obtained by immersing the dehydrated sample to water for 1 day at room temperature. The XRPD patterns of **2**, **2-A** and **2-A'** are shown in Figure 12.

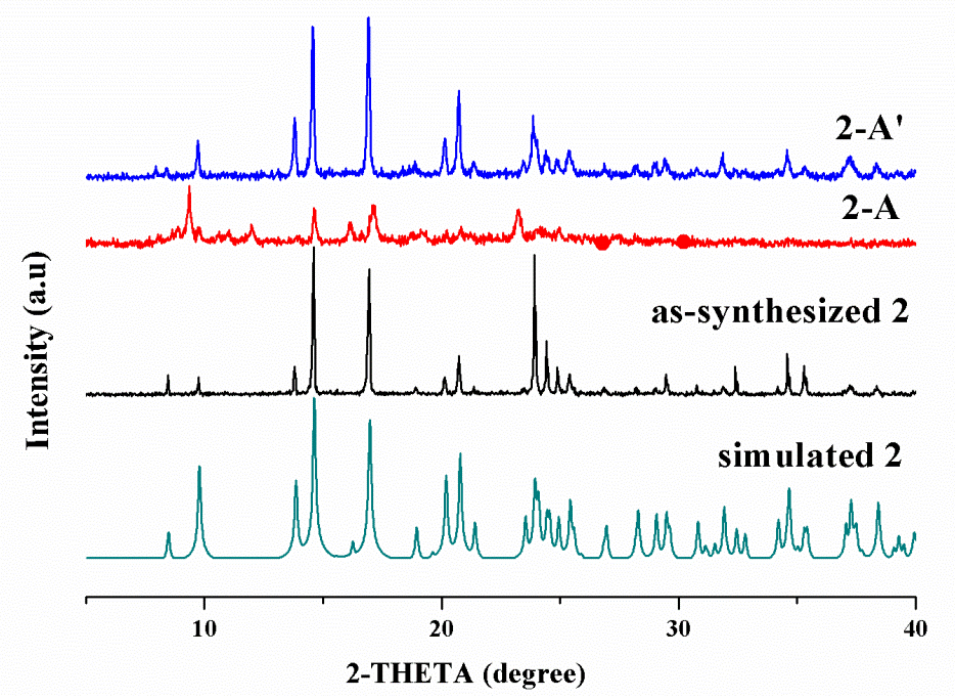

Figure 12 XRPD patterns: simulated from single-crystal X-ray data of **2**; as synthesized **2**, the dehydrated form **2-A**; the rehydrated form **2-A'**

The elemental analysis of **2-A** (Anal. Calcd for $CuC_{16}H_{12}N_4O_4$: C, 49.55; H, 3.12; N, 14.45%. Found: C, 49.30; H, 3.16; N, 14.30%.) and XRPD results indicate that the anhydrous $[Cu(cna)_2(bpy)]_n$ (**2-A**) reveals no significant change of crystalline phase which the main peaks are duplicate to those of XRPD pattern of as-synthesized **2**. The new peaks appear at 9.37º and 23.26º are ascribed to the drastic change in the coordination environments around Cu(II) center during dehydration process. Moreover, the original crystalline phase $[Cu(cna)_2(bpy)(H_2O)_2]_n$ (**2-A'**) can be restored from **2-A** after rehydration process, confirmed by the coincidence in XRPD patterns and elemental analysis (Anal. Calcd $CuC_{16}H_{16}N_4O_6$: C, 45.34; H, 3.80; N, 13.22%. Found: C, 45.26; H, 3.69; N, 13.00%.). This result confirms the rigid supramolecular framework of **2** during thermal dehydration and rehydration processes. Furthermore, this behavior has been further verified by TGA, IR and solid-state UV-vis diffuse reflectance spectra. The TGA profiles of **2** and **2-A'** (Figure 13) are identical showing the release of two coordination water molecules at the first step of weight loss (Anal. Calcd: 8.50% Found: 8.33% for **2-A'**), whereas the TGA profile of anhydrous form **2-A** shows no weight loss, remaining stable up to ~107ºC and then the structure gradually collapses.

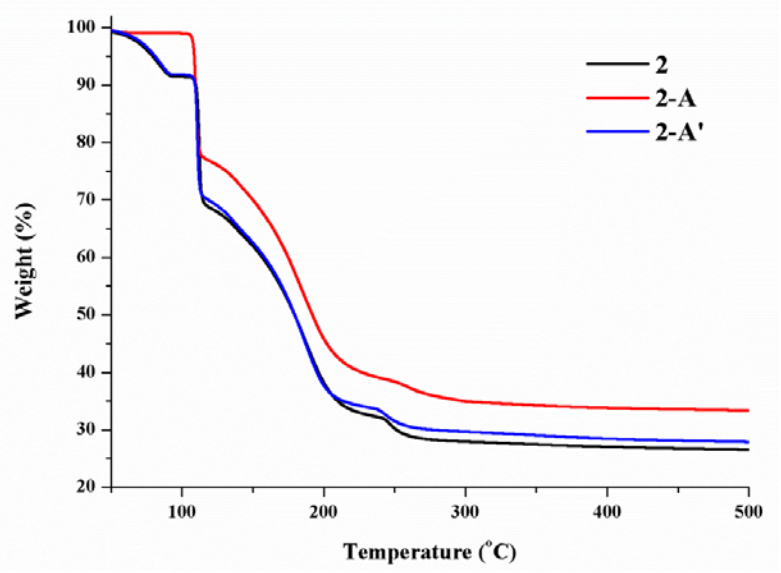

Figure 13 TGA curves of **2**, the dehydrated form **2-A**, and rehydrated form **2-A'**

The UV-vis spectra clearly show that the parallel bands observed in **2** and **2-A'** implying the same Cu(II) environments (Figure 14). Whereas the anhydrous **2-A** shows the blue-shifted absorption broadband with λ_{max} around ~590 nm, giving the deep blue color. In fact these values of the transition energy are in the usual range for the pseudo-octahedral geometry of Cu(II) center.[57] In addition, these results agree with the reversible change in IR spectra for ν(O–H) of coordination water molecules around 3544-3200 cm^{-1} and the ν_s(OCO) of cyanoacetate at ~1600 cm^{-1} and the fingerprint region below 818 cm^{-1} (Figure 15). All of the results prove the supramolecular robustness of **2**. Interestingly, this phenomenon is not observed in the isomorphous analogues containing Co(II) (**2-Co**) and Ni(II) (**2-Ni**) centers. The crystal structures of **2-Co** and **2-Ni** are confirmed by XRD, IR spectra, TGA and elemental analysis (Figure 16-3.18).

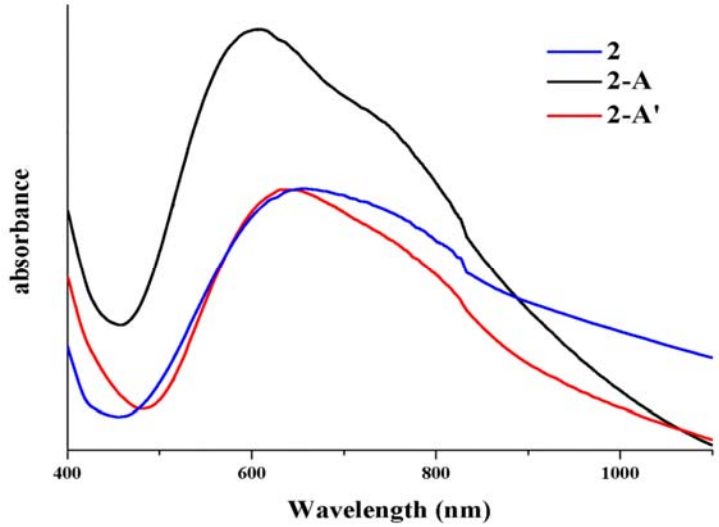

Figure 14 The UV-vis diffuse reflectance spectra of as-synthesize **2-Cu** (black line), the dehydrated form **2-Cu-A** (red line), and the rehydrated form **2-Cu-A'** (blue line)

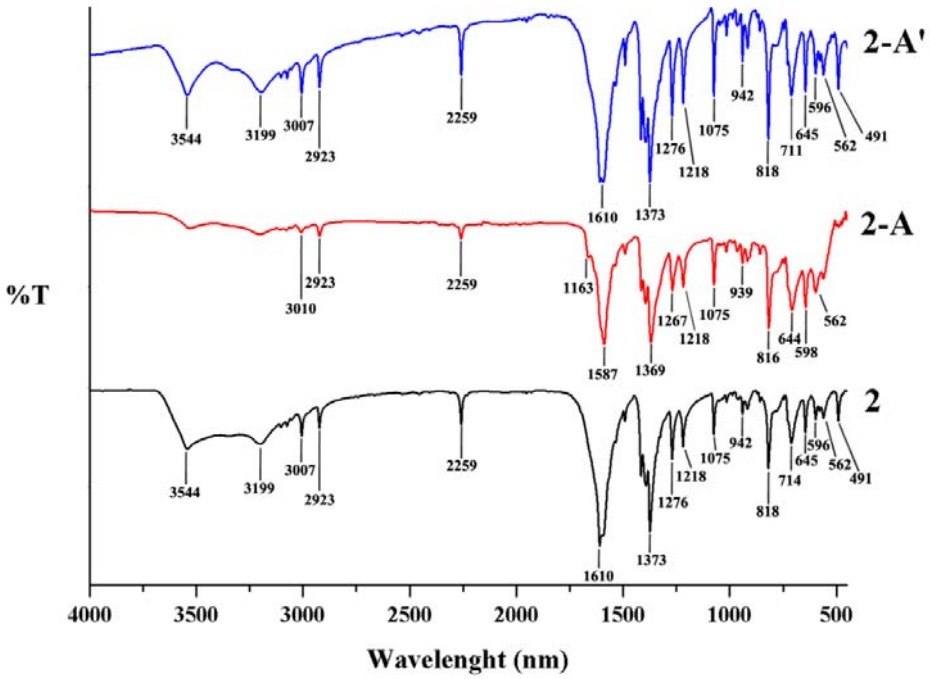

Figure 15 IR spectra of as-synthesize **2**, the dehydrated form **2-A**, and rehydrated form **2-A'**

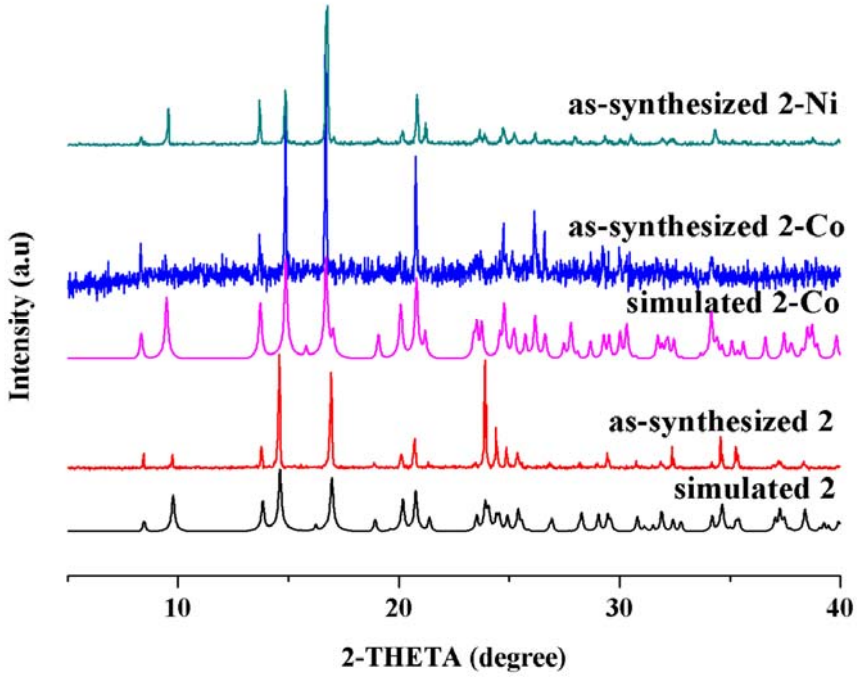

Figure 16 XRPD patterns of simulated from single-crystal X-ray data of **2** and as-synthesized of **2**, **2-Co** and **2-Ni**

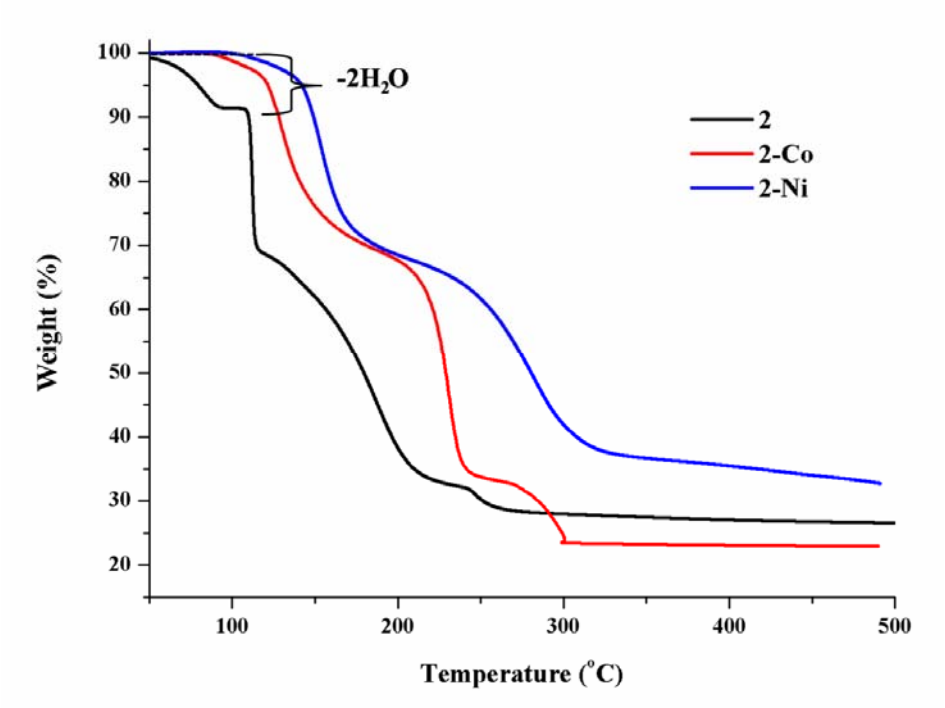

Figure 17 TGA curves of compounds **2**, **2-Co** and **2-Ni**

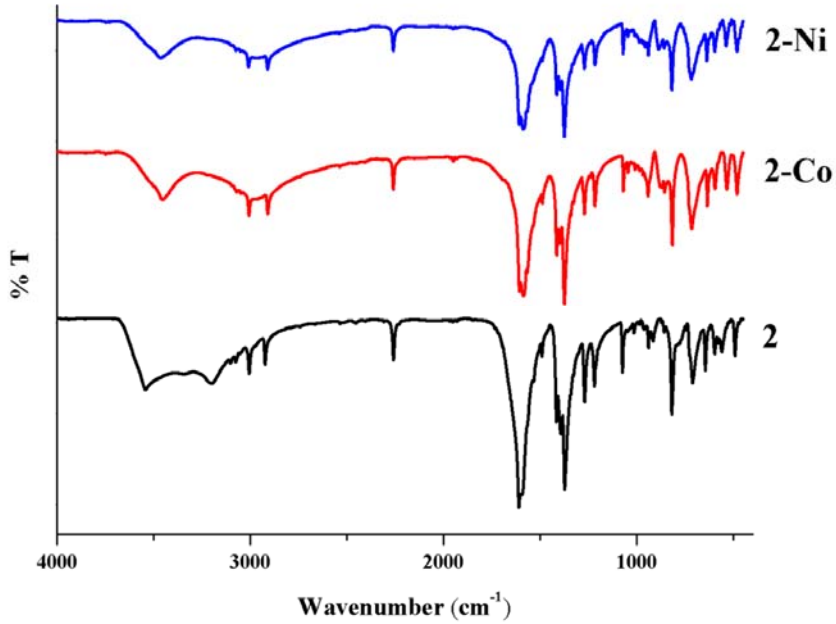

Figure 18 IR spectra (4000-450 cm^{-1}) for as-synthesize **2**, **2-Co** and **2-Ni**.

Table 3 Crystallographic data for compound **2-Co**

	2-Co
Formula	$CoC_{16}H_{16}N_4O_6$
MW	419.26
T (K)	293(2)
Crystal system	orthorhombic
Space group	*Pccn*
a (Å)	12.8995(5)
b (Å)	18.6577(8)
c (Å)	7.1839(3)
α (deg)	90.00°
β (deg)	90.00°
γ (deg)	90.00°
V (Å^3)	1728.99(12)
Z	4
ρ_{calcd} (g cm^{-3})	1.611
μ (Mo Kα) (mm^{-1})	1.036
Data collected	2150
Unique data	1923
$R_1{}^a/wR_2{}^b$ [$I > 2\sigma(I)$]	0.0258/0.0743
$R_1{}^a/wR_2{}^b$ [all data]	0.0290/0.0766
GOF	1.046
Max/min electron density (e Å^{-3})	0.272/-0.306

$^aR = \sum||F_o|-|F_c||/\sum|F_o|$. $^bR_w = \{ \sum[w(|F_o|-|F_c|)]^2/\sum[w|F_o|^2] \}^{1/2}$

Table 4 Selected bond lengths (Å) and angles (deg) for compound **2-Co**

Compound 2-Co			
Co1–O1	2.0932(9)	Co1–N1	2.1375(10)
Co1–O1^i	2.0932(9)	Co1–O2^i	2.1429(9)
Co1–N1^i	2.1375(10)	Co1–O2	2.1429(9)
O1–Co1–O1^i	180.00(4)	N1^i–Co1–O2^i	92.01(4)
O1–Co1–N1^i	89.85(4)	N1–Co1–O2^i	87.99(4)
O1^i–Co1–N1^i	90.15(4)	O1–Co1–O2	90.44(4)
O1–Co1–N1	90.15(4)	O1^i–Co1–O2	89.56(4)
O1^i–Co1–N1	89.85(4)	N1^i–Co1–O2	87.99(4)
N1^i–Co1–N1	180.00	N1–Co1–O2	92.01(4)
O1–Co1–O2^i	89.56(4)	O2^i–Co1–O2	180.00
O1^i–Co1–O2^i	90.44(4)		

(i) 2–*x*, 1–*y*, –*z*

The coincidence in XRPD patterns and IR spectra of **2**, **2-Co** and **2-Ni** imply the identical crystalline structures. Whereas the TGA profiles of **2-Co** and **2-Ni** reveal the releases of two coordination water molecules at the higher temperature range 85-120ºC for **2-Co** and 95-140 ºC for **2-Ni**. Then, the structures continuously decompose with the no observed stable anhydrous phases in TGA profiles. The dehydrated form of **2-Co-A** and **2-Ni-A** were examined and obtained by heating the polycrystalline sample at 115ºC, 135ºC for 20

min for **2-Co** and **2-Ni**, respectively and the colors changed from orange to brown for **2-Co-A**; blue to green for **2-Ni-A** (Figure 19).

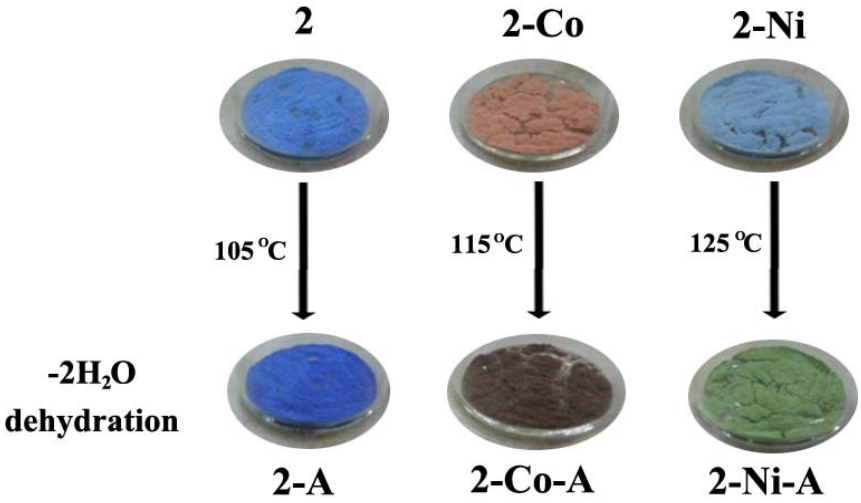

Figure 19 The colors of as-synthesized **2**, **2-Co** and **2-Ni** and dehydrated forms of **2-A**, **2-Co-A**, **2-Ni-A**

The XRPD results indicate that **2-Co-A** and **2-Ni-A** are amorphous forming by the collapse of supramolecular structure. Moreover, these anhydrous amorphous phases cannot be regenerated to the original crystal structure after immersion into water for 1 day (Figure 20 and 3.21).

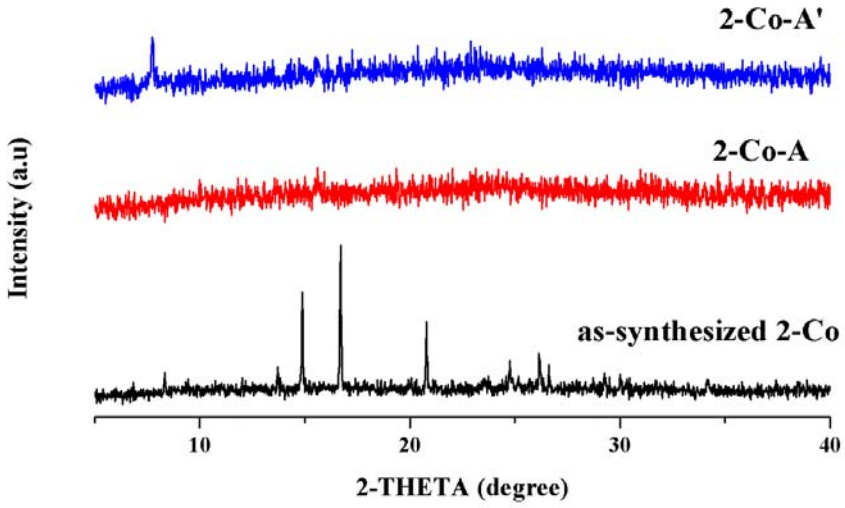

Figure 20 XRPD patterns: as-synthesized **III2-Co**, the dehydrated form **2-Co-A**; and **2-Co-A'** was obtained by soaking the dehydrated **2-Co-A** in water for 1 day

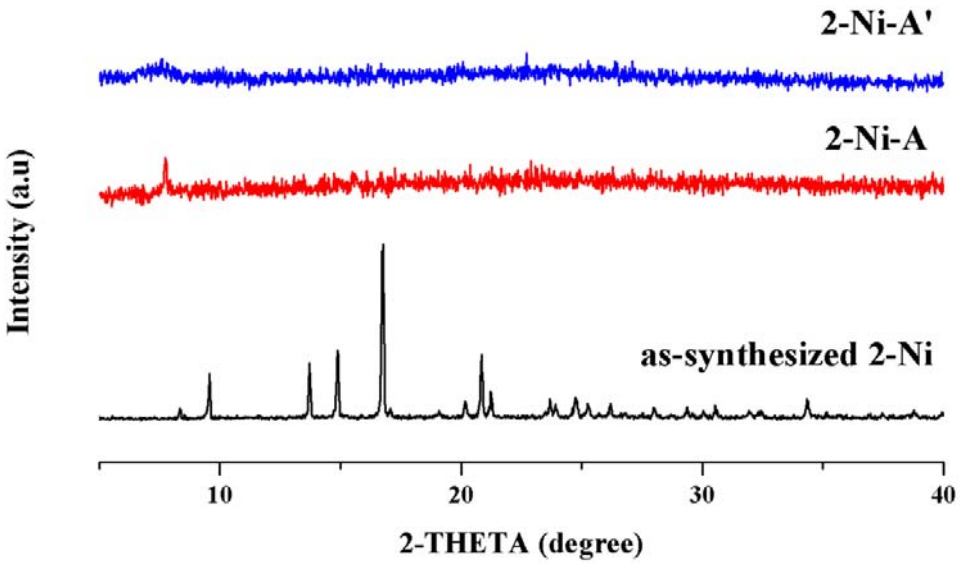

Figure 21 XRPD patterns: as-synthesized **2-Ni**, the dehydrated form **2-Ni-A**; and **2-Ni-A'** was obtained by soaking the dehydrated **2-Ni-A** in water for 1 day

The observation of the robust framework of **2** may be attributed to the cooperative effects between the diverse intermolecular interactions stabilizing noncovalent supramolecular motifs together with the Jahn-Teller distortion in Cu(II) d^9 system. The X-ray analysis of **2** revealed that two coordination water molecules in the role of H-donors display the individual intermolecular hydrogen bonds only through unbound oxygen atoms from terminal cyanoacetate as H-acceptors (Figure 7). Thus, upon eliminating the coordination water in **2**, these unbound carboxylic oxygen atoms possibly weakly interact with the vacant Cu(II) sites leading to the elongated octahedral geometry, as evidenced by electronic spectra of **2-A** (Figure 14).

In addition, the coordination bridge *via* rigid bpy backbone plays a role for supporting the structural skeleton, as well as, the other noncovalent interactions especially the 1D hydrogen bonding array involving terminal cyano groups and C–H···π interactions together efficiently support the stabilization of overall supramolecular framework of **2-A** (Figure 22). Furthermore, the structural collapses of the anhydrous analogues, **2-Co-A** and **2-Ni-A** point out that besides noncovalent interactions and coordination bridges, the Jahn-Teller effect in Cu(II), d^9 system play a significant role on stabilizing the distorted octahedral coordination sphere[65-67], giving rise to the structural flexibility that is not found in **2-Co-A** and **2-Ni-A** analogues. Remarkably, the dehydration process in **2-A** can be reversed after immersing the dehydrated sample in water, regenerating the original crystalline phase which is an indication of the robust but flexible supramolecular framework constructed by 1D polymeric chains in **2**.

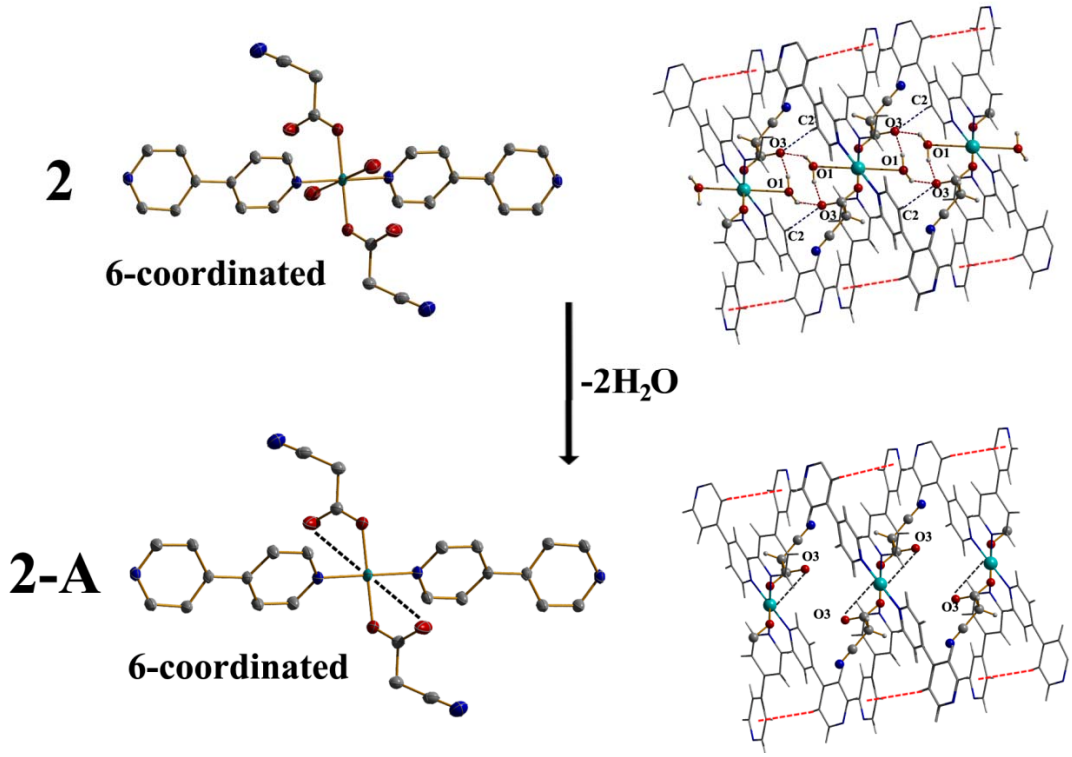

Figure 22 The proposed coordination environment of Cu(II) center in the dehydrated form**.**

Magnetic measurements

The magnetic susceptibilities of powdered sample of **1** and **3** were measured between 2 and 300 K under a constant *dc* magnetic field of 0.1 T (Figure 23 and 3.24**)**. At 300 K the $\chi_M T$ values are 0.45 and 0.41 cm^3 K mol^{-1} for **1** and **3**, respectively, which are typical of Cu(II) and above that expected for uncoupled Cu(II) centers (0.375 cm^3 K mol^{-1} for $g = 2$) because of spin-orbit coupling, i.e. $g > 2$. The $\chi_M T$ values of **1** slowly decrease, in a linear fashion, down to ~15 K then, more rapidly, reaching 0.33 cm^3 K mol^{-1} at 2 K. In contrast, the $\chi_M T$ values for **3** are practically constant until ~10 K, and then the $\chi_M T$ values abruptly decrease to reach 0.19 cm^3 K mol^{-1} at 2 K. The corresponding plots of χ_M vs. T for **1** and **3** show Curie-like behavior with a hint of a maximum in χ_M beginning below 2 K in **3**. The data are generally indicative of very weak antiferromagnetic coupling, this being responsible for the rapid decreases in $\chi_M T$ at very low temperatures,[18,49,68] although Zeeman level thermal depopulation effects may play a part in this region. There is no evidence in the temperature range studied for any long-range magnetic ordering.

In attempting to quantify the magnetic data, the 2D sheet motif of **1** ideally requires a two J model one for the *syn,anti*-η^1:η^3:μ_2-cyanoacetate bridged chains, the other for the pyrazine bridged chains. Landee and Turnbull have recently reviewed low-dimensional Cu(II) molecular magnets[69] including related 2D rectangular sheets such as $[Cu(HCO_2)(pyz)(NO_3)]_n$ that showed a mixed antiferromagnetic (pyrazine bridge)/ferromagnetic (formate bridge) behaviour and was fitted by Monte Carlo methods.[70] $[Cu(HCO_2)(pyz)(NO_3)]_n$ showed a broad maximum in $\chi_M T$ at 25.3 K, due to ferromagnetic exchange, and a maximum in χ_M at 6.5 K due to antiferromagnetic exchange. Clearly were do not observe such χ_M or $\chi_M T$ maxima in **1** so we conclude that antiferromagnetic exchange occurs along the cyanoacetate- and pyz-bridged chains, and is smaller in magnitude than in $[Cu(HCO_2)(pyz)(NO_3)]_n$. As in the case of 2D β-$[Cu(dca)_2(pyz)]_n$ where dca = $\mu_{1,5}$-NC(N)CN[71] we have used a model by Lines[72] for 2D systems with $S = 1/2$, based on that of Rushbrooke and Wood.[73] A good fit of the data was

obtained (Figure 25) using a single J of –0.24 cm^{-1} but the g value of 1.89 is lower than expected for Cu(II) and the $N\alpha$ (temperature independent susceptibility) of 400 x 10^{-6} cm^3 mol^{-1} is much higher than the normal 60 x 10^{-6} cm^3 mol^{-1}. The size of J is at the lower end of values found for *syn*,*anti*-η^1:η^3:μ_2-carboxylate and pyrazine bridges. It is possible there are traces of impurity in the sample of **1** that affect the $\chi_M T$ behavior and the fitting thereof.[69]

The $\chi_M T$ plot for **3** is indicative of very weak to zero exchange coupling and this is not surprising in view of the large Cu···Cu separations and the poor superexchange pathways provided by the 1,2-di(4-pyridyl)ethylene linkers, along the ladder chains.

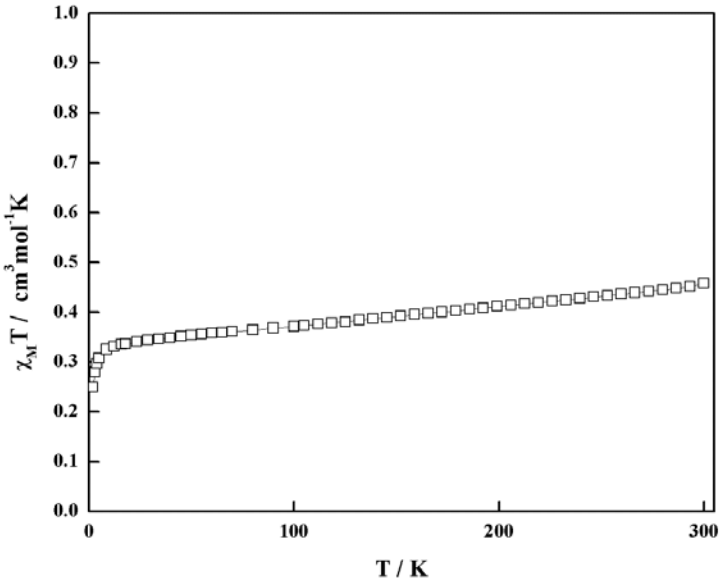

Figure 23 Temperature dependence of $\chi_M T$ of compound **1**

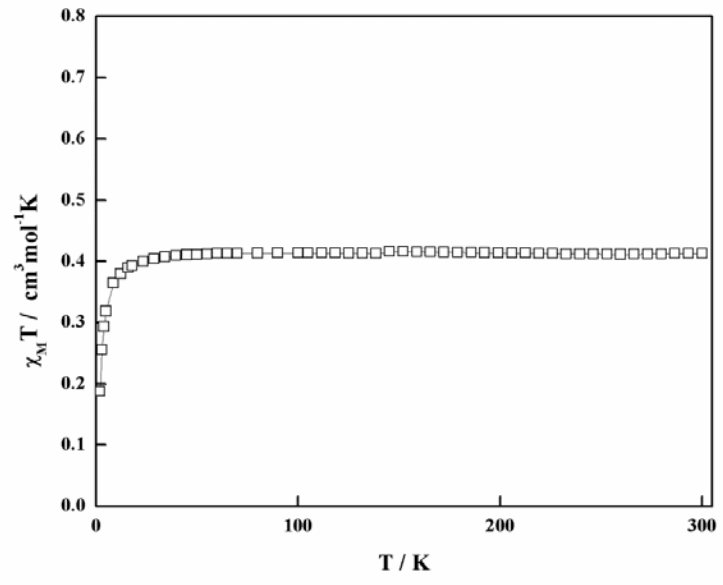

Figure 24 Temperature dependence of $\chi_M T$ of compound **3**

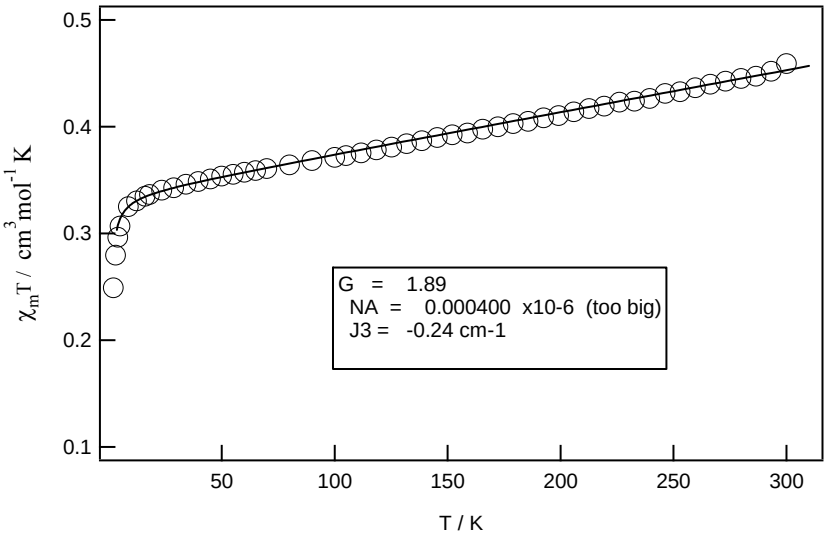

Figure 25 Best fit of the $\chi_M T$ data for compound **1** using the Lines model described in the text. NB-NA = temperature independent susceptibility is usually 60 x 10^{-6} cm^3 mol^{-1} for Cu(II)

Conclusions

Five new coordination polymers constructed by self-assembly of the auxiliary *N,N′*-ditopic spacers and copper(II) cyanoacetates have been structurally characterized. Compounds **2-5** exhibit polymeric chain structure while **1** shows 2D layer. This result demonstrated that the length of auxiliary spacers effectively influences on the structural dimensionalities. The shortest pyrazine with Cu(II) cyanoacetate well provides the construction of 2D coordination polymer in **1**. Likewise, the structural diversity greatly results from the carboxylate groups in cyanoacetate that can coordinate with Cu(II) center in various ways. The μ_2-1,3(*syn,anti*) bridging mode for **1**, **3** and **5**, and μ_2-1,1 monoatomic bridge in **4** are found, whereas cyanoacetate in **2** behaves as terminal monodentate ligand. Besides the various coordination modes of carboxylates, the nitrile group in cyanoacetate has an influence on the established supramolecular interactions *via* either hydrogen bonding or N···π interactions, which mainly contributes to the stabilization of the overall supramolecular architecture. Particularly, compound **2** exhibits a robust supramolecular framework constructed by 1D polymeric chains during thermal dehydration and rehydration processes that is not observed in the isomorphous series containing Co(II) and Ni(II) ions. This result demonstrates the significant role of Jahn-Teller distortions in octahedral Cu(II) center accompanied by various intermolecular noncovalent interactions among interlaced polymeric chains for encouraging the design of a "soft" supramolecular framework with low dimensional building blocks.

References

(1) Cheetham, A. K.; Rao, C. N. R.; Feller, R. K. *Chem. Commun.* **2006**, 4780.
(2) Janiak, C. *Dalton Trans.* **2003**, 2781.
(3) Kitagawa, S.; Kitaura, R.; Noro, S.-i. *Angew. Chem. Int. Ed.* **2004**, *43*, 2334.
(4) Kuppler, R. J.; Timmons, D. J.; Fang, Q.-R.; Li, J.-R.; Makal, T. A.; Young, M. D.; Yuan, D.; Zhao, D.; Zhuang, W.; Zhou, H.-C. *Coord. Chem. Rev.* **2009**, *253* 3042.

(5) Schneemann, A.; Bon, V.; Schwedler, I.; Senkovska, I.; Kaskel, S.; Fischer, R. A. *Chem. Soc. Rev.* **2014**, *43*, 6062.
(6) Stock, N.; Biswas, S. *Chem. Rev.* **2012**, *112*, 933.
(7) O'Keeffe, M.; Yaghi, O. M. *Chem. Rev.* **2012**, *112*, 675.
(8) Suh, M. P.; Park, H. J.; Prasad, T. K.; Lim, D.-W. *Chem. Rev.* **2012**, *112*, 782.
(9) Yoon, M.; Srirambalaji, R.; Kim, K. *Chem. Rev.* **2012**, *112*, 1196.
(10) Carballo, R.; Castineiras, A.; Covelo, B.; Vazquez-Lopez, E. M. *Polyhedron* **2001**, *20*, 899.
(11) Hu, H.-L.; Suen, M.-C.; Yeh, C.-W.; Chen, J.-D. *Polyhedron* **2005**, *24*, 1497.
(12) Jassal, A. K.; Sharma, S.; Hundal, G.; Hundal, M. S. *Cryst. Growth Des.* **2015**, *15*, 79.
(13) Liu, Q.-Y.; Yuan, D.-Q.; Xu, L. *Cryst. Growth Des.* **2007**, *7*, 1832.
(14) Wang, H.; Zhang, D.; Sun, D.; Chen, Y.; Zhang, L.-F.; Tian, L.; Jiang, J.; Ni, Z.-H. *Cryst. Growth Des.* **2009**, *9*, 5273.
(15) Wang, X.-F.; Zhang, Y.-B.; Huang, H.; Zhang, J.-P.; Chen, X.-M. *Cryst. Growth Des.* **2008**, *8*, 4559.
(16) Zhu, H.-F.; Zhang, Z.-H.; Sun, W.-Y.; Okamura, T.-a.; Ueyama, N. *Cryst. Growth Des.* **2005**, *5*, 177.
(17) Mikuriya, M.; Yoshioka, D.; Handab, M. *Coord. Chem. Rev.* **2006**, *250*, 2194.
(18) Boonmak, J.; Youngme, S.; Chaichit, N.; Albada, G. A. v.; Reedijk, J. *Cryst. Growth Des.* **2009**, *9*, 3318.
(19) Boonmak, J.; Youngme, S.; Chotkhun, T.; Engkagul, C.; Chaichit, N.; Albada, G. A. v.; Reedijk, J. *Inorg. Chem. Commun.* **2008**, *11*, 1231.
(20) Kurmoo, M. *Chem. Soc. Rev.* **2009**, *38*, 1353.
(21) Wang, X.-Y.; Wang, Z.-M.; Gao, S. *Chem. Commun.* **2008**, 281.
(22) Sokolova, M. N.; Budantseva, N. A.; Fedoseev, A. M. *Russ. J. Coord. Chem.* **2011**, *37*, 478.
(23) Feng, X.; Shi, X.-G.; Ruan, F. *Z. Kristallogr. NCS* **2009**, *224*, 193.
(24) Feng, X.; FengII, T.-C.; ZhaoIII, J.-S.; ShiI, X.-G.; RuanI, F. *Z. Kristallogr. NCS* **2009**, *224*, 541.
(25) S. G. Shova; Simonov, Y. A.; Gdaniec, M.; Novitchi, G. V.; Lazarescu, A.; Turta, K. I. *Russ. J. Inorg. Chem.* **2002**, *47*, 946.
(26) Novitskii, G.; Shova, S.; Voronkova, V. K.; Korobchenko, L.; Gdanec, M.; Simonov, Y. A.; Turte, K. *Russ. J. Coord. Chem.* **2001**, *27*, 791.
(27) Nakamoto, T.; Hanaya, M.; Katada, M.; Endo, K.; Kitagawa, S.; Sano, H. *Inorg. Chem.* **1997**, *36*, 4347.
(28) Darensbourg, D. J.; Holtcamp, M. W.; Longridge, E. M.; Khandelwal, B.; Klausmeyer, K. K.; Reibenspies, J. H. *J. Am. Chem. Soc.* **1995**, *117*, 318.
(29) Wasson, J. R.; Shyr, C.-I.; Trapp, C. *Inorg. Chem.* **1968**, *7*, 469.
(30) Leong, W. L.; Vittal, J. J. *Chem. Rev.* **2011**, *111*, 688.
(31) Vittal, J. J. *Coord. Chem. Rev.* **2007**, *251*, 1781.
(32) Hu, S.; He, K.-H.; Zeng, M.-H.; Zou, H.-H.; Jiang, Y.-M. *Inorg. Chem.* **2008**, *47*, 5218.
(33) Yu, F.; Li, D.-D.; Cheng, L.; Yin, Z.; Zeng, M.-H.; Kurmoo, M. *Inorg. Chem.* **2015**, *54*, 1655.
(34) Lee, E. Y.; Suh, M. P. *Angew. Chem. Int. Ed.* **2004**, *43*, 2798.
(35) Cingolani, A.; Galli, S.; Masciocchi, N.; Pandolfo, L.; Pettinari, C.; Sironi, A. *J. Am. Chem. Soc.* **2005**, *127*, 6144.

(36) Piromchom, J.; Wannarit, N.; Boonmak, J.; Pakawatchai, C.; Youngme, S. *Inorg. Chem. Commun.* **2014**, *40*, 59–61.
(37) Kitagawa, S.; Uemura, K. *Chem. Soc. Rev.* **2005**, *34*, 109.
(38) Boonmak, J.; Nakano, M.; Chaichit, N.; Pakawatchai, C.; Youngme, S. *Dalton Trans.* **2010**, *39*, 8161.
(39) Hogan, G. A.; Rath, N. P.; Beatty, A. M. *Cryst. Growth Des.* **2011**, *11*, 3740.
(40) Kawano, M.; Fujita, M. *Coord. Chem. Rev.* **2007**, *251*, 2592.
(41) Parshamoni, S.; Sanda, S.; Jena, H. S.; Tomar, K.; Konar, S. *Cryst. Growth Des.* **2014**, *14*, 2022.
(42) Fan, L.; Zhang, X.; Sun, Z.; Zhang, W.; Ding, Y.; Fan, W.; Sun, L.; Zhao, X.; Lei, H. *Cryst. Growth Des.* **2013**, *13*, 2462.
(43) Niu, D.; Yang, J.; Guo, J.; Kan, W.-Q.; Song, S.-Y.; Du, P.; Ma, J.-F. *Cryst. Growth Des.* **2012**, *12*, 2397.
(44) Chang, Z.; Zhang, D.-S.; Chen, Q.; Li, R.-F.; Hu, T.-L.; Bu, X.-H. *Inorg. Chem.* **2011**, *50*, 7555.
(45) Drabent, K.; Ciunik, Z. *Cryst. Growth Des.* **2009**, *9*, 3367.
(46) Tian, A.-x.; Ying, J.; Peng, J.; Sha, J.-q.; Pang, H.-j.; Zhang, P.-p.; Chen, Y.; Zhu, M.; Su, Z.-m. *Cryst. Growth Des.* **2008**, *8*, 3717.
(47) Liu, G.-X.; Huang, Y.-Q.; Chu, Q.; Okamura, T.-a.; Sun, W.-Y.; Liang, H.; Ueyama, N. *Cryst. Growth Des.* **2008**, *8*, 3233.
(48) Brown, S.; Cao, J.; Musfeldt, J. L.; Conner, M. M.; McConnell, A. C.; Southerland, H. I.; Manson, J. L.; Schlueter, J. A.; Phillips, M. D.; Turnbull, M. M.; Landee|, C. P. *Inorg. Chem.* **2007**, *46*, 8577.
(49) Carballo, R.; Covelo, B.; Fallah, M. S. E.; Ribas, J.; Vazquez-Lopez, E. M. *Cryst. Growth Des.* **2007**, *7*, 1069.
(50) Phuengphai, P.; Youngme, S.; Mutikainen, I.; Gamez, P.; Reedijk, J. *Polyhedron* **2012**, *42*, 10.
(51) *SMART 5.6* Bruker AXS Inc.: Madison, WI, 2000.
(52) *APEX2*; Bruker AXS Inc.: Madison, WI, 2014.
(53) *SAINT 4.0 Software Reference Manual*; Siemens Analytical X-Ray Systems Inc.: Madison, WI, 2000.
(54) Sheldrick, G. M. *SADABS, Program for Empirical Absorption correction of Area Detector Data*; University of Göttingen: Göttingen, Germany, 2000.
(55) Sheldrick, G. M. *Acta Crystallogr.* **2008**, *A64*, 112.
(56) Chai, X.-C.; Sun, Y.-Q.; Lei, R.; Chen, Y.-P.; Zhang, S.; Cao, Y.-N.; Zhang, H.-H. *Cryst. Growth Des.* **2010**, *10*, 658.
(57) Tabbì, G.; Giuffrida, A.; Bonomo, R. P. *J. Inorg. Biochem.* **2013**, *128* 137.
(58) Youngme, S.; Wannarit, N.; Remsungnen, T.; Chaichit, N.; Albada, G. A. v.; Reedijk, J. *Inorg. Chem. Commun.* **2008**, *11*, 179.
(59) Youngme, S.; Cheansirisomboon, A.; Danvirutai, C.; Pakawatchai, C.; Chaichit, N. *Inorg. Chem. Commun.* **2008**, *11*, 57.
(60) Youngme, S.; Chotkhun, T.; Leelasubcharoen, S.; Chaichit, N.; Pakawatchai, C.; Albada, G. A. v.; Reedijk, J. *Polyhedron* **2007**, *26*, 725.
(61) Addison, A. W.; Rao, T. N.; Reedijk, J.; Van Rijn, J.; Verschoor, G. C. *J. Chem. Soc., Dalton Trans.* **1984**, 1349.
(62) Jasiewicz, B.; Warzajtis, B.; Rychlewska, U. *Polyhedron* **2011**, *30*, 1703.
(63) Mooibroek, T. J.; Gamez, P.; Reedijk, J. *CrystEngComm* **2008**, *10*, 1501.
(64) Lin, Z.; Han, D.; Li, S. *J. Therm. Anal. Calorim.* **2012**, *107*, 471.

(65) Kozlevcar, B.; Golobic, A.; Strauch, P. *Polyhedron* **2006**, *25*, 2824.
(66) Zabierowski, P.; Szklarzewicz, J.; Kurpiewska, K.; ski, K. L.; Nitek, W. *Polyhedron* **2013**, *49*, 74.
(67) Youngme, S.; Wannarit, N.; Pakawatchai, C.; Chaichit, N.; Somsook, E.; Turpeinen, U.; Mutikainen, I. *Polyhedron* **2007**, *26*, 1459.
(68) Phuengphai, P.; Youngme, S.; Pakawatchai, C.; Albada, G. A. v.; Quesada, M.; Reedijk, J. *Inorg. Chem. Commun.* **2006**, *9*, 147.
(69) Landee, C. P.; Turnbull, M. M. *Eur. J. Inorg. Chem* **2013**, *2013*, 2266.
(70) Keith, B. C.; Landee, C. P.; Valleau, T.; Turnbull, M. M.; Harrison, N. *Phys. Rev. B* **2011**, *84*, 104442.
(71) Jensen, P.; Batten, S. R.; Fallon, G. D.; Hockless, D. C. R.; Moubaraki, B.; Murray, K. S.; Robson, R. *J. Solid State Chem.* **1999**, *145*, 387.
(72) Lines, M. E. *J. Phys. Chem. Solids* **1970**, *31*, 101.
(73) Rushbrooke, G. S.; Wood, P. J. *Molec. Phys.* **1958**, *1*, 257.

PART II
STRUCTURAL DIVERSITY AND LUMINESCENT PROPERTIES OF CYANOACETATO ZINC/CADMIUM COORDINATION POLYMERS WITH *N,N'*-DITOPIC AUXILIARY LIGANDS

Introduction

The synthesis and design of coordination polymers (CPs) have attracted great attention owing to their interesting topologies and their potential applications in catalysis, gas storage, magnetism and non-linear optical properties and so on[1-10]. However, from a crystal engineering viewpoint, how to construct the predictable networks with desired properties still remains a great challenge owing to the large number of intermolecular forces which are affected by many variable factors such as reaction stoichiometry, temperature, solvent, counterions and so on[1,6,11]. It is well-known that the most common synthetic method for the construction of novel CPs is the mixed-ligands strategy[2,12-15]. The combination of different ligands can effectively contribute a variety of structural frameworks with fascinating properties[2,12-14,16-19]. One of the most powerful ligand used for such strategy is carboxylate anions that can bind toward metal centers in various ways, such as terminal monodentate, chelating to one metal center, bridging bidentate in a *syn–syn*, *syn–anti*, and *anti–anti* configurations and multiple bridges, resulting in the formation of various new structural types of metal carboxylates[20-25]. On the other hand, many rod-like *N,N′*-ditopic organic co-ligands have been widely used as additional building blocks for the construction of several multidimensional CPs[2,26-28]. Coordination polymers constructed from d^{10} transition metal ions, particularly, abundant zinc(II) and cadmium(II) ions, together with luminescent organic ligands containing conjugated π systems and aromatic rings have been a growing interest because of their potential applications in chemical sensors and electroluminescent display[2,4,9,29-33]. In addition, the coordination environment and the arrangement of organic linkers within CPs can strongly affect the luminescent properties.

Therefore, controlling molecular interactions is crucial to tuning the luminescent properties of CPs[9,16,17,29,32,34-39]. In this work, we choose a cyanoacetate anion (cna) and *N,N'*-ditopic spacers luminescent spacer incorporating zinc(II) and cadmium(II) ions to develop new luminescent coordination networks. The cyanoacetate ($NC_2H_2CO_2^-$) anion contains both nitrile (−C≡N) and carboxylic groups which not only well provides rich coordination sites but also effectively serves as intermolecular hydrogen-accepter sites, as well as fabricating the N···π interaction toward neighboring aromatic moieties[40-43]. These versatile connection sites allow cyanoacetate to be a good candidate for constructing 3D supramolecular structures. Meanwhile, the mixed-ligands strategy, including *N,N'*-ditopic organic coligands with different lengths and flexibility, has successfully demonstrated various novel CPs. In order to study the effect of different *N,N'*-ditopic spacers on the self-assembly process of CPs, we have herein taken cyanoacetate and different pyridine-based coligands in Zn(II)/Cd(II) system and yielded seven new coordination polymers, $[Zn(cna)_2(dpe)]_n$ **(II-1),** $[Zn(cna)_2(dpe)]_n$ **(II-2) ,** $[Cd(cna)_2(dpe)]_n$ **(II-3)** $[Zn(cna)_2(bpy)(H_2O)_2]_n$ **(II-4)**, $[Cd_3(cna)_6(bpy)_3]_n$ **(II-5)**, $[Zn(cna)_2(bpa)]_n$ **(II-6)** and $[Cd(cna)_2(bpa)]_n$ **(II-7)** (bpy = 4,4'-bipyridyl, 1,2-di(4-pyridyl)ethylene (dpe) and bpa = 1,2-di(4-pyridyl)ethane). The characterization has been done through X-ray crystallography, IR spectroscopy, and elemental analysis. The luminescent properties of **II-1-3** and **II-6-7** have also been studied in detail.

Experimental

Materials and physical measurements

All chemical were obtained from commercial sources and were used without further purification. Elemental analyses (C, H, N) were carried out with a Perkin-Elmer PE 2400CHNS analyzer. FT-IR spectra were obtained in KBr disks on a Perkin-Elmer Spectrum One FT-IR spectrophotometer in 4000-450 cm^{-1} spectral range. The X-ray powder diffraction (XRPD) data were collected on a Bruker D8 ADVANCE diffractometer using monochromatic Cu Kα radiation, and the recording speed was 0.5 s/step over the 2θ range of 5-40° at room temperature. Photoluminescent spectra of the sample powders were performed on a Shimadzu RF-5301PC spectrofluorometer in the wavelength range of 300-560 nm. The excitation and emission pass widths are 1.5 and 3.0 nm, respectively.

Synthesis

Preparation of $[Zn(cna)_2(dpe)]_n$ (II-1) and (II-2). The solution containing $Zn(O_2CCH_3)_2{\cdot}2H_2O$ (109 mg, 0.5 mmol) and cyanoacetic acid (85 mg, 1 mmol) in water and methanol (4 mL, 1:1 v/v) was mixed with 1,2-di(4-pyridyl)ethylene (90 mg, 0.5 mmol) in dimethylformamide (2 mL). This mixture solution was allowed to stand undisturbed at room temperature. After five days, deep yellow rhomboid-shaped crystals of **II-1** and small pale yellow crystals of **II-2** were obtained. These crystals were manually separated, washed with water and dried in air. Yield for **II-1**: 75 mg (36%) based on zinc salt. Anal. Calcd for $ZnC_{18}H_{14}N_4O_4$: C, 52.00; H, 3.39; N, 13.48%. Found: C, 51.79; H, 3.21; N, 13.30%. IR (KBr, cm^{-1}): 3060w, 2918w, 2261m (ν(C≡N)), 1664s, 1623s (ν_{as}(OCO)), 1512w, 1401m, 1371m (ν_s(OCO)), 1269m, 1077w, 1027m, 844m, 733w, 612w, 561m. Yield for **II-2**: 125 mg (60%) based on zinc salt. Anal. Calcd for $ZnC_{18}H_{14}N_4O_4$: C, 52.00; H, 3.39; N, 13.48%. Found: C, 51.23; H, 3.33; N, 13.23%. IR (KBr, cm^{-1}): 3066w, 2261m (ν(C≡N)), 1642s, 1612s (ν_{as}(OCO)), 1513m, 1423s, 1383s (ν_s(OCO)), 1263m, 1204m, 1074m, 1015m, 994m, 915m, 836m, 716w, 557s.

Preparation of $[Cd(cna)_2(dpe)]_n$ (II-3). The solution containing $Cd(NO_3)_2{\cdot}4H_2O$ (154 mg, 0.5 mmol) and cyanoacetic acid (85 mg, 1 mmol) in water (4mL) was mixed with 1,2-di(4-pyridyl)ethylene (90 mg, 0.5 mmol) in dimethylformamide (2 mL). This mixture solution was allowed to stand undisturbed at room temperature, yielding pale yellow crystals of **II-3** after four days. Yield: 145 mg (63%) based on cadmium salt. Anal. Calcd for $CdC_{18}H_{14}N_4O_4$: C, 46.72; H, 3.05; N, 12.11%. Found: C, 46.15; H, 2.92; N, 11.70%. IR (KBr, cm^{-1}): 2261m (ν(C≡N)), 1609s (ν_{as}(OCO)), 1502w, 1370s (ν_s(OCO)), 1270w, 1201w, 1081w, 1021m, 981m, 892w, 831m, 713w, 544(m).

Preparation of $[Zn(cna)_2(bpy)(H_2O)_2]_n$ (II-4). The solution containing $Zn(NO_3)_2{\cdot}6H_2O$ (148 mg, 0.5 mmol) and cyanoacetic acid (85 mg, 1 mmol) in water and dimethylformamide (4 mL, 1:1 v/v) was mixed with the methanolic solution (2 mL) of 4,4'-bipyridyl (78 mg, 0.5 mmol). This mixture solution was allowed to stand undisturbed at room temperature, yielding colorless block-shaped crystals of **II-4** after two weeks. Yield: 52 mg (24%) based on zinc salt. Anal. Calcd for $ZnC_{16}H_{16}N_4O_6$: C, 45.14; H, 3.79; N, 13.16%. Found: C, 45.73; H, 3.52; N, 12.98%. IR (KBr, cm^{-1}): 3413br (ν(OH)), 2258w (ν(C≡N)), 1612s (ν_{as}(OCO)), 1436w, 1367s (ν_s(OCO)), 1270w, 1220w, 1083w, 1015m, 907w, 829m, 720w, 551w, 488m.

Preparation of $[Cd_3(cna)_6(bpy)_3]_n$ (II-5). An ethanolic solution (4 mL) of cyanoacetic acid (85 mg, 1 mmol) and 4,4'-bipyridyl (78 mg, 0.5 mmol) was carefully layered on an aqueous solution (2 mL) of $Cd(NO_3)_2{\cdot}4H_2O$ (154 mg, 0.5 mmol). After three weeks, colorless needle-shaped crystals of **II-5** were obtained. Yield for **II-5**: 225 mg (34%) based on cadmium salt. Anal. Calcd for $Cd_3C_{48}H_{36}N_{12}O_{12}$: C, 44.01; H, 2.77; N, 12.83%. Found: C,

43.76; H, 2.51; N, 12.73%. IR (KBr, cm^{-1}): 2263w (ν(C≡N)), 1635s (ν_{as}(OCO)), 1396s (ν_s(OCO)), 1217w, 1078m, 1007m, 899w, 807m, 635m.

Preparation of $[Zn(cna)_2(bpa)]_n$ (II-6). The solution containing $Zn(O_2CCH_3)_2{\cdot}2H_2O$ (109 mg, 0.5 mmol) and cyanoacetic acid (85 mg, 1 mmol) in water and dimethylformamide (4 mL, 1:1 v/v) was mixed with 1,2-di(4-pyridyl)ethane (92 mg, 0.5 mmol) in methanol (2 mL). This mixture solution was allowed to stand undisturbed at room temperature, yielding colorless rod-shaped crystals of **II-6** after three days. Yield: 134 mg (64%) based on zinc salt. Anal. Calcd for $ZnC_{18}H_{16}N_4O_4$: C, 51.75; H, 3.86; N, 13.41%. Found: C, 51.43; H, 3.62; N, 13.21%. IR (KBr, cm^{-1}): 2258w (ν(C≡N)), 1610s (ν_{as}(OCO)), 1433w, 1368s (ν_s(OCO)), 1270w, 1221w, 1083m, 1023w, 986w, 835m, 550m.

Preparation of $[Cd(cna)_2(bpa)]_n$ (II-7). Compound **II-7** was synthesized similarly to **II-6** using $Cd(NO_3)_2{\cdot}4H_2O$ (154 mg, 0.5 mmol) instead of $Zn(O_2CCH_3)_2{\cdot}2H_2O$ (109 mg, 0.5 mmol)**.** After three days, colorless rod-shaped crystals of **II-7** were obtained. Yield: 106 mg (45%) based on cadmium salt. Anal. Calcd for $CdC_{18}H_{16}N_4O_4$: C, 46.52; H, 3.47; N, 12.06%. Found: C, 46.13; H, 3.31; N, 11.95%. IR (KBr, cm^{-1}): 2258w (ν(C≡N)), 1619s (ν_{as}(OCO)), 1419w, 1366s (ν_s(OCO)), 1273w, 1216w, 1072w, 1048w, 1010w, 942w, 809m, 724w, 638m.

X-ray crystallography

The reflection data of **II-1-7** were collected on a Bruker D8 Quest PHOTON 100 CMOS detector with graphite-monochromated Mo*K*α radiation using the APEX2 program. [44] Raw data frame integration was performed with SAINT[45], which also applied correction for Lorentz and polarization effects. An empirical absorption correction by using the SADABS program[46] was applied. The structure was solved by direct methods and refined by full-matrix least-squares method on F^2 with anisotropic thermal parameters for all non-hydrogen atoms using the SHELXTL software package.[47] All hydrogen atoms were placed in calculated positions and refined isotropically. The unbound and coordination oxygen atoms (O4 and O3) of one terminal cyanoacetate for **II-6** are disordered. The occupancies of two conformations were refined to 0.4 and 0.6.

Results and Discussion

Description of the structures

$[Zn(cna)_2(dpe)]_n$ (II-1). Single-crystal structure analysis reveals that all compounds crystallize in the triclinic system, $P\bar{1}$ space group (Table 1). The asymmetric unit of $[Zn(cna)_2(dpe)]_n$ (**II-1**) is shown in Figure 1a. Each Zn(II) ion is coordinated by two oxygen atoms from two different monodentate cyanoacetate anions and two nitrogen atoms from two 1,2-di(4-pyridyl)ethylene molecules, showing a distorted tetrahedral ZnN_2O_2 choromophore. The ZnN_2O_2 moiety shows coordination distances and angles in ranges of 1.937(1)-2.038(1) Å and 109.03(6)-119.76(5)°, respectively (Table 2). The adjacent zinc ions are bridged *via* μ_2-dpe spacers along *a* axis generating 1D zigzag chain of **II-1** with the Zn···Zn separations of 13.233(6) and 13.452(5) Å (Figure 1b).

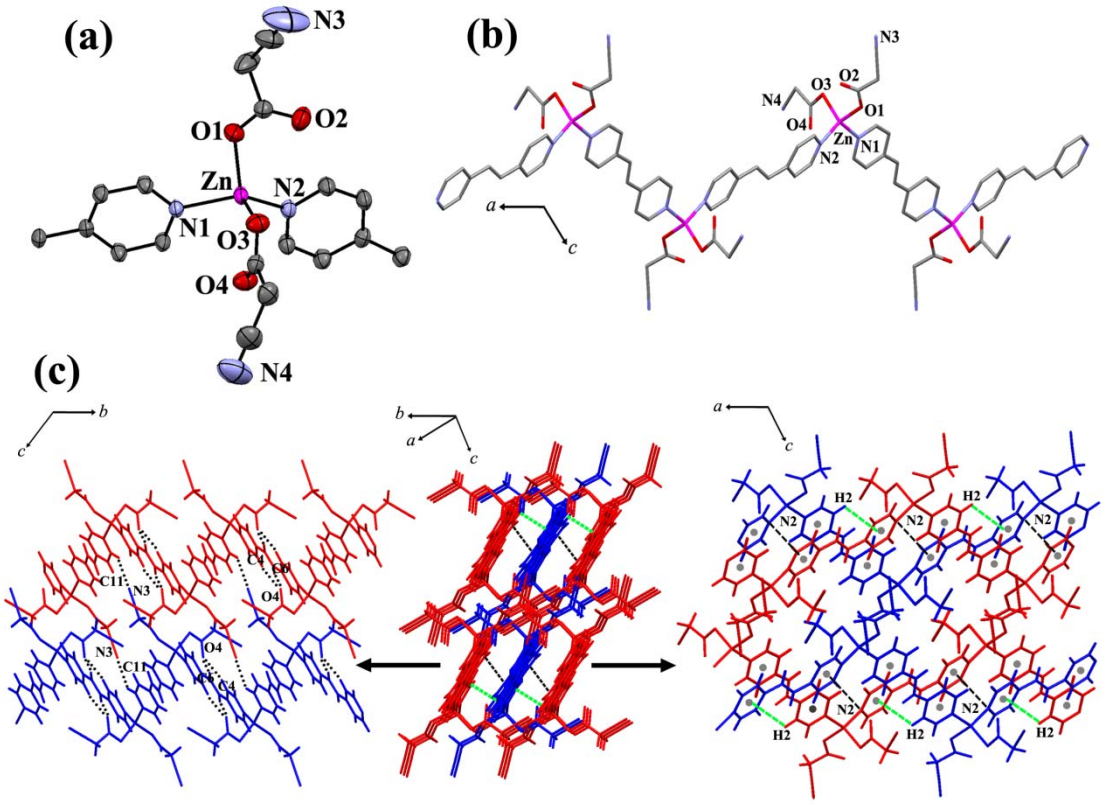

Figure 1 (a) Asymmetric unit and atom labeling scheme of **II-1**. The ellipsoids are shown at 50% probability level. All hydrogen atoms are omitted for clarity. (b) 1D zigzag chain along *a* axis. (c) 3D packing diagram of **II-1** showing the assemblage of six polymeric chains *via* C–H···π (green broken lines) and N···π interactions (black broken lines). 2D sheet structure of **II-1** built from weak hydrogen bonding (black dotted lines) extending parallel to the *bc* plane (left). Another view in *ac* plane, 2D sheet structure formed by C–H···π (green broken lines) and $N_{pyridyl}$···π (black broken lines) interactions (right).

The two pyridine rings of bipyridyl moieties are not coplanar with the dihedral angle between the two planar pyridine rings of 13.59°. The conformation of μ_2-dpe molecule is *anti* with C–CH=CH–C torsion angle of 125.59°. In the packing motif, each zigzag polymeric chain of **II-1** is assembled by the intermolecular weak H-bonding interactions (Figure 1c) relating terminal nitrile–N from cyanoacetate and pyridyl–H from μ_2-dpe spacer (C11H···N3), unbound oxygen atoms from cyanoacetate acting as H-acceptor and pyridyl–H (C4H···O4), as well as ethylene–H from μ_2-dpe acting as H-donors (C6H···O4) (Table 3). In addition, the interchain C2–H···π interaction is observed between the neighboring μ_2-dpe moieties in *ac* plane with the separation of 3.435 Å. Moreover, the pyridyl–N atom from μ_2-dpe can also interact with the adjacent dpe rings with $N_{pyridyl}$···centroid(dpe) distance of 3.595 Å (Figure 1c). All interactions complete the overall 3D supramolecular motif of **II-1** with the closest interchain Zn···Zn separation of 5.509(5) Å.

Table 1 Crystallographic data for compounds **II-1-3**

	II-1	**II-2**	**II-3**
Formula	$C_{18}H_{14}N_4O_4Zn$	$C_{18}H_{14}N_4O_4Zn$	$C_{18}H_{14}N_4O_4Cd$
Molecular weight	415.72	415.72	462.74
T (K)	293(2)	293(2)	293(2)
Crystal system	triclinic	triclinic	triclinic
Space group	$P\bar{1}$	$P\bar{1}$	$P\bar{1}$
a (Å)	9.1501(4)	7.7072(3)	8.0430(3)
b (Å)	10.7211(5)	10.5091(4)	10.7219(4)
c (Å)	11.3426(5)	11.7022(5)	11.5496(4)
α (deg)	106.610(1)	70.292(1)	70.838(1)
β (deg)	107.798(1)	86.023(1)	82.340(1)
γ (deg)	109.208(1)	72.587(1)	69.025(1)
V (Å^3)	903.36(7)	850.89(6)	878.33(6)
Z	2	2	2
ρ_{calcd} (g cm^{-3})	1.528	1.623	1.750
μ (Mo Kα) (mm^{-1})	1.391	1.477	1.276
Data collected	3697	3249	4727
Unique data (Rint)	3463(0.0150)	2771(0.0261)	4339(0.0169)
$R_1{}^a/wR_2{}^b$ [$I > 2\sigma(I)$]	0.0253/0.0667	0.0424/0.1029	0.0248/0.0578
$R_1{}^a/wR_2{}^b$ [all data]	0.0276/0.0680	0.0545/0.1081	0.0288/0.0594
GOF	1.060	1.059	1.094
Max/min electron density (e Å^{-3})	0.320/-0.253	1.195/-0.504	0.562/-0.323

$^a R = \sum||F_o|-|F_c||/\sum|F_o|$. $^b R_w = \{ \sum[w(|F_o|-|F_c|)]^2/\sum[w|F_o|^2] \}^{1/2}$

$[Zn(cna)_2(dpe)]_n$ (II-2) and $[Cd(cna)_2(dpe)]_n$ (II-3). Compounds **II-2** and **II-3** are isostructural exhibiting 1D ladder-like structures. For **II-2**, each Zn(II) ion is five-coordination showing a distorted trigonal bipyamidal ZnN_2O_3 chromophore with a τ = 0.71 (Addison's parameter[48] τ = 0 for square pyramid and τ = 1 for trigonal bipyramid) (Figure 2a). The equatorial trigonal plane around the zinc atom is composed of three oxygen atoms from three different cyanoacetates, indicated by the angles of O1–Zn1–O3, O1–Zn1–O4 and O4–Zn1–O3 being 134.17(12)°, 97.28(13)° and 128.53(13)°, respectively. The axial position is occupied by two nitrogen atoms from two different μ_2-dpe spacers with N1–Zn–N2 angle of 176.63(10)°. The average Zn–O and Zn–N distances are 2.048(3) and 2.163(3) Å, respectively (Table 2). For compound **II-3**, each Cd(II) ion shows six-coordination formed by four carboxylate oxygen atoms from three different cyanoacetates and two nitrogen atoms from two μ_2-dpe molecules, generating a distorted octahedral CdN_2O_4 chromophore (Figure 2b). The coordination distances around Cd(II) center are in the range of 2.294(2)-2.484(2) Å (Table 2).

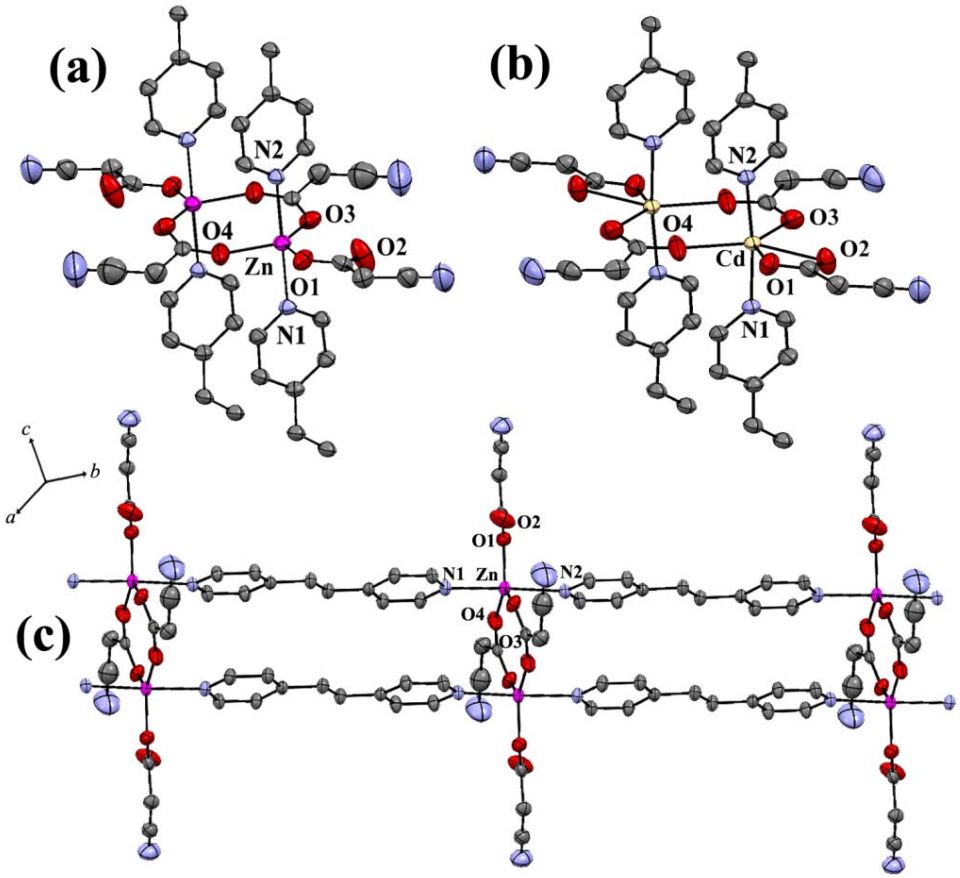

Figure 2 Part of 1D ladder chain structures of **II-2**(a) and **II-3**(b) with used atom labeling. The ellipsoids are shown at 50% probability level. All hydrogen atoms are omitted for clarity. (c) 1D ladder-like structure of **II-2**

Table 2 Selected bond lengths /Å and angles /° for **II-1-3**

II-1			
Zn–O1	1.9373(13)	Zn–O3	1.9899(13)
Zn–N2	2.0268(13)	Zn–N1	2.0381(13)
O1–Zn–O3	109.03(6)	O1–Zn–N2	111.99(6)
O3–Zn–N2	108.39(6)	O1–Zn–N1	97.13(6)
O3–Zn–N1	109.85(6)	N2–Zn–N1	119.76(5)
II-2			
Zn–O1	2.035(3)	Zn–O4	2.048(3)
Zn–O3	2.061(3)	Zn–N1	2.146(3)
Zn–N2	2.180(3)	O1–Zn–O4	97.28(13)
O1–Zn–O3	134.17(12)	O4–Zn–O3	128.53(13)
O1–Zn–N1	93.83(10)	O4–Zn–N1	88.77(11)
O3–Zn–N1	89.09(10)	O1–Zn–N2	89.45(10)
O4–Zn–N2	91.58(11)	O3–Zn–N2	88.07(10)
N1–Zn–N2	176.63(10)		
II-3			
Cd–N2	2.2938(15)	Cd–O3	2.3043(17)
Cd–O4	2.3059(15)	Cd–N1	2.3105(15)
Cd–O2	2.3595(16)	Cd–O1	2.4836(16)
N2–Cd–O3	87.00(6)	N2–Cd–O4	89.66(6)
O3–Cd–O4	127.54(8)	N2–Cd–N1	173.11(5)
O3–Cd–N1	87.76(6)	O4–Cd–N1	89.98(6)
N2–Cd–O2	96.81(6)	O3–Cd–O2	96.88(8)
O4–Cd–O2	135.45(6)	N1–Cd–O2	88.26(6)
N2–Cd–O1	86.75(6)	O3–Cd–O1	148.79(8)
O4–Cd–O1	82.97(6)	N1–Cd–O1	100.04(6)
O2–Cd–O1	53.68(5)		

The carboxylate bridges for μ_2-cna of **II-2** and **II-3** exhibit a double-*syn,anti*-η^1:η^3:μ_2 coordinative mode connecting between metal ions, giving rise to the dinuclear units with M···M separations of 3.397(5) and 4.013(2) Å for **II-2** and **II-3**, respectively. Additional cyanoacetate acts as terminal monodentate ligand for **II-2** and terminal chelating ligand for **II-3**. Moreover, the carboxyl-bridged dinuclear units are extended along the particular direction by paired μ_2-dpe spacers to create the infinite 1D ladder-like structures, as shown in Figure 2c. The M···M separations across μ_2-dpe are 13.706(6) Å for **II-2** and 13.956(4) Å for **II-3**. The two pyridine rings of bipyridyl moieties are not coplanar with the dihedral angles between the two planar pyridine ring of 4.39° and 5.26° for **II-2** and **II-3**, respectively. The conformations of dpe molecules is *anti* with C–CH=CH–C torsion angles of 179.81° for **II-2** and 178.45° for **II-3**. The 3D packing structures of **II-2** and **II-3** are stabilized by various weak interchain H-bonding interactions (Figure 3) involving terminal nitrile–N and oxygen atoms from cyanoacetates as H-acceptors and pyridyl, ethylene–H atoms from μ_2-dpe and alkyl–H atom from cyanoacetate as H-donors (Table 3). Furthermore, the nitrile–N from the terminal cyanoacetate can interact with the adjacent electron-deficient μ_2-dpe rings with N3···π distances of 3.382 and 3.388 Å for **II-2** and **II-3**, respectively, stabilizing the overall packing structures of **II-2** and **II-3**. The closest interchain M···M separations are 6.201(7) and 6.602(5) Å for **II-2** and **II-3**, respectively.

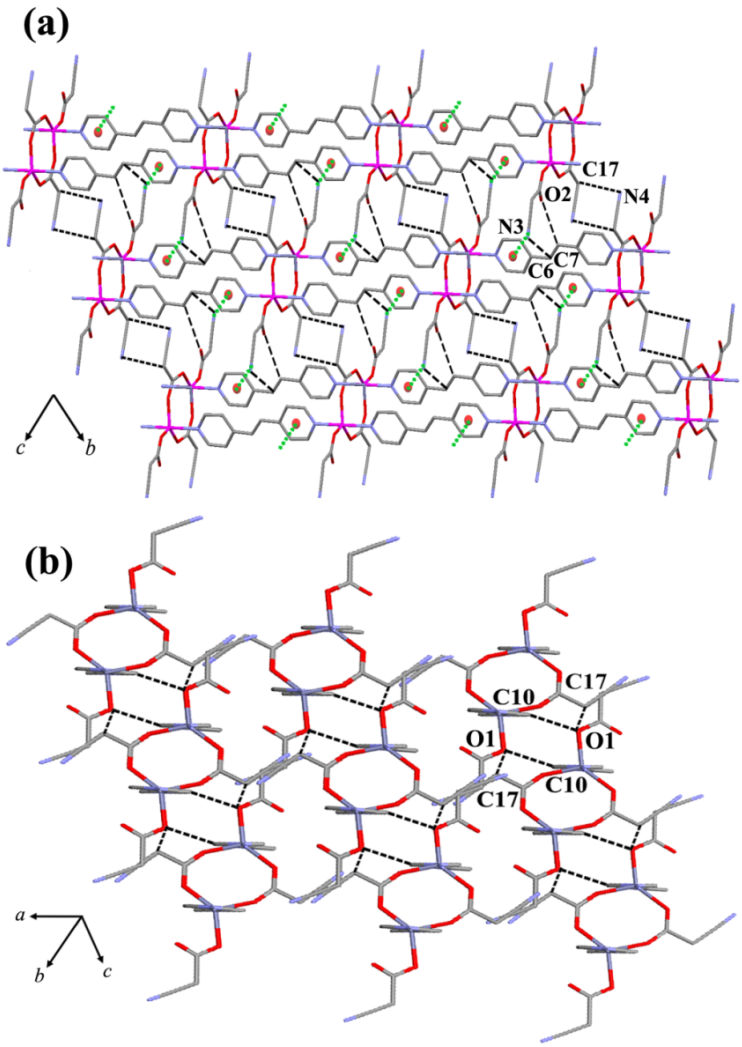

Figure 3 (a) The packing diagram of ladder chains of **II-2** in *bc* plane showing weak hydrogen bonding (black broken lines) and $N_{nitrile}\cdots\pi$ interaction (green dotted lines). (b) Another view of 3D packing diagram showing weak hydrogen bonding through carboxylate oxygen from cyanoacetates**.**

$[Zn(cna)_2(bpy)(H_2O)_2]_n$ (II-4). Compound **II-4** crystallizes in the orthorhombic with *Pccn* space group, exhibiting a 1D chain structure, as shown in Figure 4a. The structure of **II-4** is isomorphous with previously reported complexes, $[M(cna)_2(bpy)(H_2O)_2]_n$ (M = Cu(II)[120], Mn(II)[27]). Each Zn(II) ion is coordinated by two nitrogen atoms from two μ_2-bpy spacers, two oxygen atoms from two terminal cyanoacetates and two oxygen atoms from two coordination water molecules, adopting a distorted octahedral geometry.

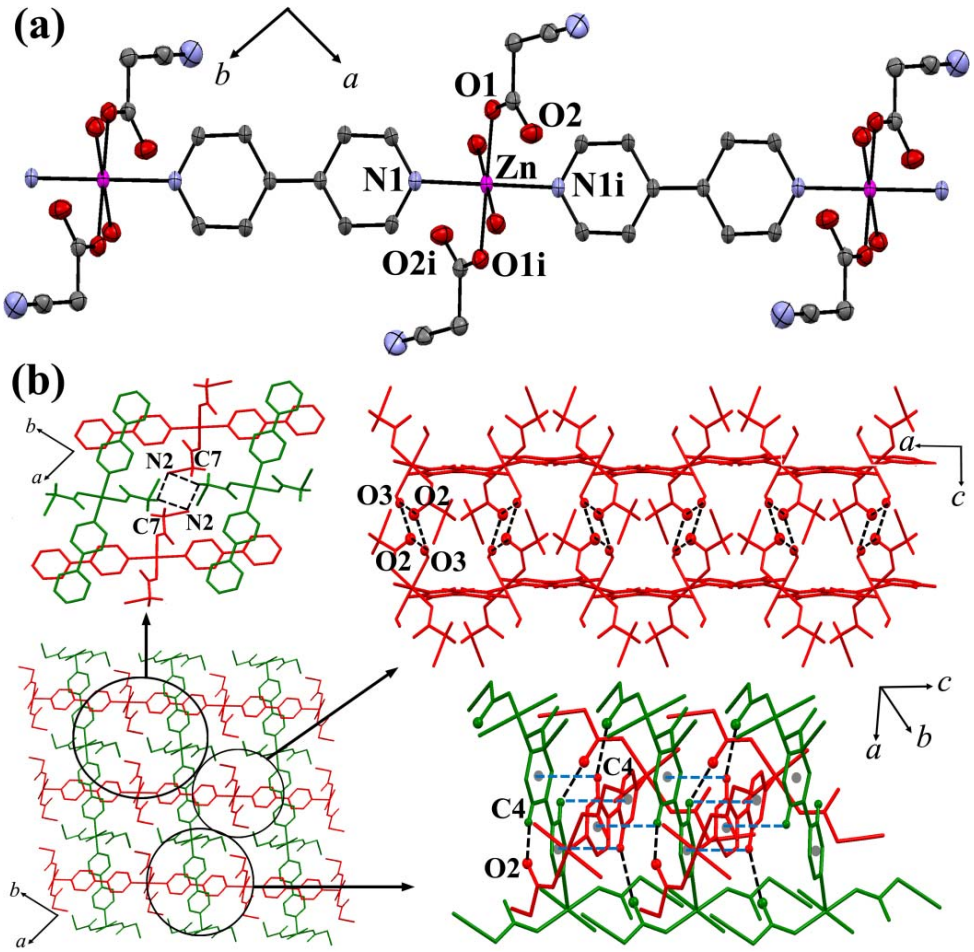

Figure 4 (a) 1D linear chain structure of **II-4** with used atom labeling. The ellipsoids are shown at 35% probability level. The hydrogen atoms are omitted for clarity (i) = -*x*, 1-*y*, 1-*z*. (b) The packing diagram of **II-4** formed by the interchain hydrogen bonding (black broken lines) and C–H···π interactions (blue broken lines)

The ZnN_2O_4 moiety shows coordination distances in the ranges of 2.118(9)-2.172(6) Å. The adjacent zinc(II) ions are bridged *via* μ_2-bpy spacers generating 1D linear chain of **1** with the Zn···Zn separation of 11.314(3) Å. The two pyridine rings of bipyridyl moieties are not coplanar with the dihedral angles between the two planar pyridine rings of 15.78°. Each 1D chain of **1** is assembled by various interchain hydrogen bonding among terminal cyanoacetates ($C7H\cdots N2_{nitrile}$) (Figure 4b, Table 4), between unbound O atom from cyanoacetate and H atom from coordination water molecule (O3H···O2), as well as, the pyridyl H atom from μ_2-bpy and O atom from coordination water molecule (C4H···O2). Moreover, the C4–H···π interaction is observed among the adjacent μ_2-bpy moieties along the *c* axis with the separation of 3.394 Å (Figure 4b). These weak interactions complete the 3D supramolecular motif of **1** with the closest interchain Zn···Zn separation of 7.208(2) Å.

$[Cd_3(cna)_6(bpy)_3]_n$ (II-5). Compound **II-5** crystallizes in the monoclinic *C*2/c space group, exhibiting a 1D triple-stranded chain structure, as shown in Figure 5a. The 1D triple-stranded chain of **II-5** contains three Cd(II) centers with two different geometries, i.e., two distorted pentagonal bipyramidal $Cd1N_2O_5$ and one distorted octahedral $Cd2N_2O_4$ chromophores. In the $Cd1N_2O_5$ moiety, each Cd1 center is surrounded by five carboxylate O

atoms from three different cyanoacetate ligands (Cd1–O = 2.275(7) –2.475(6) Å) and two N atoms from two μ_2-bpy ligands (Cd1–N = 2.311(6) and 2.334(7) Å), while, each Cd2 center is six-coordination, surrounded by four carboxylate O atoms from four different μ_2-cyanoacetates (Cd2–O = 2.328(6)–2.393(6) Å) and two N atoms from two μ_2-bpy molecules (Cd2–N = 2.284(9) and 2.302(9) Å). The Cd–O and Cd–N bond distances are in normal ranges for Cd(II) complexes[121-122]. The Cd2 is bridged to two symmetry-related Cd1 ions *via* double-*syn,anti*-η^1:η^3:μ_2-cyanoacetates and double-chelating bridging bidentate modes of cyanoacetates, generating a linear trinuclear (Cd1, Cd2, Cd1a) unit with the Cd···Cd separation of 4.184(2) Å. Moreover, each trinuclear unit is linked by μ_2-bpy spacers, giving rise to a 1D triple-stranded chains of **II-5** with the Cd···Cd separation across μ_2-bpy of 11.687(2) Å. The two pyridine rings of bpy moieties are not coplanar with the dihedral angle between the two planar pyridine rings of 12.66° (Cd1) and 21.13° (Cd2). For the packing motif (Figure 5b), each chain of **II-5** is assembled by the intermolecular weak hydrogen bonding among nitrile–N atoms from terminal cyanoacetates, coordination oxygen atoms from cyanoacetates, and pyridyl–H atoms from μ_2-bpy (C20H···N5, C16H···O1, and C11H···O1) (Figure 5b, Table 4). All interactions complete the overall 3D packing structure motif of **II-5** with the closest interchain Cd···Cd separation of 6.672(2) Å.

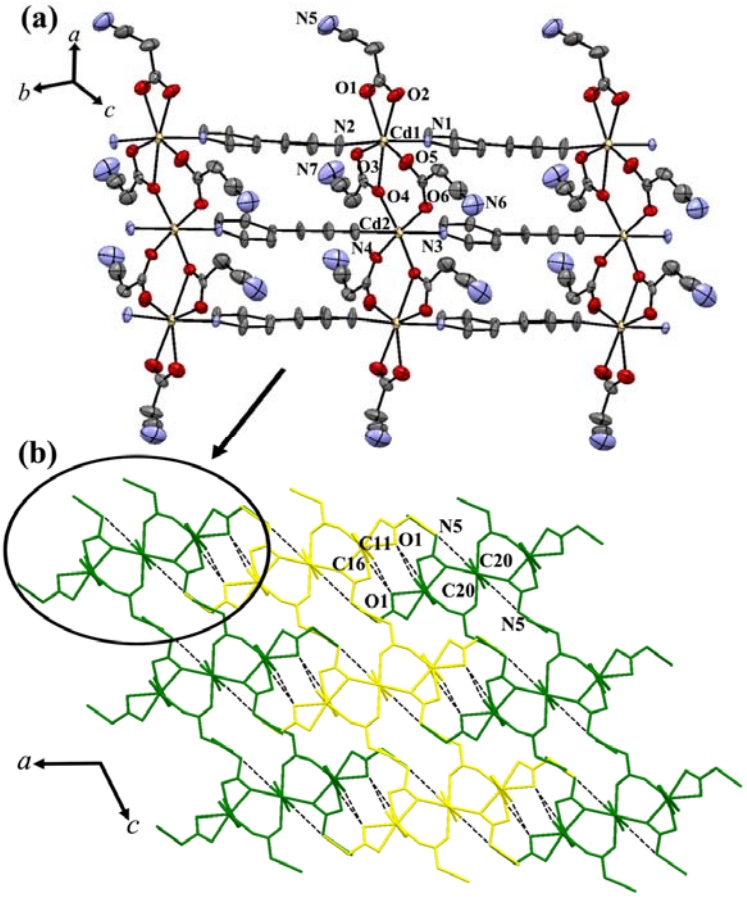

Figure 5 1D triple-stranded chain structure of **II-5** with used atom labeling. The ellipsoids are shown at 35% probability level. All hydrogen atoms are omitted for clarity. (b) The packing diagram of triple-stranded chains in **II-5** formed by various weak hydrogen bonding in *ac* plane

[Zn(cna)$_2$(bpa)]$_n$ (II-6). Compound **II-6** crystallizes in the triclinic $P\bar{1}$ space group, exhibiting a 1D zigzag chain structure, as shown in Figure 6a. Each Zn(II) ion is coordinated by two oxygen atoms from two different monodentate cyanoacetates and two nitrogen atoms from two bpa spacers, adopting a distorted tetrahedral ZnN_2O_2 chromophore. The coordination distances and angles are in ranges of 1.869(4)-2.094(6) Å and 92.08(16)-126.03(12)°, respectively. The adjacent zinc(II) ions are bridged by μ_2-bpa spacers generating 1D zigzag chains of **II-6** with the Zn···Zn separation of 13.253(6) and 13.239(5) Å. The conformation of μ_2-bpa molecule is *anti* with the C–CH_2–CH_2 angle of 112.17°. The two pyridine rings of bipyridyl moieties are perfectly coplanars. For the packing motif, each 1D zigzag chain of **II-6** is assembled by various intermolecular weak hydrogen bonding among terminal nitrile–N atoms and unbound oxygen atoms from cyanoacetates acting as H-acceptor and pyridyl–H, ethyl–H atoms from μ_2-bpa acting as H-donors (C5H···N3, C4H···O2, and C6H···O2) (Figure 6b, Table 4). In addition, the nitrile N atoms from the terminal cyanoacetates can interact with the adjacent electron deficient μ_2-bpa ring with $N3_{nitrile}$·· π distance of 3.482 Å (Figure 6b). Moreover, the C7–H···π interaction is observed between the interchain μ_2-bpa moieties with the separation of 3.551 Å, and the pyridyl–N atom from μ_2-bpa also interacts with the adjacent bpa rings with $N_{pyridyl}$···π distance of 3.767 Å (Figure 6c). All interaction completes the overall 3D supramolecular motif of **II-6** with the closest interchain Zn···Zn separation of 6.324(5) Å.

[Cd(cna)$_2$(bpa)]$_n$ (II-7). Compound **II-7** crystallizes in the triclinic $P\bar{1}$ space group, exhibiting a 1D ladder-like chain structure, as shown in Figure 7. Each Cd(II) ion is six-coordinated, surrounded by four carboxylate oxygen atoms from three different cyanoacetates and two nitrogen atoms from two μ_2-bpa molecules, generating a distorted octahedral CdN_2O_4 chromophore. The CdN_2O_4 moiety shows coordination distances and angles in ranges of 2.294(2)-2.420(2) Å and 83.97(8)-149.17(10)°, respectively.

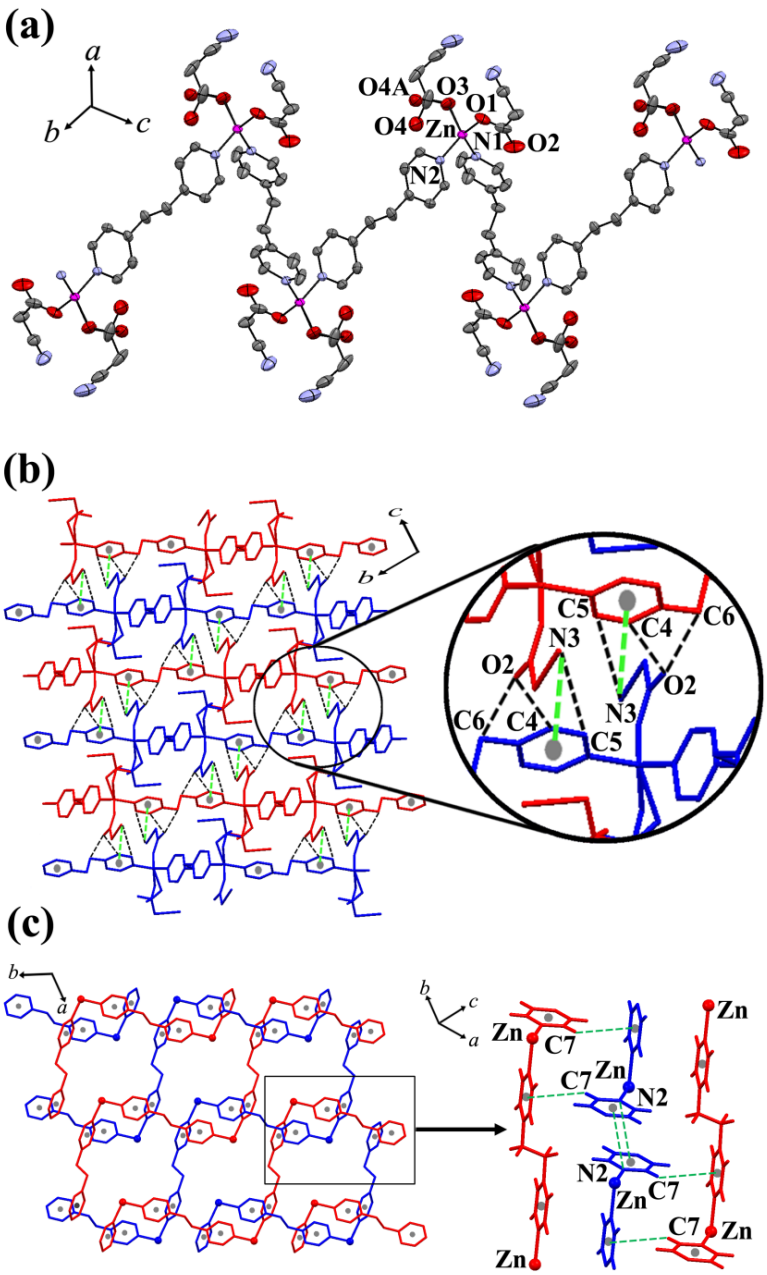

Figure 6 (a) 1D zigzag chain structure of **II-6** with used atom labeling. The ellipsoids are shown at 50% probability level. All hydrogen atoms are omitted for clarity. (b) 2D sheet structure of **II-6** built from weak hydrogen bonding (black broken lines) and $N_{nitrile}\cdots\pi$ interaction (green broken lines) in *bc* plane. (c) Another view in *ab* plane showing 2D sheet structure formed by C–H$\cdots\pi$ and $N_{pyridyl}\cdots\pi$ interactions. The cyanoacetates are omitted for clarity

The carboxylate bridges from two cyanoacetates exhibit a double-*syn,anti*-η^1:η^3:μ_2 coordinative modes connecting between Cd(II) centers, adopting a dinuclear Cd(II) unit with Cd···Cd separation of 3.961(6) Å. An additional cyanoacetate acts as terminal chelating ligand. Moreover, the carboxyl-bridged dinuclear units are assembled by paired μ_2-bpa spacers to create the infinite 1D ladder-like structures (Figure 7a). The Cd···Cd separation across μ_2-bpa is 6.877(5) Å. The two pyridine rings of bipyridyl moieties are not coplanar with the dihedral angles between the two planar pyridine rings of 9.88°. The conformation of

bpa molecules is *anti* with C–CH_2–CH_2 angles of 115.98° and 117.22°, and C–CH_2–CH_2–C torsion angle of 171.69°. For the packing diagram (Figure 7b, Table 4), each 1D ladder chain of **II-7** is assembled by the intermolecular weak hydrogen bonding between terminal nitrile–N from cyanoacetate and ethyl–H from μ_2-bpa (C6H···N4), coordination oxygen atoms and alkyl–H from cyanoacetates (C14H···O3) and ethyl–H from μ_2-bpa (C11H···O3). In addition, the nitrile–N atoms from the terminal cyanoacetates effectively interact with the adjacent μ_2-bpa moieties with N···π distance of 3.412 Å, as shown in Figure 7b.

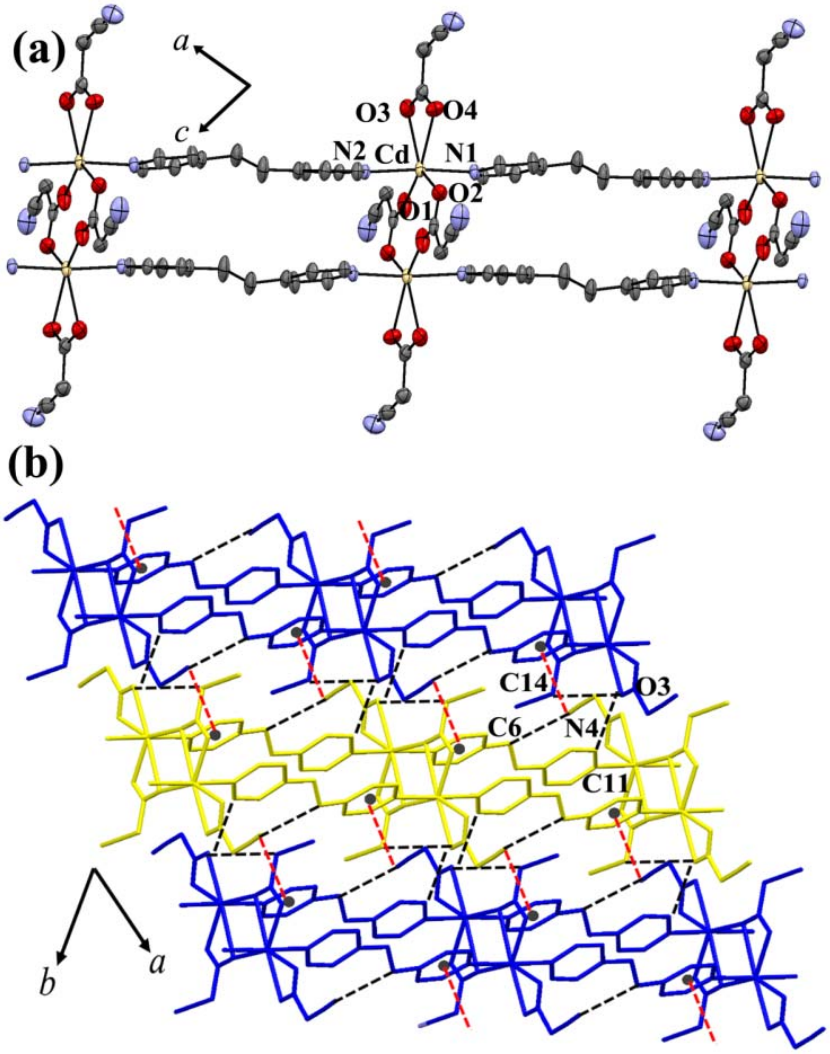

Figure 7 (a) 1D ladder chain structure of **II-7** with used atom labeling. The ellipsoids are shown at 50% probability level. All hydrogen atoms are omitted for clarity. (b) The packing diagram of **II-7** formed by weak interchain hydrogen bonding (black broken lines) and $N_{nitrile}$···π interaction (red broken lines) in *ab* plane

Table 3 Crystallographic data for compounds **II-4-7**

compound	**II-4**	**II-5**	**II-6**	**IV-7**
Formula	$ZnC_{16}H_{16}N_4O_6$	$Cd_3C_{48}H_{36}N_{12}O_{12}$	$ZnC_{18}H_{16}N_4O_4$	$CdC_{18}H_{14}N_4O_4$
Molecular weight	425.72	1310.09	417.72	464.75
T (K)	293(2)	293(2)	293(2)	293(2)
Crystal system	orthorhombic	monoclinic	triclinic	triclinic
Space group	*Pccn*	*C*2/c	$P\bar{1}$	$P\bar{1}$
a (Å)	12.9041(5)	24.9894(19)	9.5264(3)	8.3470(3)
b (Å)	18.5888(7)	11.6868(9)	9.7703(4)	10.7131(5)
c (Å)	7.2082(2)	20.7170(15)	10.9211(4)	11.5269(4)
α (deg)	90.00	90.00	112.2500(10)	70.459(2)
β (deg)	90.00	123.260(2)	96.906(10)	81.386(10)
γ (deg)	90.00	90.00	98.6510(10)	67.1380(10)
V (Å^3)	1729.04(11)	5059.16(7)	912.49(6)	894.85(6)
Z	4	4	2	2
ρ_{calcd} (g cm^{-3})	1.635	1.720	1.520	1.725
μ (Mo Kα) (mm^{-1})	1.464	1.324	1.378	1.253
Data collected	4890	5195	4473	4230
Unique data (*R*int)	3136(0.0307)	5195(0.1666)	3821(0.0173)	3519(0.0340)
$R_1{}^a/wR_2{}^b$ [$I > 2\sigma(I)$]	0.0404/0.0925	0.0711/0.1096	0.0420/0.1086	0.0338/0.0657
$R_1{}^a/wR_2{}^b$ [all data]	0.0776/0.1060	0.1890/0.1394	0.0527/0.1159	0.0497/0.0715
GOF	1.067	1.007	1.036	1.099
Max/min electron density (e Å^{-3})	0.395/-0.738	1.164/-0.841	0.946/-0.467	0.693/-0.726

$^aR = \sum||F_o|-|F_c||/\sum|F_o|$. $^bR_w = \{ \sum[w(|F_o|-|F_c|)]^2/\sum[w|F_o|^2] \}^{1/2}$

Table 4 Selected bond lengths (Å) and angles (°) for compounds **II-4-7**

Compound **II-4**			
Zn1–O1	2.118(9)	Zn1–O1^i	2.118(9)
Zn1–N1	2.130(9)	Zn1–N1^i	2.130(9)
Zn1–O3	2.172(10)	Zn1–O3^i	2.172(10)
O1–Zn1–O1^i	180.00	O1–Zn1–N1^i	90.23(4)
O1^i –Zn1–N1^i	89.77(4)	O1 –Zn1–N1	89.77(4)
O1^i –Zn1–N1	90.23(4)	N1^i –Zn1–N1	180.00
O1–Zn1–O3^i	90.87(4)	O1^i –Zn1–O3^i	89.13(4)
N1^i –Zn1– O3^i	88.01(4)	N1–Zn1– O3^i	91.99(4)
O1–Zn1–O3	89.13(4)	O1^i –Zn1–O3	90.87(4)
N1^i –Zn1– O3	91.99(4)	N1 –Zn1– O3	88.01(4)
O3^i –Zn1– O3	180.00		
Compound **II-5**			
Cd1–O1	2.451(6)	Cd1–O2	2.404(6)
Cd1–O3	2.364(6)	Cd1–O4	2.475(6)
Cd1–O5	2.275(7)	Cd1–N1	2.311(6)
Cd1^{ii}–N2	2.334(7)	Cd1–N2^{iii}	2.334(7)
Cd2^{ii}–N4	2.284(9)	Cd2–N4^{iii}	2.284(9)
Cd2–O6^i	2.328(6)	Cd2–O4^i	2.393(6)
O5—Cd1—N1	92.8(2)	O1—Cd1—O4	136.4(2)
O5—Cd1—N2^{iii}	85.7(2)	O5—Cd1—C4	114.9(3)
N1—Cd1—N2^{iii}	175.3(2)	N1—Cd1—C4	84.3(2)

O5—Cd1—O3	140.9(2)	$N2^{iii}$—Cd1—C4	92.3(2)
N1—Cd1—O3	88.1(2)	O3—Cd1—C4	26.3(2)
$N2^{iii}$—Cd1—O3	90.2(2)	O2—Cd1—C4	160.7(3)
O5—Cd1—O2	84.3(2)	O1—Cd1—C4	108.7(3)
N1—Cd1—O2	93.1(2)	O4—Cd1—C4	27.7(2)
$N2^{iii}$—Cd1—O2	91.2(3)	O5—Cd1—C1	109.9(3)
O3—Cd1—O2	134.7(2)	N1—Cd1—C1	97.0(3)
O5—Cd1—O1	136.1(2)	$N2^{iii}$—Cd1—C1	87.6(3)
N1—Cd1—O1	96.2(2)	O3—Cd1—C1	108.7(3)
$N2^{iii}$—Cd1—O1	87.9(2)	O2—Cd1—C1	26.3(2)
O3—Cd1—O1	82.4(2)	O1—Cd1—C1	26.3(2)
O2—Cd1—O1	52.4(2)	O4—Cd1—C1	162.7(3)
O5—Cd1—O4	87.4(2)	C4—Cd1—C1	135.0(3)
N1—Cd1—O4	82.6(2)	$N4^{iii}$—Cd2—N3	180.000
$N2^{iii}$—Cd1—O4	92.9(2)	$N4^{iii}$—Cd2—O6	92.77(14)
O3—Cd1—O4	54.0(2)	N3—Cd2—O6	87.23(14)
O2—Cd1—O4	170.4(2)	$N4^{iii}$—Cd2—$O6^{i}$	92.77(14)
N3—Cd2—$O6^{i}$	87.23(14)	$O6^{i}$—Cd2—O4	79.6(2)
O6—Cd2—$O6^{i}$	174.5(3)	$N4^{iii}$—Cd2—$O4^{i}$	87.03(13)
$N4^{iii}$—Cd2—O4	87.03(13)	N3—Cd2—$O4^{i}$	92.97(13)
N3—Cd2—O4	92.97(13)	O6—Cd2—$O4^{i}$	79.6(2)
O6—Cd2—O4	100.7(2)		

Compound **II-6**

Zn1–O3A	1.869(4)	Zn1–O3	2.094(6)
Zn1–O1	1.956(2)	Zn1–N2	2.039(2)
Zn1–N1	2.041(2)	O3A–Zn1–O1	92.08(16)
O3A–Zn1–N2	117.60(18)	O1–Zn1–N2	126.03(12)
O3A–Zn1–N1	115.63(18)	O1–Zn1–N1	103.05(10)
N2–Zn1–N1	102.44(8)	O1–Zn1–O3	108.10(2)
N2–Zn1–O3	94.49(19)	N1–Zn1–O3	124.90(2)

Compound **II-7**

Cd1–N1	2.294(2)	Cd1–N2	2.298(2)
Cd1–O1	2.331(2)	Cd1–$O2^{i}$	2.366(2)
Cd1–O2	2.366(2)	Cd1–O4	2.415(2)
Cd1–O3	2.420(2)	N1–Cd1–N2	174.36(8)
N1–Cd1–O1	87.15(8)	N2–Cd1–O1	87.80(8)
N1–Cd1–$O2^{i}$	89.38(8)	N2–Cd1–$O2^{i}$	91.57(8)
O1–Cd1–$O2^{i}$	126.21(10)	N1–Cd1–O4	87.06(8)
N2–Cd1–O4	98.56(8)	O1–Cd1–O4	149.17(10)
$O2^{i}$ –Cd1–O4	83.97(8)	N1–Cd1–O3	95.75(8)
N2–Cd1–O3	87.36(8)	O1–Cd1–O3	96.92(10)
$O2^{i}$ –Cd1–O3	136.80(8)	O4–Cd1–O3	53.67(8)

Symmetry codes for **II-4**: (i) -*x*, 1-*y*, 1-*z*. For **II-5**: (i) 1–*x*, *y*, 1/2-*z*; (ii) *x*, 1+*y*, *z*; (iii) *x*, -1+*y*, *z*. For **II-7**: (i) -*x*, 2-*y*, 1-*z*.

Photoluminescent properties

Photoluminescence studies of d^{10} metal–organic CPs with luminescent organic ligands containing aromatic rings have been a subject of immense current research interest because their emissions can be adjusted involving the coordination environment, the rigidity and the arrangement of organic linkers within CPs. Recently, the luminescent properties of d^{10} complexes containing di(pyridyl) ligands have been reported. The solid-state photoluminescent properties of **II-1-3** and **II-6-7** were investigated at ambient temperature. To compare the luminescent intensities, all emission spectra were determined with the same excitation wavelength (λ_{ex}= 285 nm) and the same spectral pass widths. As depicted in Figure 8, compound **II-1** shows the intense emission band with maximum at 362 nm and shoulder bands near 380 and 450 nm, upon excitation at 285 nm. In contrast, the isostructures **II-2** and **II-3** show much weaker emission intensity with broad band with maxima around 470 nm. To understand the nature of emission bands, the luminescent spectrum of the free dpe ligand was also examined. The emission peaks of free dpe display the maximum in the 340-420 nm region and a broadband around 530 nm (λ_{ex} = 285 nm)[39,49], which may be assigned to intraligand π–π* and n–π* transitions[16,17,37,39]. Typically, in the compounds containing Zn(II)/Cd(II) ion with d^{10} configuration, there is no emission originates from the metal-to-ligand (MLCT) or ligand-to-metal charge transfer (LMCT), since the d^{10} metal ions are normally difficult to be oxidized or reduced[9,30,35,37]. Thus, the emission of **II-1-3** may be attributed to intraligand charge transition. Compared with the free dpe ligand, the emission patterns of **II-1-3** are quite similar to that of free dpe, implying the ligand-centered nature of the emission and display the blue-shifts which were attributed to coordination effects of dpe ligand to the metal centers[9,32,35,37]. The divergences of the emission spectra between **II-1** and isostructures **II-2** and **II-3** are attributed to the differences in coordination environments and the arrangement of π-conjugation between dpe moieties within supramolecular motifs[9,32].

Excitation of the samples at 285 nm leads to the generation of similar emissions in the compounds **II-6**, **II-7** and free bpa ligand with the peak maxima occurring at 352 nm for **II-6**, 357 nm for **II-7** and 370 nm for free bpa (Figure 9). These emissions may be assigned to the intraligand π–π* transition since the Zn(II) and Cd(II) ions are difficult to oxidize or to reduce due to the d^{10} configuration. The spectra of **II-6** and **II-7** exhibit more intense and the emission peaks are blue-shifted by about 15 nm compared to free bpa ligand, which may be attributed to the arrangement and the coordination interactions of the bpa ligand to the Zn(II) and Cd(II) ions.

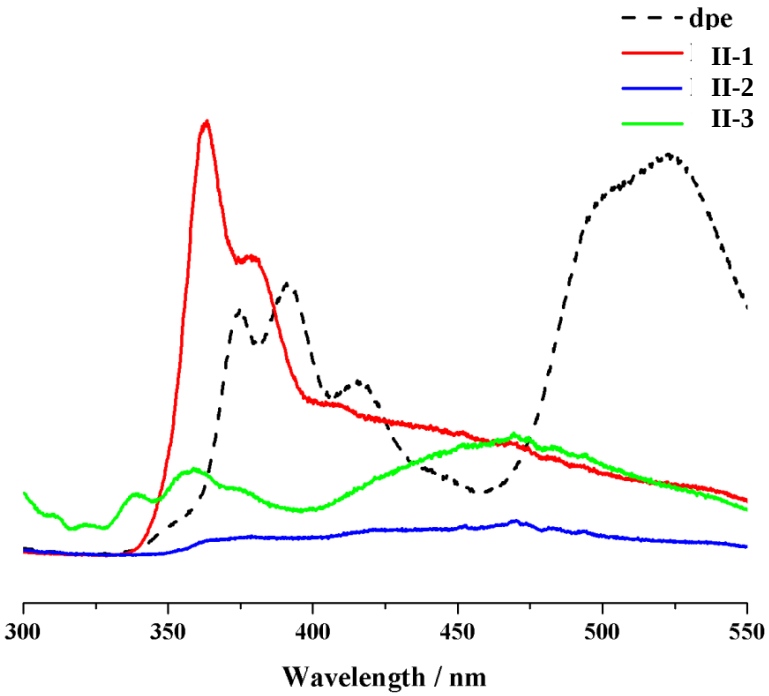

Figure 8 The solid-state emission spectra of the free dpe and compounds **II-1-3** at room temperature

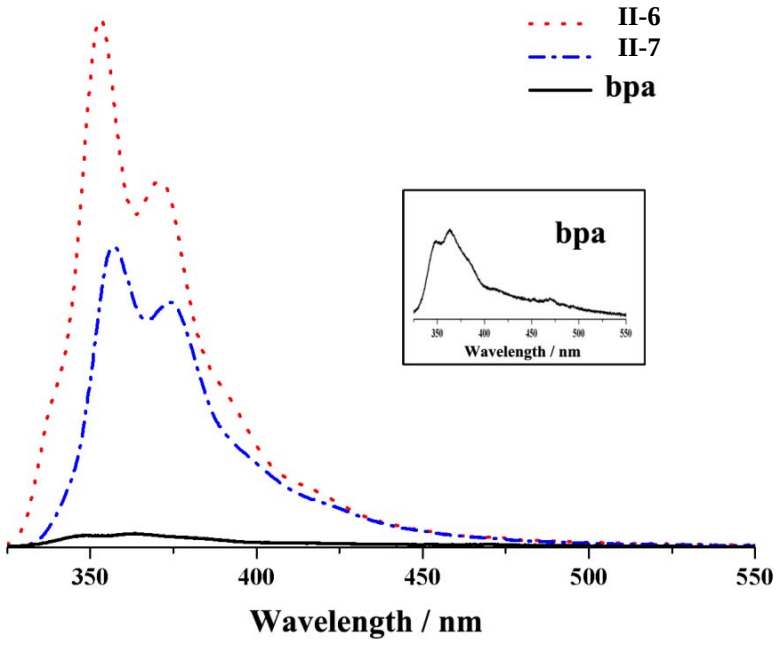

Figure 9 The solid-state photoluminescent spectra of compounds **II-6**, **II-7** and free bpa ligand at room temperature. The inset shows the zoom-in for emission of free bpa ligand

Conclusion

In summary, sevens new 1D coordination polymers have been synthesized by self-assemblies of cyanoacetate with Zn(II)/Cd(II) ions and *N*,*N*'-ditopic spacers. Cyanoacetate well provides coordination site through carboxylate oxygen atoms, as well as, presents either various interchain H-bonding or N···π interactions through nitrile functional group, stabilizing

whole 3D supramolecular frameworks. The result of photoluminescence for **II-1-3** and **II-6-7** in the solid state demonstrated that the orientation and the coordination environment of organic spacer within supramolecular frameworks powerfully affect the luminescent properties, and supports the idea that non-covalent supramolecular assemblies have great potential for utility in the chemistry of luminescent materials.

References

(1) Cheetham, A. K.; Rao, C. N. R.; Feller, R. K. *Chem. Commun.* 2006, 4780.
(2) Janiak, C. *Dalton Trans.* 2003, 2781.
(3) Kitagawa, S.; Kitaura, R.; Noro, S.-i. *Angew. Chem. Int. Ed.* 2004, *43*, 2334.
(4) Kuppler, R. J.; Timmons, D. J.; Fang, Q.-R.; Li, J.-R.; Makal, T. A.; Young, M. D.; Yuan, D.; Zhao, D.; Zhuang, W.; Zhou, H.-C. *Coord. Chem. Rev.* 2009, *253* 3042.
(5) O'Keeffe, M.; Yaghi, O. M. *Chem. Rev.* 2012, *112*, 675.
(6) Stock, N.; Biswas, S. *Chem. Rev.* 2012, *112*, 933.
(7) Suh, M. P.; Park, H. J.; Prasad, T. K.; Lim, D.-W. *Chem. Rev.* 2012, *112*, 782.
(8) Yoon, M.; Srirambalaji, R.; Kim, K. *Chem. Rev.* 2012, *112*, 1196.
(9) Cui, Y.; Yue, Y.; Qian, G.; Chen, B. *Chem. Rev.* 2012, *112*, 1126.
(10) Li, Y.-W.; Li, J.-R.; Wang, L.-F.; Zhou, B.-Y.; Chena, Q.; Bu, X.-H. *J. Mater. Chem.* 2014, *1*, 495.
(11) Noro, S.-i.; Kitagawa, S.; Akutagawa, T.; Nakamura, T. *Prog. Polym. Sci.* 2009, *34*, 240.
(12) Jiang, G.; Wu, T.; Zheng, S.-T.; Zhao, X.; Lin, Q.; Bu, X.; Feng, P. *Cryst. Growth Des.* 2011, *11*, 3713.
(13) Du, M.; Jiang, X.-J.; Zhao, X.-J. *Inorg. Chem.* 2011, *46*, 3984.
(14) Mao, H.; Zhang, C.; Li, G.; Zhang, H.; Hou, H.; Li, L.; Wu, Q.; Zhub, Y.; Wanga, E. *Dalton Trans.* 2004, 3918.
(15) Tian, D.; Chen, Q.; Li, Y.; Zhang, Y.-H.; Chang, Z.; Bu, X.-H. *Angew. Chem. Int. Ed.* 2014, *53*, 837.
(16) Zhao, Y.; He, L.-L.; Xu, H.; Li, X.-Y.; Zang, S.-Q. *Inorg. Chim. Acta.* 2013, *404*, 201.
(17) Wang, C.-C.; Yang, C.-C.; Chung, W.-C.; Lee, G.-H.; Ho, M.-L.; Yu, Y.-C.; Chung, M.-W.; Sheu, H.-S.; Shih, C.-H.; Cheng, K.-Y.; Chang, P.-J.; Chou, P.-T. *Chem. Eur. J.* 2011, *17*, 9232.
(18) Carballo, R.; Castineiras, A.; Covelo, B.; Vazquez-Lopez, E. M. *Polyhedron* 2001, *20*, 899.
(19) Liang, X.-Q.; Zhou, X.-H.; Chen, C.; Xiao, H.-P.; Li, Y.-Z.; Zuo, J.-L.; You, X.-Z. *Cryst. Growth Des.* 2009, *9*, 1041.
(20) Boonmak, J.; Youngme, S.; Chotkhun, T.; Engkagul, C.; Chaichit, N.; Albada, G. A. v.; Reedijk, J. *Inorg. Chem. Commun.* 2008, *11*, 1231.
(21) Wang, H.; Zhang, D.; Sun, D.; Chen, Y.; Zhang, L.-F.; Tian, L.; Jiang, J.; Ni, Z.-H. *Cryst. Growth Des.* 2009, *9*, 5273.
(22) Wang, X.-F.; Zhang, Y.-B.; Huang, H.; Zhang, J.-P.; Chen, X.-M. *Cryst. Growth Des.* 2008, *8*, 4559.
(23) Boonmak, J.; Youngme, S.; Chaichit, N.; Albada, G. A. v.; Reedijk, J. *Cryst. Growth Des.* 2009, *9*, 3318.
(24) Phuengphai, P.; Youngme, S.; Chaichit, N.; Reedijk, J. *Inorg. Chim. Acta.* 2013, *403*, 35.
(25) Kima, Y.; Jung, D.-Y. *CrystEngComm* 2012, *14*, 4567.

(26) Chang, Z.; Zhang, D.-S.; Chen, Q.; Li, R.-F.; Hu, T.-L.; Bu, X.-H. *Inorg. Chem.* 2011, *50*, 7555.
(27) Fan, L.; Zhang, X.; Sun, Z.; Zhang, W.; Ding, Y.; Fan, W.; Sun, L.; Zhao, X.; Lei, H. *Cryst. Growth Des.* 2013, *13*, 2462.
(28) Liu, G.-X.; Huang, Y.-Q.; Chu, Q.; Okamura, T.-a.; Sun, W.-Y.; Liang, H.; Ueyama, N. *Cryst. Growth Des.* 2008, *8*, 3233.
(29) Bruhwiler, D.; Calzaferri, G.; Torres, T.; Ramm, J. H.; Gartmann, N.; Dieu, L.-Q.; Lopez-Duartec, I.; Martinez-Dıaz, M. V. *J. Mater. Chem.* 2009, *19*, 8040.
(30) Zhang, Q.; Hu, F.; Zhang, Y.; Bi, W.; Wang, D.; Sun, D. *Inorg. Chem. Commun.* 2012, *24*, 195.
(31) Jin, S.; Wang, D.; Chen, W. *Inorg. Chem. Commun.* 2007, *10*, 685.
(32) Zhang, X.; Hou, L.; Liu, B.; Cui, L.; Wang, Y.-Y.; Wu, B. *Cryst. Growth Des.* 2013, *13*, 3177.
(33) Xu, B.; Xie, J.; Hu, H.-M.; Yang, X.-L.; Dong, F.-X.; Yang, M.-L.; Xue, G.-L. *Cryst. Growth Des.* 2014, *14*, 1629.
(34) Chen, X.-L.; Qiao, Y.-L.; Gao, L.-J.; Cui, H.-L.; Zhang, M.-L.; Lv, J.-F.; Hou, X.-Y. *Z. Anorg. Allg. Chem.* 2013, *639*, 403.
(35) Yang, G.-b.; Sun, Z.-H. *Inorg. Chem. Commun.* 2013, *29*, 94.
(36) Wang, X.; Qin, C.; Wang, E.; Li, Y.; Hao, N.; Hu, C.; Xu, L. *Inorg. Chem.* 2004, *43*, 1850.
(37) Sen, R.; Mal, D.; Branda, P.; Ferreira, R. A. S.; Lin, Z. *Cryst. Growth Des.* 2013, *13*, 5272.
(38) Ye, J.; Zhao, L.; Bogale, R. F.; Gao, Y.; Wang, X.; Qian, X.; Guo, S.; Zhao, J.; Ning, G. *Chem. Eur. J.* 2015, *21*, 2029.
(39) Kang, J.-G.; Shin, J.-S.; Cho, D.-H.; Jeong, Y.-K.; Park, C.; Soh, S. F.; Lai, C. S.; Tiekink, E. R. T. *Cryst. Growth Des.* 2010, *10*, 1247.
(40) Darensbourg, D. J.; Atnip, E. V.; Reibenspies, J. H. *Inorg. Chem.* 1992, *31*, 4475.
(41) Nakamoto, T.; Hanaya, M.; Katada, M.; Endo, K.; Kitagawa, S.; Sano, H. *Inorg. Chem.* 1997, *36*, 4347.
(42) Novitskii, G.; Shova, S.; Voronkova, V. K.; Korobchenko, L.; Gdanec, M.; Simonov, Y. A.; Turte, K. *Russ. J. Coord. Chem.* 2001, *27*, 791.
(43) Sokolova, M. N.; Budantseva, N. A.; Fedoseev, A. M. *Russ. J. Coord. Chem.* 2011, *37*, 478.
(44) *APEX2*; Bruker AXS Inc.: Madison, WI, 2014.
(45) *SAINT 4.0 Software Reference Manual*; Siemens Analytical X-Ray Systems Inc.: Madison, WI, 2000.
(46) Sheldrick, G. M. *SADABS, Program for Empirical Absorption correction of Area Detector Data*; University of Göttingen: Göttingen, Germany, 2000.
(47) Sheldrick, G. M. *Acta Crystallogr.* 2008, *A64*, 112.
(48) Addison, A. W.; Rao, T. N.; Reedijk, J.; Van Rijn, J.; Verschoor, G. C. *J. Chem. Soc., Dalton Trans.* 1984, 1349.
(49) Zhu, W.; Zheng, R.; Fu, X.; Fu, H.; Shi, Q.; Zhen, Y.; Dong, H.; Hu, W. *Angew. Chem. Int. Ed.* 2015, *54*, 6785.

OUTPUT OF THE RESEARCH

MSc. Students:

1) Miss Porntiva Suvanvapee (2012-2015): **"**Series of cyanoacetato coordination polymers with various *N,N'*-organic bridges: syntheses, crystal structures, luminescent and magnetic properties**"** Master of Science Thesis in Chemistry, Graduate School, Khon Kaen University.

Publication papers:

1) P. Suvanvapee, J. Boonmak*, F. Klongdee, C. Pakawatchai, B. Moubaraki, K.S. Murray, S. Youngme, A Series of cyanoacetato copper(II) coordination polymers with various *N,N'*-ditopic spacers: Structural diversity, supramolecular robustness and magnetic properties. *Crystal Growth & Design*, **2015**, 15(8), 3804. (IF 2014 = 4.89)

2) P. Suvanvapee, J. Boonmak*, S. Youngme, Structural diversity and luminescent properties of cyanoacetato zinc/cadmium coordination polymers with *N,N'*-ditopic auxiliary ligands**.** *Polyhedron,* **2015**, 102, 693. (IF 2014 = 2.01)

3) P. Suvanvapee, J. Boonmak*, S. Youngme, Synthesis, crystal structure and luminescent properties of three new zinc/cadmium coordination polymers containing cyanoacetate and 1,2-di(4-pyridyl)ethylene. *Inorganica Chimica Acta*, **2015**, 437, 11. (IF 2014 = 2.05)

Awards:

1) Pacifichem2015 Early Career Chemist award by 2015 International Chemical Congress of Pacific Basin Societies on December 15 – 20, 2015 at Honolulu, Hawaii, USA.

Presentations:

1) J. Boonmak*, "Cyanoacetato copper(II) coordination polymers with various *N,N'*-ditopic spacers: Structural diversity, supramolecular robustness and magnetic properties" ***Invited speaker*** *(Inorganic Chemistry) at The 41th Congress on Science and Technology of Thailand, November 6 - 8, 2015* at Suranaree University of Technology, Nakhonratchasima, Thailand.

2) J. Boonmak*, "Series of azido-bridged cobalt(II) coordination networks and cyanoacetato metal-organic frameworks: structural diversities and magnetic properties" ***Invited speaker*** *(A Special Session to Commemorate the International Year of Crystallography) at The 40th Congress on Science and Technology of Thailand*, Khon Kaen, Thailand. December 2-4, 2014

3) J. Boonmak*,P. Suvanvapee, F. Klongdee, C. Pakawatchai, K.S. Murray, S. Youngme, Series of cyanoacetato copper(II) coordination polymers with various N,N'-ditopic spacers: Structural diversity, supramolecular robustness and magnetic properties, ***Poster*** *presented at* 2015 International Chemical Congress of Pacific Basin Societies (PACHEM2015), December 15 – 20, 2015 at Honolulu, Hawaii, USA. *(Pacifichem2015 Early Career Chemist award)*

4) P. Suvanvapee, J. Boonmak*, C. Pakawatchai, K. Chainok, K.S. Murray, S. Youngme, A series of cyanoacetato copper(II) coordination polymers with various *N,N'*-ditopic spacers: structural diversity, supramolecular robustness and magnetic properties, ***Poster*** *presentated at 40th Congress on Science and Technology of Thailand*, Hotel Pullman Khon Kaen Raja Orchid, Khon Kaen, Thailand. December 2-4, 2014.

5) P. Suvanvapee, J. Boonmak*, C. Pakawatchai, K. S. Murray, S.Youngme, Syntheses, Crystal Structures and Magnetic Properties of Copper(II) Coordination Networks Containing 1,2-Di(4-pyridyl)ethylene and Cyanoacetic Acid, ***Poster*** *presented at* Pure and Applied Chemistry

International Conference 2014 (PACCON 2014), Centara Hotel and Convention Centre Khon Kaen, Thailand. January 8-10, 2014

6) J. Boonmak*, F. Klongdee, P. Suvanvapee, C. Pakawatchai and S. Youngme, Robust metal supramolecular frameworks constructed from interlaced chain coordination polymers containing 4,4′- bipyridyl and cyanoacetate, ***Poster*** *presented at 4th Asian Conference on Coordination Chemistry (ACCC 4)*, the International Convention Center, Jeju, Korea. November 4-7, 2013.

APPENDICES

Publication paper of PART I

1) P. Suvanvapee, J. Boonmak*, F. Klongdee, C. Pakawatchai, B. Moubaraki, K.S. Murray, S. Youngme, A Series of cyanoacetato copper(II) coordination polymers with various *N*,*N*'-ditopic spacers: Structural diversity, supramolecular robustness and magnetic properties. *Crystal Growth & Design*, **2015**, 15(8), 3804. (IF 2014 = 4.89)

Publication papers of PART II

1) P. Suvanvapee, J. Boonmak*, S. Youngme, Structural diversity and luminescent properties of cyanoacetato zinc/cadmium coordination polymers with *N*,*N*'-ditopic auxiliary ligands**.** *Polyhedron*, **2015**, 102, 693. (IF 2014 = 2.01)

2) P. Suvanvapee, J. Boonmak*, S. Youngme, Synthesis, crystal structure and luminescent properties of three new zinc/cadmium coordination polymers containing cyanoacetate and 1,2-di(4-pyridyl)ethylene. *Inorganica Chimica Acta*, **2015**, 437, 11. (IF 2014 = 2.05)

Polyhedron 102 (2015) 693–698

Contents lists available at ScienceDirect

Polyhedron

journal homepage: www.elsevier.com/locate/poly

Structural diversity and luminescent properties of cyanoacetato zinc/cadmium coordination polymers with *N*,*N*′-ditopic auxiliary ligands

Porntiva Suvanvapee, Jaursup Boonmak*, Sujittra Youngme

Materials Chemistry Research Center, Department of Chemistry and Center of Excellence for Innovation in Chemistry, Faculty of Science, Khon Kaen University, Khon Kaen 40002, Thailand

ARTICLE INFO

Article history:
Received 5 August 2015
Accepted 25 October 2015
Available online 31 October 2015

Keywords:
Coordination polymer
Cyanoacetate
4,4′-Bipyridyl
1,2-Di(4-pyridyl)ethane
Luminescence properties

ABSTRACT

By using the carboxylate ligand cyanoacetate (cna) and *N*,*N*′-ditopic organic neutral spacers, four new Zn(II)/Cd(II) coordination polymers, formulated as $[Zn(cna)_2(bpy)(H_2O)_2]_n$ (**1**), $[Cd_3(cna)_6(bpy)_3]_n$ (**2**), $[Zn(cna)_2(bpa)]_n$ (**3**) and $[Cd(cna)_2(bpa)]_n$ (**4**) (bpy = 4,4′-bipyridyl and bpa = 1,2-di(4-pyridyl)ethane) have been obtained. All compounds exhibit one-dimensional (1D) chain coordination polymers with diverse topologies. Compound **1** reveals a linear chain structure which is formed by μ_2-bpy bridging between $[Zn(cna)_2(H_2O)_2]_n$ units. Compound **2** shows a triple-stranded chain consisting of six- and seven-coordinated Cd(II) centers. Compound **3** exhibits a zigzag chain coordination polymer containing μ_2-bpa spacers bridging between tetrahedral Zn(II) ions. Whereas **4** shows a ladder-like structure which is built from double μ_2-bpa spacers connecting between Cd(II) cyanoacetate dimeric units. All compounds are further extended into a 3D supramolecular architectures through non-covalent weak hydrogen bonds and N···π and/or C–H···π interactions. The free bpa ligand exhibits very weak photoluminescence in the solid state, while this property is significantly enhanced in **3** and **4**.

1. Introduction

The construction of coordination polymers (CPs) has attracted attention due to their diverse structural topologies and potential applications such as gas storage, magnetism, catalysis, and luminescence [1–9]. The rational design of CPs is an important goal for synthetic chemistry as it provides an opportunity to modify their functional properties at the molecular level. To date, many CPs have been prepared on the basis of the connector and linker approach [4,6,10]. Connectors are often transition metal ions that can yield different coordination geometries. Linkers are typically organic molecules such as functionalized carboxylates and pyridine-based linkers. Coordination polymers constructed from divalent zinc and cadmium ions have been an active research area because the absence of crystal field stabilization energy in the d^{10} electronic configuration allows these metal ions to have no significant coordination preferences [11–14]. Thus, they can form a variety of structures depending on the organic linker. In the present studies, the cyanoacetate ($NC_2H_2CO_2$, cna) is used for binding metal ions through carboxylate bridge. It contains both nitrile (–C≡N) and carboxylic groups which not only provides many coordination sites but also effectively serves as hydrogen bonding sites and the intermolecular $N_{nitrile}\cdots\pi$ interaction toward neighboring electron-deficient aromatic moieties. These versatile connection sites allow cyanoacetate to be a good candidate for constructing the CPs [15–23]. Meanwhile, the mixed-ligands strategy, including *N*,*N*′-ditopic organic neutral coligands with different lengths and flexibility, has successfully demonstrated various novel CPs [10,24,25]. Recently, we reported a series of cyanoacetato coordination polymers in the Cu(II) system [23]. In consequence, to extend the study of the self-assembly process in d^{10} metal CPs, we have herein taken cyanoacetate and different pyridine-based neutral coligands in the Zn(II)/Cd(II) system (see Scheme 1). The four new 1D coordination polymers, $[Zn(cna)_2(bpy)(H_2O)_2]_n$ (**1**), $[Cd_3(cna)_6(bpy)_3]_n$ (**2**), $[Zn(cna)_2(bpa)]_n$ (**3**) and $[Cd(cna)_2(bpa)]_n$ (**4**) (bpy = 4,4′-bipyridyl and bpa = 1,2-di(4-pyridyl)ethane) have been synthesized. The characterizations have been done through X-ray crystallography, IR spectroscopy, and elemental analysis. The solid-state photoluminescent properties at room temperature have also been studied and this property is significantly enhanced in **3** and **4**.

* Corresponding author. Fax: +66 43 202 373.
E-mail address: Jaursup@kku.ac.th (J. Boonmak).

http://dx.doi.org/10.1016/j.poly.2015.10.043
0277-5387/

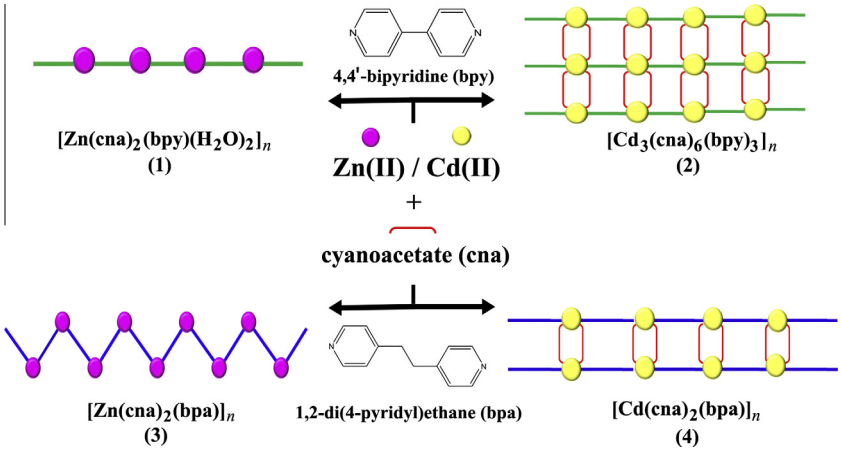

Scheme 1. The coordination polymers **1**–**4**.

2. Experimental

2.1. General remarks

All chemical were obtained from commercial sources and were used without further purification. Elemental analyses (C, H, N) were carried out with a PerkinElmer PE 2400CHNS analyzer. FT-IR spectra were obtained in KBr disks on a PerkinElmer Spectrum One FT-IR spectrophotometer in 4000–450 cm^{-1} spectral range. The X-ray powder diffraction (XRPD) data were collected on a Bruker D8 ADVANCE diffractometer using monochromatic Cu Kα radiation, and the recording speed was 0.5 s/step over the 2θ range of 5–40° at room temperature to determine the phase purity. Photoluminescent spectra of the sample powders were performed on a Shimadzu RF-5301PC spectrofluorophotometer in the wavelength range of 300–550 nm with the spectral band widths at 3 nm for excitation and emission.

2.2. Preparation of $[Zn(cna)_2(bpy)(H_2O)_2]_n$ (**1**)

The solution containing $Zn(NO_3)_2{\cdot}6H_2O$ (148 mg, 0.5 mmol) and cyanoacetic acid (85 mg, 1 mmol) in water and dimethylformamide (4 mL, 1:1 v/v) was mixed with the methanolic solution (2 mL) of 4,4′-bipyridyl (78 mg, 0.5 mmol). This mixture solution was allowed to stand undisturbed at room temperature, yielding colorless block-shaped crystals of **1** after 2 weeks. Yield: 52 mg (24%) based on zinc salt. *Anal.* Calc. for $ZnC_{16}H_{16}N_4O_6$: C, 45.14; H, 3.79; N, 13.16. Found: C, 45.73; H, 3.52; N, 12.98%. IR (KBr, cm^{-1}): 3413br (ν(OH)), 2258w (ν(C≡N)), 1612s (ν_{as}(OCO)), 1436w, 1367s (ν_s(OCO)), 1270w, 1220w, 1083w, 1015m, 907w, 829m, 720w, 551w, 488m.

2.3. Preparation of $[Cd_3(cna)_6(bpy)_3]_n$ (**2**)

An ethanolic solution (4 mL) of cyanoacetic acid (85 mg, 1 mmol) and 4,4′-bipyridyl (78 mg, 0.5 mmol) was carefully layered on an aqueous solution (2 mL) of $Cd(NO_3)_2{\cdot}4H_2O$ (154 mg, 0.5 mmol). After 3 weeks, colorless needle-shaped crystals of **2** were obtained. Yield for **2**: 225 mg (34%) based on cadmium salt. *Anal.* Calc. for $Cd_3C_{48}H_{36}N_{12}O_{12}$: C, 44.01; H, 2.77; N, 12.83. Found: C, 43.76; H, 2.51; N, 12.73%. IR (KBr, cm^{-1}): 2263w (ν(C≡N)), 1635s (ν_{as}(OCO)), 1396s (ν_s(OCO)), 1217w, 1078m, 1007m, 899w, 807m, 635m.

2.4. Preparation of $[Zn(cna)_2(bpa)]_n$ (**3**)

The solution containing $Zn(OAc)_2{\cdot}2H_2O$ (109 mg, 0.5 mmol) and cyanoacetic acid (85 mg, 1 mmol) in water and dimethylformamide (4 mL, 1:1 v/v) was mixed with 1,2-di(4-pyridyl)ethane (92 mg, 0.5 mmol) in methanol (2 mL). This mixture solution was allowed to stand undisturbed at room temperature, yielding colorless rod-shaped crystals of **3** after 3 days. Yield: 134 mg (64%) based on zinc salt. *Anal.* Calc. for $ZnC_{18}H_{16}N_4O_4$: C, 51.75; H, 3.86; N, 13.41. Found: C, 51.43; H, 3.62; N, 13.21%. IR (KBr, cm^{-1}): 2258w (ν(C≡N)), 1610s (ν_{as}(OCO)), 1433w, 1368s (ν_s(OCO)), 1270w, 1221w, 1083m, 1023w, 986w, 835m, 550m.

2.5. Preparation of $[Cd(cna)_2(bpa)]_n$ (**4**)

Compound **4** was synthesized in a similar manner to **3** using $Cd(NO_3)_2{\cdot}4H_2O$ (154 mg, 0.5 mmol) instead of $Zn(OAc)_2{\cdot}2H_2O$. After 3 days, colorless rod-shaped crystals of **4** were obtained. Yield: 106 mg (45%) based on cadmium salt. *Anal.* Calc. for $CdC_{18}H_{16}N_4O_4$: C, 46.52; H, 3.47; N, 12.06. Found: C, 46.13; H, 3.31; N, 11.95%. IR (KBr, cm^{-1}): 2258w (ν(C≡N)), 1619s (ν_{as}(OCO)), 1419w, 1366s (ν_s(OCO)), 1273w, 1216w, 1072w, 1048w, 1010w, 942w, 809m, 724w, 638m.

2.6. X-ray crystallography

The reflection data of **1**–**4** were collected on a Bruker D8 Quest PHOTON100 CMOS detector with graphite-monochromated Mo Kα radiation using the APEX2 program [26]. Raw data frame integration was performed with SAINT [26]. An empirical absorption correction by using the SADABS program [26] was applied. The structure was solved by direct methods and refined by full-matrix least-squares method on F^2 with anisotropic thermal parameters for all non-hydrogen atoms using the SHELXTL software package [27]. All hydrogen atoms were placed in calculated positions and refined isotropically, with the exception of the hydrogen atoms of coordination water molecules in **1** which were found *via* difference Fourier maps, and then restrained at fixed positions. The unbound and coordination oxygen atoms (O4 and O3) of a terminal cyanoacetate for **3** are disordered. The occupancies of two conformations were refined to 0.4 and 0.6. The details of crystal data, selected bond lengths and angles for **1**–**4** are listed in Tables 1 and S1.

Table 1
Crystallographic data for compounds **1**–**4**.

Compound	**1**	**2**	**3**	**4**
Formula	$ZnC_{16}H_{16}N_4O_6$	$Cd_3C_{48}H_{36}N_{12}O_{12}$	$ZnC_{18}H_{16}N_4O_4$	$CdC_{18}H_{14}N_4O_4$
Molecular weight	425.72	1310.09	417.72	464.75
T (K)	293(2)	293(2)	293(2)	293(2)
Crystal system	orthorhombic	monoclinic	triclinic	triclinic
Space group	*Pccn*	*C*2/*c*	$P\bar{1}$	$P\bar{1}$
a (Å)	12.9041(5)	24.9894(19)	9.5264(3)	8.3470(3)
b (Å)	18.5888(7)	11.6868(9)	9.7703(4)	10.7131(5)
c (Å)	7.2082(2)	20.7170(15)	10.9211(4)	11.5269(4)
α (°)	90.00	90.00	112.2500(10)	70.459(2)
β (°)	90.00	123.260(2)	96.906(10)	81.386(10)
γ (°)	90.00	90.00	98.6510(10)	67.1380(10)
V (Å^3)	1729.04(11)	5059.16(7)	912.49(6)	894.85(6)
Z	4	4	2	2
ρ_{calcd} (g cm^{-3})	1.635	1.720	1.520	1.725
μ (Mo Kα) (mm^{-1})	1.464	1.324	1.378	1.253
Data collected	4890	5195	4473	4230
Unique data (R_{int})	3136(0.0307)	5195(0.1666)	3821(0.0173)	3519(0.0340)
R_1[a]/wR_2[b] [$I > 2\sigma(I)$]	0.0404/0.0925	0.0711/0.1096	0.0420/0.1086	0.0338/0.0657
R_1[a]/wR_2[b] [all data]	0.0776/0.1060	0.1890/0.1394	0.0527/0.1159	0.0497/0.0715
Goodness-of-fit (GOF)	1.067	1.007	1.036	1.099
Maximum/minimum electron density (e Å^{-3})	0.395/−0.738	1.164/−0.841	0.946/−0.467	0.693/−0.726

[a] $R = \Sigma||F_o|-|F_c||/\Sigma|F_o|$.
[b] $R_w = \{\Sigma[w(|F_o|-|F_c|)]^2/\Sigma[w|F_o|^2]\}^{1/2}$.

3. Results and discussion

3.1. Crystal structure of $[Zn(cna)_2(bpy)(H_2O)_2]_n$ (**1**)

Compound **1** crystallizes in the orthorhombic system with *Pccn* space group, exhibiting a 1D chain structure, as shown in Fig. 1a. The structure of **1** is isomorphous with previously reported complexes, $[M(cna)_2(bpy)(H_2O)_2]_n$ (M = Cu(II) [23], Mn(II) [16]). Each Zn(II) ion is coordinated by two nitrogen atoms from two μ_2-bpy spacers, two oxygen atoms from two terminal cyanoacetates and two oxygen atoms from two coordination water molecules, adopting a distorted octahedral geometry. The ZnN_2O_4 moiety shows coordination distances in the range of 2.118(9)–2.172(6) Å. The adjacent zinc(II) ions are bridged *via* μ_2-bpy spacers generating 1D linear chain of **1** with the Zn···Zn separation of 11.314(3) Å. The two pyridine rings of bipyridyl moieties are not coplanar with the dihedral angle between the two planar pyridine rings of 15.78°. Each 1D chain of **1** is assembled by various interchain hydrogen bonding among terminal cyanoacetates (C7H···N2$_{nitrile}$) (Fig. 1b, Table S2), and between unbound O atom from cyanoacetate and H atom from coordination water molecule (O3H···O2), as well as, the pyridyl H atom from μ_2-bpy and O atom from coordination water molecule (C4H···O2). Moreover, the C4H···π interaction is observed among the adjacent μ_2-bpy moieties along the *c* axis with the separation of 3.394 Å (Fig. 1b). These weak interactions complete the 3D supramolecular motif of **1** with the closest interchain Zn···Zn separation of 7.208(2) Å. A comparison was made with the previous mixed bridging cna-bpy Zn(II) complex, $[Zn_2(cna)_4(bpy)_2]_n(H_2O)_n$ [17], which was reported to exhibit a 1D zigzag chain constructed from terminal cyanoacetate and μ_2-bpy spacer linking between the distorted tetrahedral ZnN_2O_2 chromophores. The different structural topologies are attributed to the diverse coordination geometries of Zn(II) centers.

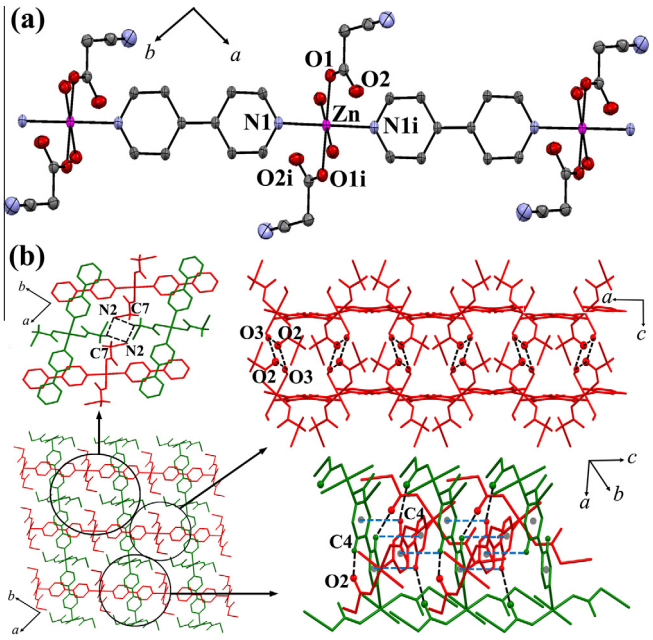

Fig. 1. (a) 1D linear chain structure of **1** with used atom labeling. The ellipsoids are shown at 35% probability level. The hydrogen atoms are omitted for clarity (i) = $-x$, $1-y$, $1-z$. (b) The packing diagram of **1** formed by the interchain hydrogen bonding (black broken lines) and C–H···π interactions (blue broken lines). (Color online.)

3.2. Crystal structure of $[Cd_3(cna)_6(bpy)_3]_n$ (**2**)

Compound **2** crystallizes in the monoclinic *C*2/*c* space group, exhibiting a 1D triple-stranded chain structure, as shown in Fig. 2a. The 1D triple-stranded chain of **2** contains two crystallographic independent Cd(II) centers of different geometries, i.e., two distorted pentagonal bipyramidal $Cd1N_2O_5$ and one distorted octahedral $Cd2N_2O_4$ chromophores. In the $Cd1N_2O_5$ moiety, each Cd1 center is surrounded by five carboxylate O atoms from three different cyanoacetate ligands (Cd1–O = 2.275(7)–2.475(6) Å) and two N atoms from two μ_2-bpy ligands (Cd1–N = 2.311(6) and 2.334(7) Å), while, each Cd2 center is six-coordination, surrounded by four carboxylate O atoms from four different μ_2-cyanoacetates (Cd2–O = 2.328(6)–2.393(6) Å) and two N atoms from two μ_2-bpy molecules (Cd2–N = 2.284(9) and 2.302(9) Å). The Cd–O and Cd–N bond distances are in normal ranges for Cd(II) complexes [28,29]. The Cd2 is bridged to two symmetry-related Cd1 ions *via* double-*syn*,*anti*-η^1:η^3:μ_2-cyanoacetates and double-chelating

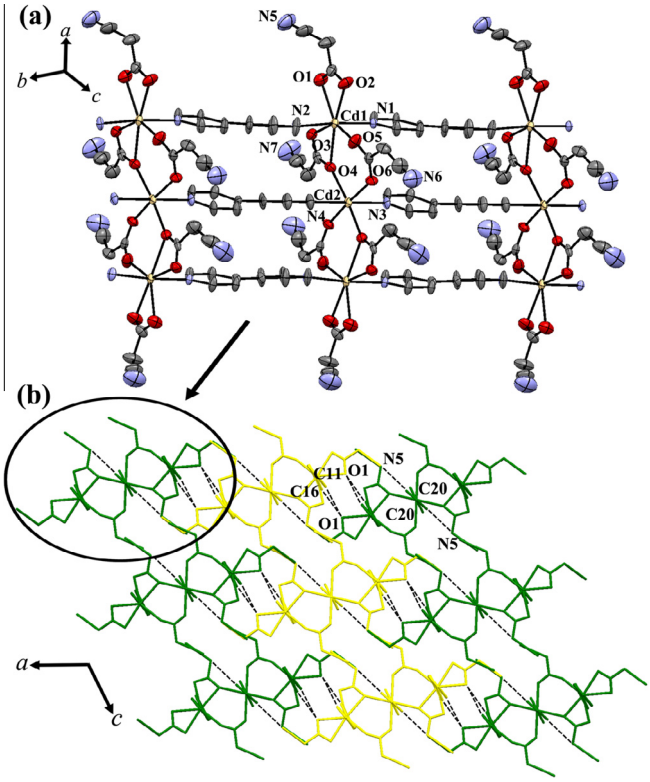

Fig. 2. 1D triple-stranded chain structure of **2** with used atom labeling. The ellipsoids are shown at 35% probability level. All hydrogen atoms are omitted for clarity. (b) The packing diagram of triple-stranded chains in **2** formed by various weak hydrogen bonding in *ac* plane.

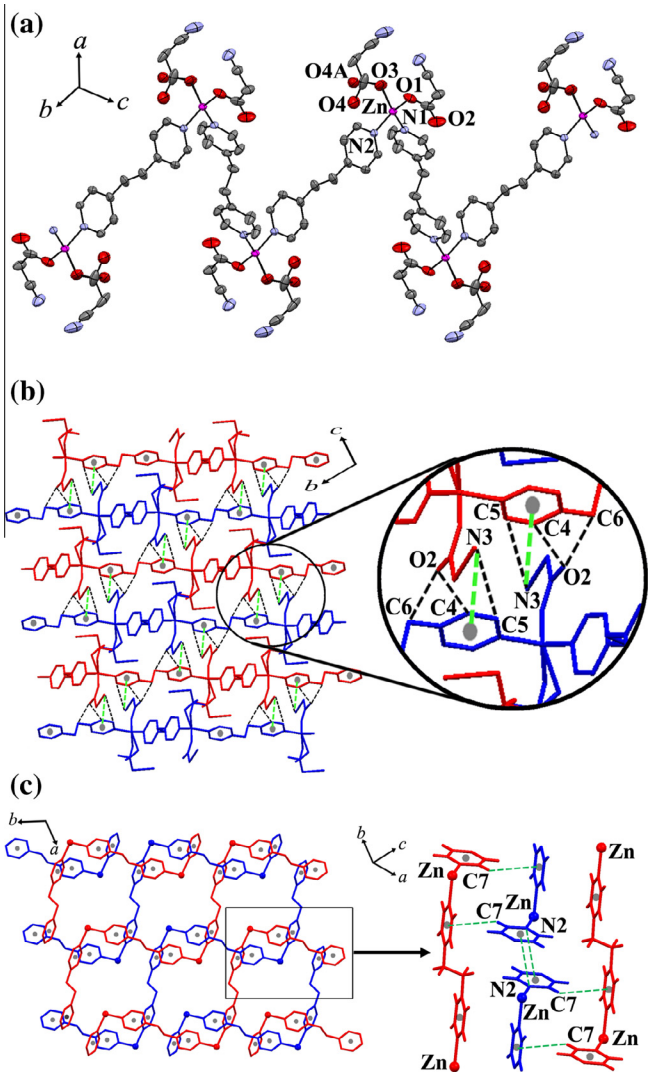

Fig. 3. (a) 1D zigzag chain structure of **3** with used atom labeling. The ellipsoids are shown at 50% probability level. All hydrogen atoms are omitted for clarity. (b) 2D sheet structure of **3** built from weak hydrogen bonding (black broken lines) and $N_{nitrile}\cdots\pi$ interaction (green broken lines) in *bc* plane. (c) Another view in *ab* plane showing 2D sheet structure formed by C–H···π and $N_{pyridyl}\cdots\pi$ interactions. The cyanoacetates are omitted for clarity. (Color online.)

bridging bidentate modes of cyanoacetates, generating a linear trinuclear (Cd1, Cd2, Cd1a) unit with the Cd···Cd separation of 4.184(2) Å. Moreover, each trinuclear unit is linked by μ_2-bpy spacers, giving rise to a 1D triple-stranded chains of **2** with the Cd···Cd separation across μ_2-bpy of 11.687(2) Å. The two pyridine rings of bpy moieties are not coplanar with the dihedral angle between the two planar pyridine rings of 12.66° (Cd1) and 21.13° (Cd2). For the packing motif (Fig. 2b), each chain of **2** is assembled by the intermolecular weak hydrogen bonding among nitrile–N atoms from terminal cyanoacetates, coordination oxygen atoms from cyanoacetates, and pyridyl–H atoms from μ_2-bpy (C20H···N5, C16H···O1, and C11H···O1,) (Fig. 2b, Table S2). All interactions complete the overall 3D packing structure motif of **2** with the closest interchain Cd···Cd separation of 6.672(2) Å.

3.3. Crystal structure of $[Zn(cna)_2(bpa)]_n$ (**3**)

Compound **3** crystallizes in the triclinic $P\bar{1}$ space group, exhibiting a 1D zigzag chain structure, as shown in Fig. 3a. Each Zn(II) ion is coordinated by two oxygen atoms from two different monodentate cyanoacetates and two nitrogen atoms from two bpa spacers, adopting a distorted tetrahedral ZnN_2O_2 chromophore. The coordination distances and angles are in ranges of 1.869(4)–2.094(6) Å and 92.08(16)–126.03(12)°, respectively. The adjacent zinc(II) ions are bridged by μ_2-bpa spacers generating 1D zigzag chains of **3** with the Zn···Zn separation of 13.253(6) and 13.239(5) Å. The *anti* conformation of μ_2-bpa molecule is observed with the C–CH_2–CH_2 angle of 112.17°. The two pyridine rings of bipyridyl moieties are perfectly coplanars, being located on a crystallographic center of symmetry. For the packing motif, each 1D zigzag chain of **3** is assembled by various intermolecular weak hydrogen bonding among terminal nitrile–N atoms and unbound oxygen atoms from cyanoacetates acting as H-acceptor and pyridyl–H, ethyl–H atoms from μ_2-bpa acting as H-donors (C5H···N3, C4H···O2, and C6H···O2) (Fig. 3b, Table S2). In addition, the nitrile N atoms from the terminal cyanoacetates can interact with the adjacent electron deficient μ_2-bpa ring with $N3_{nitrile}\cdots\pi$ distance of 3.482 Å (Fig. 3b). Moreover, the C7–H···π interaction is observed between the interchain μ_2-bpa moieties with the separation of 3.551 Å, and the pyridyl–N atom from μ_2-bpa also interacts with the adjacent bpa rings with $N_{pyridyl}\cdots\pi$ distance of 3.767 Å (Fig. 3c). All interactions complete the overall 3D supramolecular motif of **3** with the closest interchain Zn···Zn separation of 6.324(5) Å.

3.4. Crystal structure of $[Cd(cna)_2(bpa)]_n$ (**4**)

Compound **4** crystallizes in the triclinic $P\bar{1}$ space group, exhibiting a 1D ladder-like chain structure, as shown in Fig. 4. Each Cd(II) ion is six-coordinated, surrounded by four carboxylate oxygen atoms from three different cyanoacetates and two nitrogen atoms from two μ_2-bpa molecules, generating a distorted octahedral

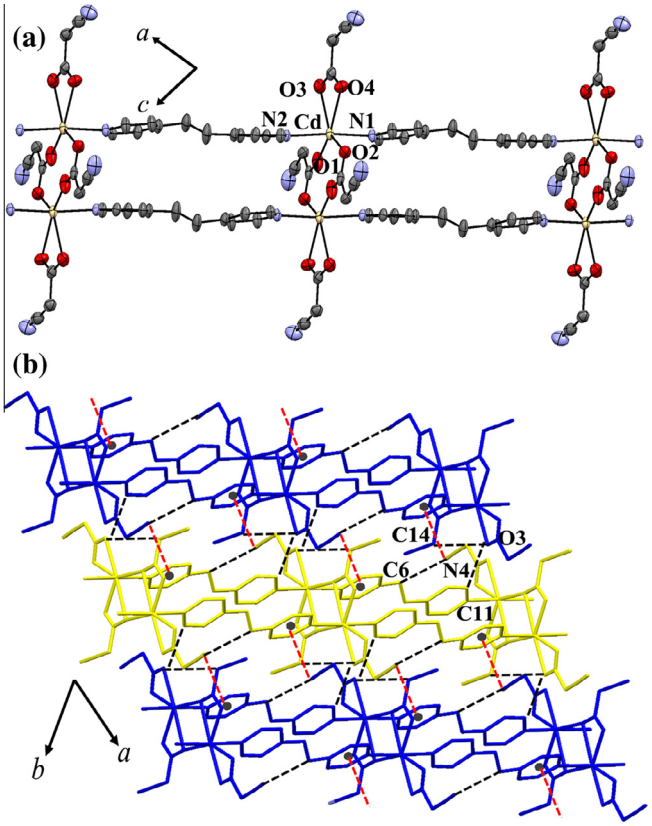

Fig. 4. (a) 1D ladder chain structure of **4** with used atom labeling. The ellipsoids are shown at 50% probability level. All hydrogen atoms are omitted for clarity. (b) The packing diagram of **4** formed by weak interchain hydrogen bonding (black broken lines) and $N_{nitrile}\cdots\pi$ interaction (red broken lines) in *ab* plane. (Color online.)

CdN_2O_4 chromophore. The CdN_2O_4 moiety shows coordination distances and angles in ranges of 2.294(2)–2.420(2) Å and 83.97(8)–149.17(10)°, respectively. The carboxylate bridges from two cyanoacetates exhibit a double-*syn*,*anti*-η^1:η^3:μ_2 coordinative modes connecting between Cd(II) centers, adopting a dinuclear Cd(II) unit with Cd···Cd separation of 3.961(6) Å. An additional cyanoacetate acts as terminal chelating ligand. Moreover, the carboxyl-bridged dinuclear units are assembled by paired μ_2-bpa spacers to create the infinite 1D ladder-like structures (Fig. 4a). The Cd···Cd separation across μ_2-bpa is 6.877(5) Å. The two pyridine rings of bipyridyl moieties are not coplanar with the dihedral angle between the two planar pyridine rings of 9.88°. The *anti* conformation of bpa molecules is observed with C–CH_2–CH_2 angles of 115.98° and 117.22°, and the C–CH_2–CH_2–C torsion angle of 171.69°. For the packing diagram (Fig. 4b, Table S2), each 1D ladder chain of **4** is assembled by the intermolecular weak hydrogen bonding between terminal nitrile–N from cyanoacetate and ethyl–H from μ_2-bpa (C6H···N4), coordination oxygen atoms and alkyl–H from cyanoacetates (C14H···O3) and ethyl–H from μ_2-bpa (C11H···O3). In addition, the nitrile–N atoms from the terminal cyanoacetates effectively interact with the adjacent μ_2-bpa moieties with N···π distance of 3.412 Å, as shown in Fig. 4b.

3.5. Photoluminescent properties

Photoluminescence studies of d^{10} metal-organic CPs with luminescent organic ligands containing aromatic rings have been a subject of immense current research interest because their emissions can be adjusted by involving the coordination environment, the rigidity and the arrangement of organic linkers within CPs [9,30–33]. Recently, the luminescent properties of d^{10} complexes

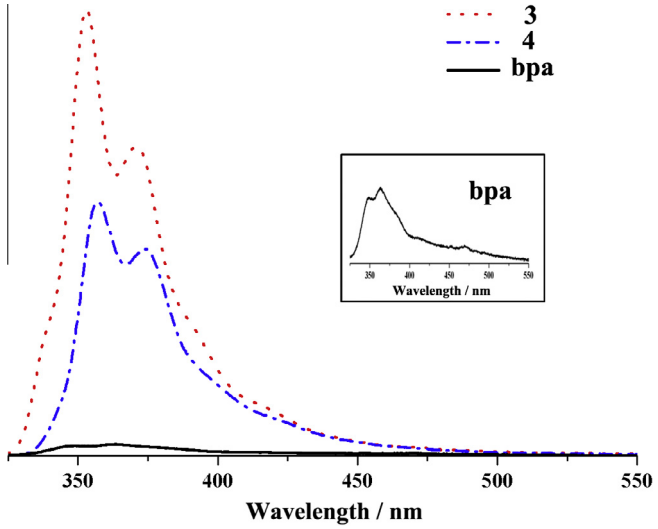

Fig. 5. The solid-state photoluminescent spectra of compounds **3**, **4**, and free bpa ligand. The inset shows the enlarged emission of free bpa.

containing bpa/dpe spacers have been reported [34–37]. Therefore, the solid-state luminescent properties of **3** and **4** were investigated at room temperature. The phase purities of **3** and **4** were confirmed by X-ray powder diffraction (XRPD) (Figs. S1 and S2), in which the experimental diffraction peaks are in good agreement with the patterns simulated from single-crystal data, implying the good phase purities of **3** and **4**. It should be mentioned that both compounds **1** and **2** contain mixed crystals with similar shapes and color and they are difficult to be manually separated to obtain pure bulk products in sufficient amount for the XRPD and photoluminescent measurements. To compare the luminescent intensities, all emission spectra were determined with the same excitation wavelength (λ_{ex} = 285 nm) and the same spectral pass widths. Excitation of the samples at 285 nm leads to the generation of similar emissions in the compounds **3**, **4** and free bpa ligand with the peak maxima occurring at 352 nm for **3**, 357 nm for **4**, and 370 nm for free bpa (Fig. 5). These emissions may be assigned to the intraligand π–π* transition since the Zn(II) and Cd(II) ions are difficult to be oxidized or reduced due to the d^{10} configuration. The spectra of **3** and **4** exhibit more intense and the emission peaks are blue-shifted by about 15 nm compared to free bpa ligand, which may be attributed to the arrangement and the increased rigidity in the bpa ligand resulting from complexation to the Zn(II) and Cd (II) ions. [30–37] A similar emission band around 350 nm has been observed previously for other related mixed-ligands coordination polymers, such as $[Cd_2(cta)(bpa)(H_2O)_3]_n(H_2O)_{5n}$ (H_4cta = cyclohexane-1,2,4,5-tetracarboxylic acid) [37], $[Zn_2(tbip)_2(bpa)(H_2O)]_n$ (H_2tbip = 5-tert-butylisophthalic acid) [38], $[Zn(cna)_2(dpe)]_n$ and $[Cd(cna)_2(dpe)]_n$ [39].

4. Conclusion

In summary, a series of four d^{10} metal coordination polymers based on cyanoacetate and *N*,*N*′-ditopic coligands has been successfully synthesized and characterized. All compounds exhibit polymeric chain structures. In comparison with mixed rigid bridging bpy and cyanoacetate in the Cu(II) system [23], the linear chain structure of **1** is isomorphous to that of Cu(II) complex, whereas **2** shows a triple-stranded chain. This structure is attributed to a larger accessible space of Cd(II) ion which can organize the bridging cyanoacetates and bpy small spacers, leading to a linear trinuclear subunit. Contrary to the flexible extended spacer bpa, compound **3**

shows a zigzag chain structure caused by the tetrahedral Zn(II) connectors, while the ladder-like chain structure of **4** is isomorphous to the Cu(II) analog. These diverse structural topologies significantly depend on the different coordination sites of Zn(II) and Cd(II) centers. Weak interactions such as hydrogen bonding and N···π and/or CH···π interactions join the polymeric chains to stabilize overall supramolecular networks. Moreover, the strong photoluminescence properties of **3** and **4** may make them as the candidates for potential photoactive materials.

Acknowledgments

Funding for this work is provided by The Thailand Research Fund: Grant No. TRG5780003 (for J.B.) and BRG5680009 (for S.Y.), the Higher Education Research Promotion and National Research University Project of Thailand, through the Advanced Functional Materials Cluster of Khon Kaen University, and the Center of Excellence for Innovation in Chemistry (PERCH–CIC), Office of the Higher Education Commission, Ministry of Education, Thailand.

Appendix A. Supplementary data

Supplementary data contains XRPD patterns of **3** and **4**. CCDC 1414051–1414054 contain the supplementary crystallographic data for compounds **1**–**4**. These data can be obtained free of charge via http://www.ccdc.cam.ac.uk/conts/retrieving.html, or from the Cambridge Crystallographic Data Centre, 12 Union Road, Cambridge CB2 1EZ, UK; fax: (+44) 1223-336-033; or e-mail: deposit@ccdc.cam.ac.uk. Supplementary data associated with this article can be found, in the online version, at http://dx.doi.org/10.1016/j.poly.2015.10.043.

References

[1] A. Schneemann, V. Bon, I. Schwedler, I. Senkovska, S. Kaskel, R.A. Fischer, Chem. Soc. Rev. 43 (2014) 6062.
[2] N. Stock, S. Biswas, Chem. Rev. 112 (2012) 933.
[3] R.J. Kuppler, D.J. Timmons, Q.-R. Fang, J.-R. Li, T.A. Makal, M.D. Young, D. Yuan, D. Zhao, W. Zhuang, H.-C. Zhou, Coord. Chem. Rev. 253 (2009) 3042.
[4] A.K. Cheetham, C.N.R. Rao, R.K. Feller, Chem. Commun. (2006) 4780.
[5] S. Kitagawa, R. Kitaura, S.-I. Noro, Angew. Chem. Int. Ed. 43 (2004) 2334.
[6] C. Janiak, Dalton Trans. (2003) 2781.
[7] Y.-W. Li, J.-R. Li, L.-F. Wang, B.-Y. Zhou, Q. Chena, X.-H. Bu, J. Mater. Chem. 1 (2014) 495.
[8] S.-I. Noro, S. Kitagawa, T. Akutagawa, T. Nakamura, Prog. Polym. Sci. 34 (2009) 240.
[9] Y. Cui, Y. Yue, G. Qian, B. Chen, Chem. Rev. 112 (2012) 1126.
[10] D. Tian, Q. Chen, Y. Li, Y.-H. Zhang, Z. Chang, X.-H. Bu, Angew. Chem. Int. Ed. 53 (2014) 837.
[11] X.-Q. Liang, X.-H. Zhou, C. Chen, H.-P. Xiao, Y.-Z. Li, J.-L. Zuo, X.-Z. You, Cryst. Growth Des. 9 (2009) 1041.
[12] L.-F. Ma, X.-Q. Li, Q.-L. Meng, L.-Y. Wang, M. Du, H.-W. Hou, Cryst. Growth Des. 11 (2011) 175.
[13] Q. Zhang, F. Hu, Y. Zhang, W. Bi, D. Wang, D. Sun, Inorg. Chem. Commun. 24 (2012) 195.
[14] Y.-R. Liu, X. Zhang, G.-R. Liang, Inorg. Chem. Commun. 37 (2013) 1.
[15] M.N. Sokolova, N.A. Budantseva, A.M. Fedoseev, Russ. J. Coord. Chem. 37 (2011) 478.
[16] X. Feng, X.-G. Shi, F. Ruan, Z. Kristallogr. NCS 224 (2009) 193.
[17] X. Feng, T.-C. Feng, J.-S. Zhao, X.-G. Shi, F. Ruan, Z. Kristallogr. NCS 224 (2009) 541.
[18] S.G. Shova, Y.A. Simonov, M. Gdaniec, G.V. Novitchi, A. Lazarescu, K.I. Turta, Russ. J. Inorg. Chem. 47 (2002) 946.
[19] G. Novitskii, S. Shova, V.K. Voronkova, L. Korobchenko, M. Gdanec, Y.A. Simonov, K. Turte, Russ. J. Coord. Chem. 27 (2001) 791.
[20] T. Nakamoto, M. Hanaya, M. Katada, K. Endo, S. Kitagawa, H. Sano, Inorg. Chem. 36 (1997) 4347.
[21] P. Startnowicz, Acta Crystallogr., Sect. C. 49 (1993) 1621.
[22] J.R. Wasson, C.-I. Shyr, C. Trapp, Inorg. Chem. 7 (1968) 469.
[23] P. Suvanvapee, J. Boonmak, F. Klongdee, C. Pakawatchai, B. Moubaraki, K.S. Murray, S. Youngme, Cryst. Growth Des. 15 (2015) 3804.
[24] P. Phuengphai, S. Youngme, N. Chaichit, J. Reedijk, Inorg. Chim. Acta 403 (2013) 35.
[25] Z. Chang, D.-S. Zhang, Q. Chen, R.-F. Li, T.-L. Hu, X.-H. Bu, Inorg. Chem. 50 (2011) 7555.
[26] APEX2, SAINT and SADABS, Bruker AXS Inc., Madison, WI, 2014.
[27] G.M. Sheldrick, Acta Crystallogr., Sect. A 64 (2008) 112.
[28] B. Xu, J. Xie, H.-M. Hu, X.-L. Yang, F.-X. Dong, M.-L. Yang, G.-L. Xue, Cryst. Growth Des. 14 (2014) 1629.
[29] P.-P. Cen, X.-Y. Jin, Inorg. Chim. Acta 421 (2014) 38.
[30] M.B. Bushuev, K.A. Vinogradova, V.P. Krivopalov, E.B. Nikolaenkova, N.V. Pervukhina, D.Y. Naumov, M.I. Rakhmanova, E.M. Uskov, L.A. Sheludyakova, A. V. Alekseev, S.V. Larionov, Inorg. Chim. Acta 371 (2011) 88.
[31] F. Guo, Inorg. Chim. Acta 399 (2013) 79.
[32] Y. Zhang, W. Luo, D. Liu, Y. Xu, S.-L. Li, J. Li, Y. Wu, Y. Zhou, M. Fang, H.-K. Liu, Inorg. Chim. Acta 409 (2014) 512.
[33] Z.-G. Kong, X.-R. Sun, L. Li, H.-X. Wang, X.-Y. Wang, S.W. Ng, Transit. Metal Chem. 38 (2013) 449.
[34] W. Zhu, R. Zheng, X. Fu, H. Fu, Q. Shi, Y. Zhen, H. Dong, W. Hu, Angew. Chem. Int. Ed. 54 (2015) 6785.
[35] J.-G. Kang, J.-S. Shin, D.-H. Cho, Y.-K. Jeong, C. Park, S.F. Soh, C.S. Lai, E.R.T. Tiekink, Cryst. Growth Des. 10 (2010) 1247.
[36] L.-F. Ma, C.-P. Li, L.-Y. Wang, M. Du, Cryst. Growth Des. 10 (2010) 2641.
[37] G.-G. Luo, H.-B. Xiong, D. Sun, D.-L. Wu, R.-B. Huang, J.-C. Dai, Cryst. Growth Des. 11 (2011) 1948.
[38] L.-F. Ma, L.-Y. Wang, J.-L. Hu, Y.-Y. Wang, G.-P. Yang, Cryst. Growth Des. 9 (2009) 5334.
[39] P. Suvanvapee, J. Boonmak, S. Youngme, Inorg. Chim. Acta 437 (2015) 11.

CRYSTAL GROWTH & DESIGN

Article

pubs.acs.org/crystal

A Series of Cyanoacetato Copper(II) Coordination Polymers with Various *N,N′*-Ditopic Spacers: Structural Diversity, Supramolecular Robustness, and Magnetic Properties

Porntiva Suvanvapee,[†] Jaursup Boonmak,*[,†] Fatima Klongdee,[†] Chaveng Pakawatchai,[‡] Boujemaa Moubaraki,[§] Keith S. Murray,[§] and Sujittra Youngme[†]

[†]Materials Chemistry Research Center, Department of Chemistry and Center of Excellence for Innovation in Chemistry, Faculty of Science, Khon Kaen University, Khon Kaen 40002, Thailand

[‡]Department of Chemistry, Faculty of Science, Prince of Songkla University, Hat Yai, Songkla 90112, Thailand

[§]School of Chemistry, Monash University, Building 23, 17 Rainforest Walk, Melbourne, Victoria 3800, Australia

Supporting Information

ABSTRACT: Five novel copper(II) coordination polymers containing cyanoacetate (cna) anion with various *N,N′*-ditopic spacers $[Cu(cna)_2(pyz)]_n$ (**1**), $[Cu(cna)_2(bpy)(H_2O)_2]_n$ (**2**), $[Cu(cna)_2(dpe)]_n$ (**3**), $[Cu(cna)_2(dpe)]_n(H_2O)_n$ (**4**), and $[Cu(cna)_2(bpa)]_n$ (**5**) (when pyz = pyrazine, bpy = 4,4′-bipyridyl, dpe = 1,2-di(4-pyridyl)ethylene, and bpa = 1,2-di(4-pyridyl)ethane) were structurally and spectroscopically characterized. Compound **1** shows a two-dimensional (2D) sheet structure constructed from μ_2-1,3(*syn,anti*) coordinative mode of cyanoacetate and μ_2-pyz linking adjacent Cu(II) centers. Compound **2** exhibits a one-dimensional (1D) polymeric chain which is formed by μ_2-bpy bridging between $[Cu(cna)_2(H_2O)_2]$ units, whereas compounds **3**−**5** reveal 1D ladder-like structures which are built from double-μ_2-dpe/bpa spacers connecting neighboring Cu(II) cyanoacetate dimers. Weak interactions such as hydrogen bonding and N···π and/or C−H···π interactions join the adjacent layers of **1** or polymeric chains of **2**−**5** to stabilize overall supramolecular networks. The thermal stabilities of **1**−**5** were investigated. Interestingly, compound **2** reveals a robust supramolecular framework constructed by 1D polymeric chains during thermal dehydration and rehydration processes, which has been further verified by spectroscopic techniques, elemental analyses, thermogravimetric analysis, and X-ray powder diffraction. Moreover, this behavior is not observed in the isomorphous series containing Co(II) and Ni(II) ions. The magnetic properties of **1** and **3** exhibit very weak antiferromagnetic interactions between Cu(II) centers.

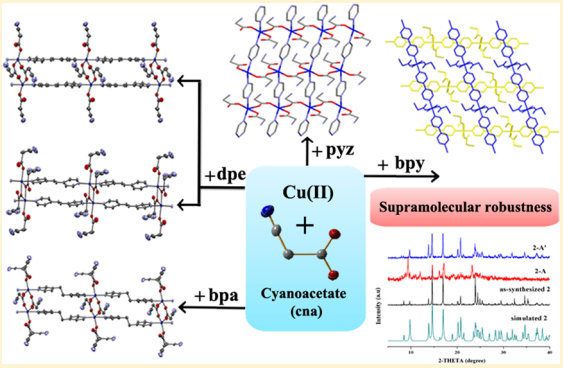

INTRODUCTION

The design and construction of coordination polymers have received much attention and have become an interesting research area of chemistry in recent decades due to their potential applications in gas storage, catalysis, luminescence, ion exchange, and magnetism.[1−9] Generally, the structural diversity and the construction of such promising materials strongly depend on the chemical nature of the main or ancillary ligands and the coordination geometries of metal ions. It is well-known that the coordination polymers containing carboxylates show various dimensional networks with interesting properties.[10−18] This diversity results from the fact that the carboxylate groups can bind metal centers in various ways and may account for the possible intermolecular hydrogen bonds spreading low dimensional materials to higher dimensional supramolecular frameworks.[1,6,13−19] Besides the structural aspect, the carboxylate bridges provide an efficient pathway for transmitting magnetic information between paramagnetic centers. Different coordination modes contribute different forms of cooperative coupling which can be principally used to modulate the overall magnetic behavior in a coordination network.[17,18,20,21] In the present studies, the cyanoacetate anion (cna) is used as a ligand for binding more than one metal ion through carboxylate bridge. The cyanoacetate ($NC_2H_2CO_2^-$) is a monocarboxylate with many interaction sites. It contains both nitrile (−C≡N) and carboxylic groups which not only provides coordination sites but also effectively serves as a hydrogen acceptor site at the cyano group as well as fabricating the intermolecular N···π interaction toward neighboring electron-deficient aromatic moieties.[22−29] In general, the intermolecular noncovalent interactions are useful tools for the construction of a soft supramolecular framework[3,5,30,31] with low dimensional molecular building blocks that can show a variety of structural dynamic behaviors, such as reversible single-crystal-to-single-crystal, reversible single crystal

Received: April 2, 2015
Revised: June 28, 2015
Published: July 2, 2015

DOI: 10.1021/acs.cgd.5b00453
Cryst. Growth Des. 2015, 15, 3804−3812

Scheme 1. A Series of Cu(II) Coordination Polymers 1−5

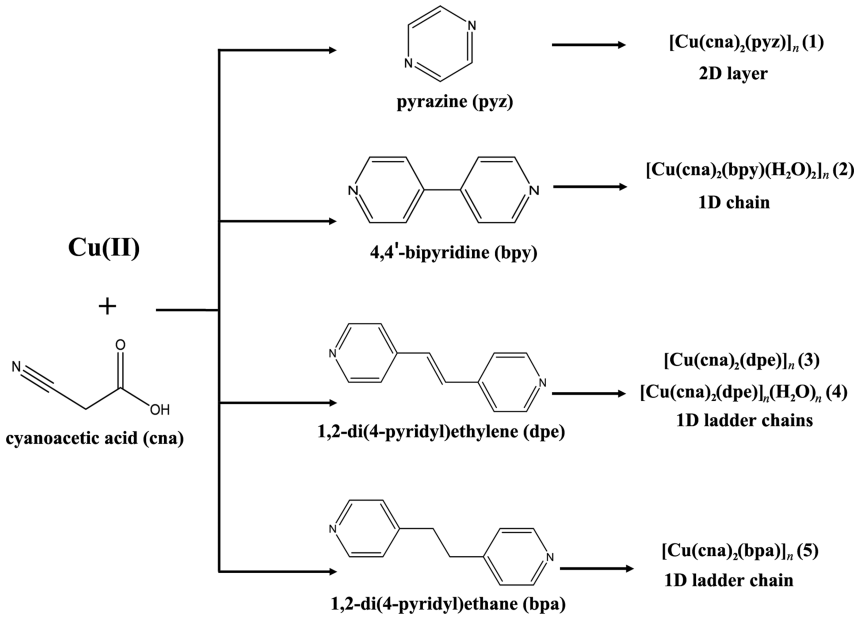

to amorphous, and also nonreversible transformations.[3,5,31−40] Therefore, these versatile connection sites allow the cyanoacetate to be a promising candidate for constructing flexible but robust coordination frameworks. However, the chemistry of coordination complexes containing cyanoacetate has been rarely explored to date.[22−29] Apart from carboxylate linkers, the *N,N′*-ditopic spacers are frequently used as ancillary ligands for dimensional extension. Their length, rigidity, and functional groups have consequential effects on the final structures of coordination networks. Therefore, the development of synthetic routes to novel coordination polymers by mixed bridging ligands remains to be much explored.[10,41−50]

Consequently, in our efforts toward rational design and systematic synthesis of coordination polymers, the use of *N,N′*-ditopic spacers acting as coligands, i.e., pyrazine (pyz), 4,4′-bipyridyl (bpy), 1,2-di(4-pyridyl)ethylene (dpe), and 1,2-di(4-pyridyl)ethane (bpa), in combination with cyanoacetate in the Cu(II) system have been used to construct a variety of new coordination polymers. We found that cyanoacetate can bind Cu(II) ions through diverse coordination modes of carboxylate to generate Cu(II) dinuclear unit and one-dimensional (1D) coordination polymeric chain. To connect these segments, an ancillary *N,N′*-ditopic spacer has been fulfilled. Herein, we report the syntheses and characterizations of a novel series of Cu(II) coordination polymers, namely, $[Cu(cna)_2(pyz)]_n$ (**1**), $[Cu(cna)_2(bpy)(H_2O)_2]_n$ (**2**), $[Cu(cna)_2(dpe)]_n$ (**3**), $[Cu(cna)_2(dpe)]_n(H_2O)_n$ (**4**) and $[Cu(cna)_2(bpa)]_n$ (**5**) (see Scheme 1). The resulting coordination networks exhibit a variation of architectures from 1D polymeric chain, 1D-ladder chain, to 2D layer depending upon the length and rigidity of the spacers and diverse coordination modes of carboxylates. The nitrile functional group in cyanoacetate plays a key role in 3D packing motifs via intermolecular hydrogen bonding and N···π interactions. Furthermore, we found that compound **2** reveals a robust supramolecular framework during dehydration and rehydration processes which is not observed in the Co(II) and Ni(II) analogues. This behavior is not common for low dimensional coordination polymers because the noncovalent supramolecular motif easily collapses upon removal of the coordination water molecules.[36,38] The result demonstrates the significant role of various weak intermolecular interactions among interlaced covalently bonded chain in **2** and the influence of Jahn−Teller distortion in octahedral Cu(II) system to preserve the crystalline phase of anhydrous frameworks of **2**. The magnetic properties of **1** and **3** have also been investigated.

EXPERIMENTAL SECTION

General. All chemicals were obtained from commercial sources and were used without further purification. Elemental analyses (C, H, N) were carried out with a PerkinElmer PE 2400CHNS analyzer. FT-IR spectra were obtained in KBr disks on a PerkinElmer Spectrum One FT-IR spectrophotometer in 4000−450 cm^{-1} spectral range. Solid-state (diffuse reflectance) electronic spectra were measured as polycrystalline samples on a PerkinElmer Lambda2S spectrophotometer, within the range 400−1100 nm. The X-ray powder diffraction (XRPD) data were collected on a Bruker D8 ADVANCE diffractometer using monochromatic Cu$K\alpha$ radiation, and the recording speed was 0.5 s/step over the 2θ range of 5−40° at room temperature. Thermogravimetric analyses (TGA) were performed using a TG-DTA 2010S MAC apparatus between 30 and 500 °C in N_2 atmosphere with heating rate of 10 °C min^{-1}. Magnetic susceptibility measurements (2−300 K) were carried out using a Quantum design MPMS-5S SQUID magnetometer. Measurements carried out using a 1 kOe dc field. Accurately weighed samples of ∼25 mg were contained in a gel capsule that was held in the center of a soda straw that was attached to the end of the sample rod. Data were corrected for magnetization of the sample holder and for diamagnetic contributions, which were estimated from Pascal constants.

Syntheses. $[Cu(cna)_2(pyz)]_n$ (1). The aqueous solution (4 mL) of $Cu(NO_3)_2{\cdot}3H_2O$ (120 mg, 0.5 mmol) and cyanoacetic acid (85 mg, 1 mmol) was mixed with pyrazine (40 mg, 0.5 mmol) in dimethylformamide (2 mL). This mixture solution was allowed to stand undisturbed at room temperature, yielding blue crystals of **1** after 2 days. Yield: 97 mg (62%) based on copper salt. Anal. Calcd for $CuC_{10}H_8N_4O_4$: C, 38.53; H, 2.59; N, 17.93%. Found: C, 37.65; H, 2.62; N, 18.03%. IR (KBr, cm^{-1}): 3096(w), 3045(w), 2255(w), 1645(s), 1600(s), 1440(m), 1365(s), 1253(m), 1160(m), 1126(m), 1075(m), 923(m), 838(m), 718(w), 574(w), 506(m). UV−vis (diffuse reflectance, cm^{-1}): 15450.

$[Cu(cna)_2(bpy)(H_2O)_2]_n$ (2). The mixture solution of $Cu(NO_3)_2{\cdot}3H_2O$ (120 mg, 0.5 mmol) and 4,4′-bipyridyl (78 mg, 0.5 mmol) in aqueous media (4 mL) was carefully layered on cyanoacetic acid (85 mg, 1 mmol) in dimethylformamide (2 mL) in 15 mL of glass vial. The vial was sealed and allowed to stand undisturbed at room temperature. After

DOI: 10.1021/acs.cgd.5b00453
Cryst. Growth Des. 2015, 15, 3804−3812

Table 1. Crystallographic Data for Compounds 1−5

compound	1	2	3	4	5
formula	$CuC_{10}H_8N_4O_4$	$CuC_{16}H_{16}N_4O_6$	$CuC_{18}H_{14}N_4O_4$	$CuC_{18}H_{16}N_4O_5$	$CuC_{18}H_{16}N_4O_4$
molecular weight	311.74	423.87	413.87	431.87	415.90
T (K)	293(2)	293(2)	293(2)	293(2)	293(2)
crystal system	monoclinic	orthorhombic	triclinic	monoclinic	triclinic
space group	$P2_1/c$	$Pccn$	$P\bar{1}$	$C2/c$	$P\bar{1}$
a (Å)	4.8966(1)	12.7963(12)	9.6394(7)	23.9507(12)	8.1148(3)
b (Å)	13.3780(4)	18.0945(17)	10.0132(7)	11.7986(6)	10.2084(3)
c (Å)	17.6679(5)	7.4363(7)	10.2337(7)	14.5996(8)	12.3390(4)
α (deg)	90.00	90.00	97.073(2)	90.00	105.745(1)
β (deg)	101.794(1)	90.00	91.002(2)	110.044(1)	95.226(1)
γ (deg)	90.00	90.00	117.107(1)	90.00	110.908(1)
V (Å^3)	1132.93(5)	1721.8(3)	869.54(11)	3875.7(3)	898.72(5)
Z	4	4	2	8	2
ρ_{calcd} (g cm^{-3})	1.828	1.635	1.581	1.473	1.537
μ (Mo Kα) (mm^{-1})	1.945	1.312	1.289	1.163	1.247
data collected	3028	2075	4324	3988	3670
unique data (Rint)	2239(0.0320)	1796(0.0192)	3493(0.0463)	3451(0.0219)	3177(0.0182)
$R_1{}^a/wR_2{}^b$ [$I > 2\sigma(I)$]	0.0567/0.1378	0.0347/0.0921	0.0467/0.1001	0.0322/0.0820	0.0331/0.0837
$R_1{}^a/wR_2{}^b$ [all data]	0.0731/0.1488	0.0395/0.0958	0.0625/0.1064	0.0405/0.0864	0.0420/0.0882
GOF	0.996	1.091	1.072	1.055	1.056
max/min electron density (e Å^{-3})	0.469/−0.775	0.332/−1.238	0.584/−0.250	0.354/−0.264	0.542/−0.217

$^aR = \sum||F_o| - |F_c||/\sum|F_o|$. $^bR_w = \{\sum[w(|F_o| - |F_c|)]^2/\sum[w|F_o|^2]\}^{1/2}$.

2 days, blue crystals of **2** were obtained. Yield: 100 mg (47%) based on copper salt. Anal. Calcd for $CuC_{16}H_{16}N_4O_6$: C, 45.34; H, 3.80; N, 13.22%. Found: C, 44.55; H, 3.53; N, 12.40%. IR (KBr, cm^{-1}): 3544(br), 3199(w), 3007(w), 2923(w), 2259(w), 1610(s), 1373(s), 1276(m), 1218(m), 1075(m), 942(w), 818(m), 714(m), 645(w), 596(w), 491(w). UV−vis (diffuse reflectance, cm^{-1}): 15470.

[Cu(cna)$_2$(dpe)]$_n$ (3) and [Cu(cna)$_2$(dpe)]$_n$(H$_2$O)$_n$ (4). A mixture solution of ethanol and water (4 mL, 1:1 v/v) was carefully layered on an aqueous solution (4 mL) containing $Cu(BF_4)_2{\cdot}nH_2O$ (118 mg, 0.5 mmol) and cyanoacetic acid (85 mg, 1 mmol) in 15 mL of glass vial. Then an ethanolic solution (2 mL) of 1,2-di(4-pyridyl)ethylene (90 mg, 0.5 mmol) was layered over the mixture layer. Then, the vial was sealed and allowed to stand undisturbed at room temperature. After 2 days, greenish-blue block-shaped crystals of **3** and blue polygonal crystals of **4** were obtained. These crystals were manually separated, washed with water and dried in air. Yield for **3**: 49 mg (24%) based on copper salt. Anal. Calcd for $CuC_{18}H_{14}N_4O_4$: C, 52.24; H, 3.41; N, 13.54%. Found: C, 51.82; H, 3.41; N, 13.27%. IR (KBr, cm^{-1}): 3088(w), 2258(w), 1633(s), 1613(s), 1496(m), 1385(s), 1266(m), 1207(m), 1073(m), 816(m), 720(w), 643(w). UV−vis (diffuse reflectance, cm^{-1}): 13770. Yield for **4**: 11 mg (5%) based on copper salt. Anal. Calcd for $CuC_{18}H_{16}N_4O_5$: C, 50.06; H, 3.73; N, 12.97%. Found: C, 50.92; H, 3.40; N, 13.07%. IR (KBr,cm^{-1}): 3419(br), 3060(w), 2933(w), 2258(w), 1626(s), 1463(s), 1372(s), 1286(s), 1080(m), 1030(m), 903(w), 844(s), 727(m), 549(m). UV−vis (diffuse reflectance, cm^{-1}): 16860. The single-crystals of **4** were synthesized in a similar manner but using dimethylformamide instead of ethanol. After 1 week, suitable single-crystals of **4** for X-ray diffraction study were obtained. The low yields of **3** and **4** are owing to the tiny crystals of the mixed products which are difficult to separate manually.

[Cu(cna)$_2$(bpa)]$_n$ (5). The solution containing $Cu(BF_4)_2{\cdot}nH_2O$ (118 mg, 0.5 mmol) and cyanoacetic acid (85 mg, 1 mmol) in water and ethanol (4 mL, 1:1 v/v) was mixed with 1,2-di(4-pyridyl)ethane (90 mg, 0.5 mmol) in dimethylformamide (2 mL). This mixture solution was allowed to stand undisturbed at room temperature. After 2 days, greenish-blue crystals of **5** were obtained. Yield: 86 mg (41%) based on copper salt. Anal. Calcd for $CuC_{18}H_{16}N_4O_4$: C, 51.98; H, 3.88; N, 13.47%. Found: C, 51.73; H, 3.78; N, 13.36%. IR (KBr, cm^{-1}): 3432(br), 2258(w), 1627(s), 1367(s), 1255(m), 1073(w), 1030(w), 901(w), 849(m), 719(w), 555(w). UV−vis (diffuse reflectance, cm^{-1}): 13770.

X-ray Crystallography. The reflection data of **1**−**4** and **2-Co** were collected on a 1 K Bruker SMART CCD area-detector diffractometer with graphite-monochromated MoKα radiation (λ = 0.71073 Å) using the SMART program.[51] The reflection data of **5** was collected on a Bruker D8 Quest PHOTON100 CMOS detector with graphite-monochromated MoKα radiation using the APEX2 program.[52] Raw data frame integration was performed with SAINT,[53] which also applied correction for Lorentz and polarization effects. An empirical absorption correction by using the SADABS program[54] was applied. The structure was solved by direct methods and refined by full-matrix least-squares method on F^2 with anisotropic thermal parameters for all non-hydrogen atoms using the SHELXTL software package.[55] All hydrogen atoms were placed in calculated positions and refined isotropically, with the exception of the hydrogen atoms of all coordination water molecules in **2** were found via difference Fourier maps, then restrained at fixed positions and refined isotropically whereas hydrogen atoms on the disordered lattice water molecule in **4** could not be located. The nitrile groups of μ-cna for **4** and those of terminal cna for **5** are disordered, so the occupancies of conformations A and B refined to 0.8 and 0.2 (for **4**) and 0.7 and 0.3 (for **5**), respectively. Therefore, there are hydrogen bonding networks and N$\cdots\pi$ interactions present via the disordered nitrile N3 atom for **4**, and both are symmetry related in which changing one interaction has a knock-on effect. The details of crystal data, selected bond lengths and angles for compounds **1**−**5** are listed in Tables 1 and S1.

RESULTS AND DISCUSSION

Description of the Structures. [Cu(cna)$_2$(pyz)]$_n$ (1). Single-crystal structure analysis reveals that **1** crystallizes in the monoclinic system $P2_1/c$ space group. The coordination environment of the Cu(II) center is shown in Figure 1a. Each Cu(II) ion is five-coordinated showing a distorted square pyramidal CuN_2O_3 chromophore with a τ value of 0.24 (Addison's parameter τ[56] = 0 for square pyramid and τ = 1 for trigonal bipyramid). The equatorial plane around the copper atom is composed of two carboxylic oxygen atoms (O1 and O2) from two different cyanoacetate groups and two nitrogen atoms from μ_2-pyz with average Cu−O and Cu−N distances of 1.959(2) and 2.030(2) Å, respectively. The apical position is

DOI: 10.1021/acs.cgd.5b00453
Cryst. Growth Des. 2015, 15, 3804−3812

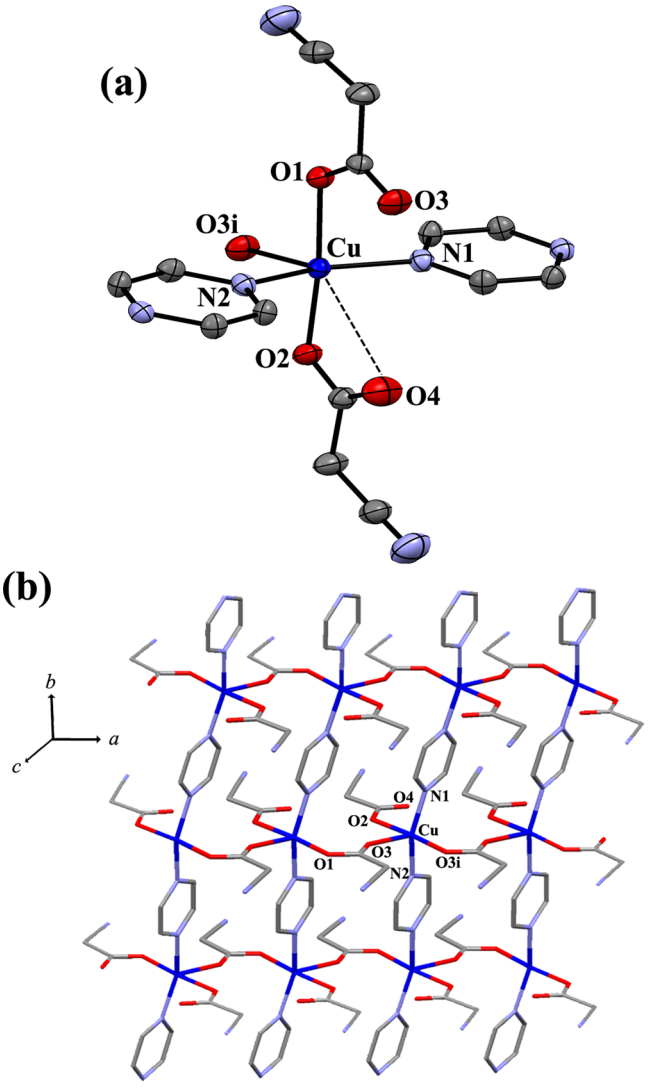

Figure 1. (a) Asymmetric unit and atom labeling scheme of **1**. The ellipsoids are shown at 50% probability level. All hydrogen atoms are omitted for clarity. The dashed line represents weak interaction in the off-the-axis position. (i) = 1 + *x*, *y*, *z*. (b) Two-dimensional sheet structure of **1**.

occupied by oxygen (O3) atom from μ_2-cyanoacetate with the Cu−O3 distance of 2.283(2) Å. The CuN_2O_2 square base is not perfectly planar with tetrahedral twists between the N2−Cu−O2 and N1−Cu−O1 planes of 24.53°. The copper atom is slightly shifted by 0.087 Å from the mean basal plane toward the apical position, which is attributed to semicoordinated O4 atom from the terminal cyanoacetate weakly interacting to copper center in off-the-axis position of an elongated octahedral geometry with the longest Cu···O4 distance of 2.970 Å.[18,57] The cyanoacetate acts as bridging and terminal ligands. The μ_2-cyanoacetate exhibits a *syn,anti*-η^1:η^3:μ_2 coordinative mode of carboxylate bridging between adjacent Cu(II) centers along the *a* axis with Cu···Cu separation of 4.896(5) Å, resulting a zigzag polymeric chain structure of **1**. Moreover, each cyanoacetato Cu(II) wavy chain is connected by μ_2-pyz along *b* axis giving rise to 2D sheet structure of **1** with Cu···Cu separation of 6.832 Å via pyz (Figure 1b). The packing motif of **1** is stabilized by weak hydrogen bonding and N···π interactions between the layers (Figure 2). The interlayer weak hydrogen bonding are constructed from the C−H on pyrazine ring and the nitrogen atom of nitrile group

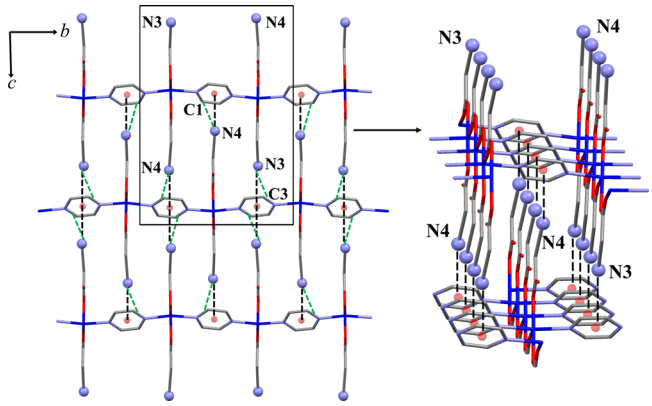

Figure 2. Packing motif of **1** in the *bc* plane; the inset presents the interlayered N···π(pyz) interactions. The green broken lines present weak hydrogen bonding between layers of **1**.

from the terminal and bridging cyanoacetates [C3H···$N3^i$ = 2.61 Å (147°), C3···$N3^i$ = 3.4290(6) Å, (i) = 3 − *x*, 1 − *y*, 1 − *z*; C1H···$N4^{ii}$ = 2.49 Å (147°), C1···$N4^{ii}$ = 3.3091(4) Å, (ii) = 1 + *x*, 1/2 − *y*, 1/2 + *z*]. Moreover, the nitrile N atoms from the terminal and μ_2-cyanoacetate can interact with the electron-deficient μ_2-pyz ring with N···centroid(pyz) distance of 3.420 Å for N3···π and 3.169 Å for N4···π, stabilizing 3D supramolecular framework of **1**, as shown in Figure 2. The distance between a R≡N donor and a centroid of six-membered heteroaromatic rings is found to be in the usual range of 3.00−3.40 Å.[58]

$[Cu(cna)_2(bpy)(H_2O)_2]_n$ (2). Single-crystal structure determination of **2** reveals 1D chain structure that crystallizes in orthorhombic *Pccn* space group. The crystal structure of **2** consists of neutral $[Cu(cna)_2(H_2O)_2]$ unit bridged *via* μ_2-bpy with the Cu···Cu separation of 11.018(8) Å. The cyanoacetate behaves as a monodentate ligand. Each Cu(II) ion is six-coordinated showing a distorted octahedral CuN_2O_4 chromophore (Figure 3a). The two nitrogen atoms from two μ_2-bpy spacers and two oxygen atoms from two terminal cyanoacetates reside in equatorial plane with Cu−N1 and Cu−O2 distances of 2.023(1) and 1.990(1) Å, respectively. Two oxygen atoms from two coordination water molecules are located in the axial positions with Cu−O1 distances of 2.500(1) Å. The adjacent Cu(II) centers are connected by μ_2-bpy forming a 1D chain coordination polymers, as shown in Figure 3b. The two pyridine rings of bipyridyl moieties are not coplanar with the dihedral angle between the two planar pyridine rings of 24.15°. The structure of **2** is isomorphous with previously reported Mn^{II} complex, $[Mn(cna)_2(bpy)(H_2O)_2]_n$.[23] However, the overall packing motif has not been entirely investigated. Each 1D chain of **2** is interlaced by 1D interchain weak hydrogen bonding array between terminal cyanoacetate ligands along *c* axis (C7H···N2) (Figure 4) and the intermolecular hydrogen bonding between unbound O atom from cyanoacetate and H atom from coordination water molecules (O1H···O3), additionally, weak hydrogen bonding between the pyridyl H atom from μ_2-bpy and coordination water molecules (C2H···O3). Moreover, the C2−H···π interaction is observed among the adjacent μ_2-bpy moieties along *c* axis with the separation of 3.372 Å (Figure 4). These weak interactions complete the overall 3D supramolecular motif of **2** with the closest interchain Cu···Cu separation of 7.4363(7) Å. [C2H···$O3^i$ = 2.59 Å (145°), C2···$O3^i$ = 3.391(2) Å, (i) = 1/2 + *x*, 1 − *y*, 1/2 − *z*; C7H···$N2^{ii}$ = 2.59 Å (122°), C7···$N2^{ii}$ = 3.213(3) Å, (ii) = *x*, 1/2 − *y*, 1/2 + *z*; O1H···$O3^{iii}$ = 2.26 Å (147°), O1···$O3^{iii}$ = 3.097(2) Å, (iii) = 1 − *x*, 1 − *y*, 1 − *z*].

DOI: 10.1021/acs.cgd.5b00453
Cryst. Growth Des. 2015, 15, 3804−3812

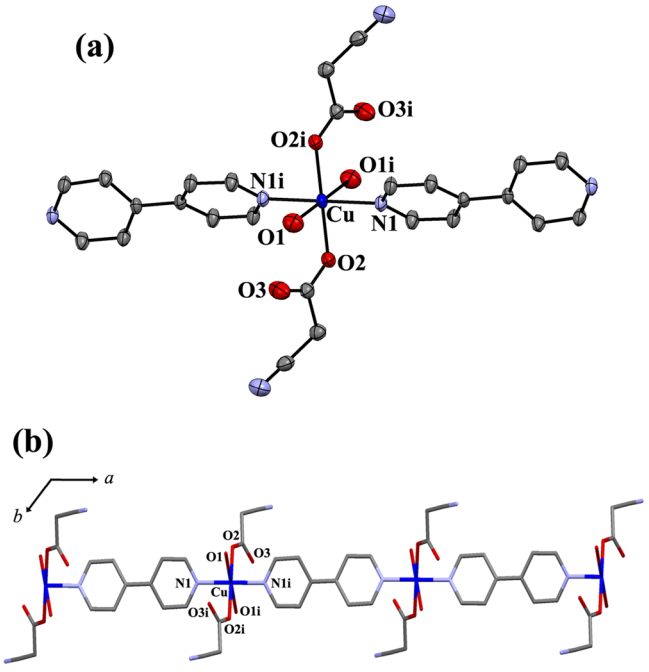

Figure 3. (a) Asymmetric unit and atom labeling scheme of **2**. The ellipsoids are shown at 50% probability level. All hydrogen atoms are omitted for clarity (i) = 1 − *x*, 1 − *y*, −*z*. (b) 1D chain structure of **2** along the *a* axis.

$[Cu(cna)_2(dpe)]_n$ (3), $[Cu(cna)_2(dpe)]_n(H_2O)_n$ (4) and $[Cu(cna)_2(bpa)]_n$ (5). Compounds **3**−**5** exhibit 1D ladder chain structures as shown in Figure 5. Single-crystal structure analysis reveals that **3** and **5** are isostructures crystallizing in the triclinic system $P\bar{1}$ space group whereas compound **4** crystallizes in the monoclinic *C*2/*c* space group. All Cu(II) ions are five-coordination showing distorted square pyramidal geometry CuN_2O_3 chromophore with τ values of 0.42, 0.04, and 0.46 for **3**−**5**, respectively. Each Cu(II) center is surrounded by two carboxylate oxygen atoms from two different cyanoacetates and two nitrogen atoms from two μ_2-dpe (for **3** and **4**) or μ_2-bpa (for **5**) living in an equatorial site with average Cu−O distances of 2.000(2), 1.968(1), and 1.990(2) Å and Cu−N distances of 2.016(2), 2.010(1), and 2.014(2) Å for **3**−**5**, respectively. The leaving one apical position is occupied by carboxylate oxygen atom from bridging cyanoacetate with the distances of Cu−O4 = 2.282(2), Cu−O1 = 2.446(1), and Cu−O2 = 2.264(2) Å for **3**−**5**, respectively. The CuN_2O_2 square base is not completely planar with tetrahedral twists between the planes of 26.61°, 14.45°, and 29.06° for **3**−**5**, respectively. The copper atoms are shifted by 0.303, 0.056, and 0.270 Å from the mean basal planes toward the apical positions for **3**−**5**, respectively. Those of slightly shifted value of **4** results from semicoordinated O4 atom from terminal cyanoacetate weakly interacting to copper center in off-the-axis position of an elongated octahedral geometry with the longest Cu···O4 distance of 2.828(2) Å. The carboxylic bridges for μ_2-cyanoacetate of **3** and **5** exhibit a double-*syn*,*anti*-η^1:η^3:μ_2 coordinative mode connecting between Cu(II) ions, generating the dinuclear Cu(II) units with Cu···Cu separation of 4.278(3) Å for **3** and 4.352(4) Å for **5**, whereas those of **4** exhibit a double-μ_2-1,1-monoatomic bridging mode with the shorter Cu···Cu separation of 3.433(4) Å. The carboxyl-bridged dinuclear Cu(II) units are extended along the particular direction by paired μ_2-dpe (for **3** and **4**) or μ_2-bpa spacers (for **5**) to create the infinite 1D ladder-like structures. The Cu···Cu separations across μ_2-dpe

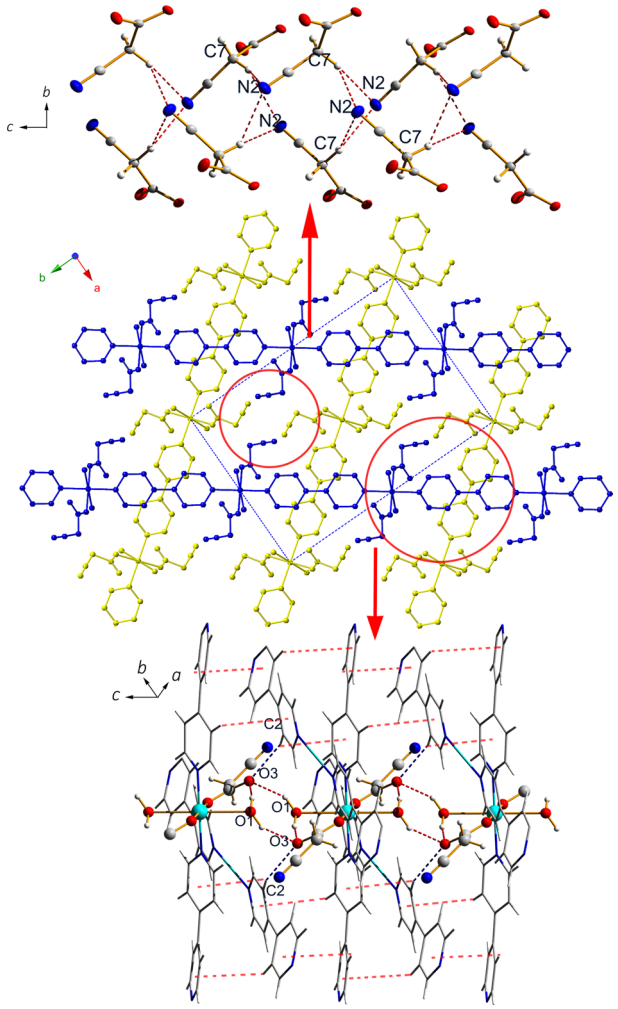

Figure 4. Interlaced chain structure of **2** in *ab* plane formed by 1D intermolecular weak hydrogen bonding array between terminal cyanoacetates along the *c* axis (top). The hydrogen bonding between unbound O3-cyanoacetate and coordination water represents in red dotted lines (bottom). The blue dotted lines represent the C2H···O3 weak hydrogen bonding and the red broken lines represent C−H···π interaction.

(for **3** and **4**) are 13.407(8), 13.349(6) Å and μ_2-bpa (for **5**) 13.288(5) Å, respectively. The two pyridine rings of bipyridyl moieties are not coplanar with the dihedral angles between the two planar pyridine rings of 9.24°, 11.59°, and 18.64° for **3**−**5**, respectively. The conformations of μ_2-dpe and μ_2-bpa ligands are *anti* with C−CH═CH−C torsion angles of 177.30° (for **3**) and 179.03° (for **4**), and C−CH_2−CH_2−C torsion angle of 179.91° (for **5**).

The supramolecular structures of **3** and **5** (Figure S1) are stabilized by weak interchain hydrogen bonding with the closest Cu···Cu distances of 6.7787(7) Å for **3** and 6.5672(5) Å for **5**. [for **3**, C15H···O2^{i}= 2.46 Å (126°), C15···O2^{i} = 3.099(4) Å, (i) = −*x*, 2 − *y*, 1 − *z*; C16H···O2^{i}= 2.60 Å (121°), C16···O2^{i} = 3.147(4) Å; for **5**, C2H···O4^{i}= 2.52 Å (152°), C2···O4^{i} = 3.373(4) Å, (i) = −*x*, −*y*, −*z*; C17H···N4^{ii} = 2.54 Å (161°), C17···N4^{ii} = 3.170(1) Å, (ii) = −*x*, 1 − *y*, 1 − *z*]. Moreover, the nitrile N atoms from the terminal and bridging cyanoacetates interact with the adjacent electron-deficient μ_2-dpe rings with N···centroid distances of 3.665 Å (for N3···π) and 3.274 Å (for N4···π), stabilizing the overall packing structure of **3**. The

DOI: 10.1021/acs.cgd.5b00453
Cryst. Growth Des. 2015, 15, 3804−3812

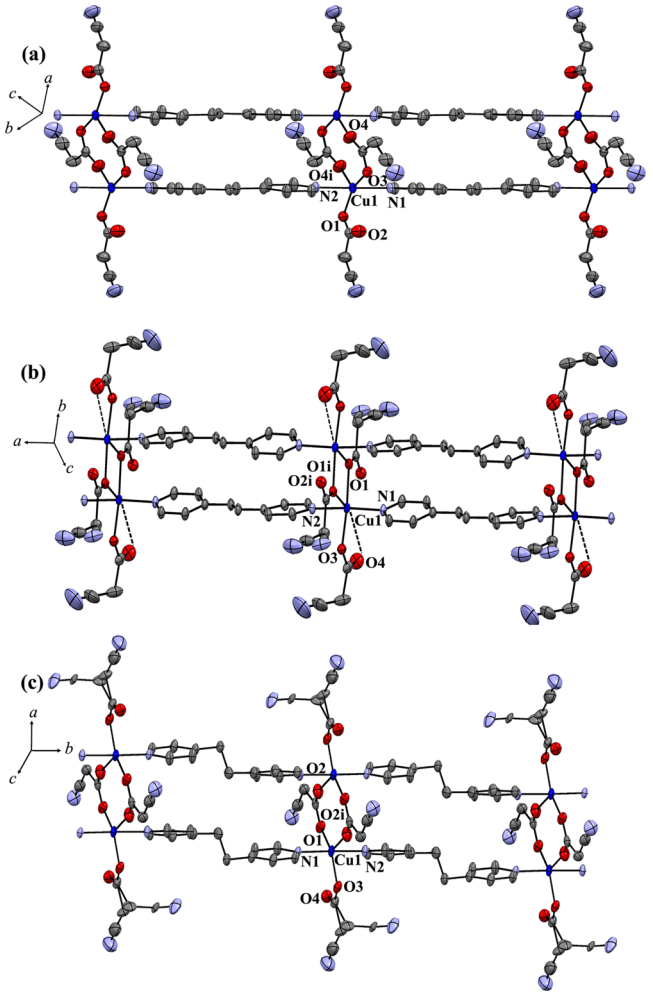

Figure 5. Part of 1D ladder chain structures of **3**(a), **4**(b), and **5**(c) with used atom labeling. The ellipsoids are shown at 35% probability level. The lattice water molecules for **4** and all hydrogen atoms are omitted for clarity. Both disordered nitrile groups of μ_2-cna for **4** and those of terminal cna for **5** are shown.

N···π(bpa) interactions in **5** is not observed because two bipyridyl moieties in a flexible μ_2-bpa spacer are notably twisted with the highest dihedral angle compared with those of **3** and **4**.

In contrast, the ladder chains of **4** are crossed by the hydrogen bonding between the nitrile N atoms from the terminal and bridging cyanoacetates and oxygen atoms from lattice water molecules with N4···O5 = 2.819 Å and N3···O5 = 3.194 Å, as well as, the hydrogen bonding between lattice water molecules with O5···O5i separation of 2.762 Å. In addition, the N3··· centroid(pyridyl) is observed with the distance of 3.328 Å and the weak hydrogen bonding among the carboxylate oxygen of cyanoacetate and pyridyl hydrogen of μ_2-dpe cooperatively stabilizes the entire 3D packing motif of **4** with the closest Cu··· Cu interchain distance of 7.2746(5) Å [C5H···N3^{i} = 2.51 Å (170°), C5···N3^{i} = 3.433(5) Å, (i) = 1/2 − x, 5/2 − y, −z; C7H··· O4^{ii} = 2.56 Å (127°), C7···O4^{ii} = 3.212(3) Å, (ii) = 1/2 − x, −1/ 2 + y, 1/2 − z; C14H···O4^{iii} = 2.50 Å (156°), C14···O4^{iii} = 3.289(4) Å, (iii) = x, 2 − y, 1/2 − z; C17H···O2^{ii} = 2.30 Å (153°), C17···O2^{ii} = 3.191(4) Å] (Figure S2).

IR and UV−visible Spectroscopy. The solid-state IR spectra of **1**−**5** in the region 4000−450 cm^{-1} are displayed in Figure S3. The IR spectra of all compounds exhibit the vibrations of the pyridyl rings for *N,N′*-ditopic spacers in the region 1650−1600 cm^{-1} overlapping the ν_{as}(OCO) bands around ∼1630−1570 cm^{-1}. The strong bands in the region 1430−1360 cm^{-1} are attributed to the ν_s(OCO). The splitting of ν(OCO) reflects that the carboxylate groups of cyanoacetate adopt a variety of coordination modes. The $\Delta\nu_{asym-sym}$ values are in range of 200−260 cm^{-1} which are consistent with monodentate and bridging coordination by the carboxylato group.[10,26,41,59] The medium sharp band at 2258 cm^{-1} can be assigned to the ν(C≡N) from cyanoacetate.[22,26,29] Compounds **2** and **4** show broad bands in the region 3200−3460 cm^{-1} due to the ν(O−H) of water molecules.

The electronic spectra of **1**−**5** were studied in solid state at room temperature (Figure S4). Compounds **1**, **2**, and **4** show a broad absorption band at higher energy around 16860−15450 cm^{-1}, corresponding to the ^2E_g to $^2T_{2g}$ (parent) transition in the distorted octahedral geometry of **2**, and this feature is also consistent with the elongated octahedral geometry with the sixth off-the-axis weakly interacting to Cu center for **1** and **4**,[18,60] while compounds **3** and **5** exhibit the single broad band in much lower transition energy around 13770 cm^{-1}, which is in agreement with the distorted square pyramidal geometry with high τ values.[61−63]

Thermal Analyses. To examine the thermal stabilities of compounds **1**−**5**, thermogravimetric analyses (TGA) were performed in the temperature range 30−500 °C in N_2 atmosphere (Figure 6). Compounds **1**, **3**, **4**, and **5** show no

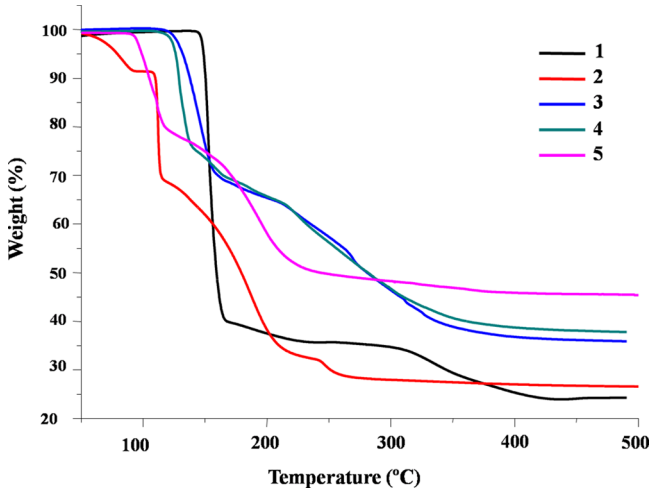

Figure 6. TGA curves of compounds **1**−**5**.

weight loss and are stable up to ∼140, 120, 110, 100 °C, respectively. Then the structures gradually decompose corresponding to the removal of lattice water molecule, cyanoacetate and organic coligands, finally giving a mixture of the CuO and Cu_2O as main products.[64] The TGA curve of **2** reveals the release of two coordination water molecules at the first step of weight loss in the temperature range 50−92 °C (found, 8.33%; Calcd, 8.50%) resulting to the dehydrated form of $[Cu(cna)_2(bpy)]_n$ (**2-A**), which is stable up to ∼107 °C and then the structure gradually collapses.

Supramolecular Robustness in 2. Aforementioned compound **2** contains two coordination water molecules and its anhydrous phase remaining stable up to 107 °C, as evidenced by the TGA profile. This inspired us to examine the dynamic structures of **2** during the dehydration and rehydration processes by elemental analyses, XRPD, and spectroscopic techniques. Consequently, the dehydrated form, $[Cu(cna)_2(bpy)]_n$ (**2-A**)

DOI: 10.1021/acs.cgd.5b00453
Cryst. Growth Des. 2015, 15, 3804−3812

was obtained by heating the polycrystalline samples of **2** at 105 °C for 20 min and the color changed from blue to deep blue. Furthermore, the rehydrated form of **2-A′** was obtained by immersing the dehydrated sample to water for 1 day at room temperature. The XRPD patterns of **2**, **2-A** and **2-A′** are shown in Figure 7. The elemental analysis of **2-A** (Anal. Calcd for

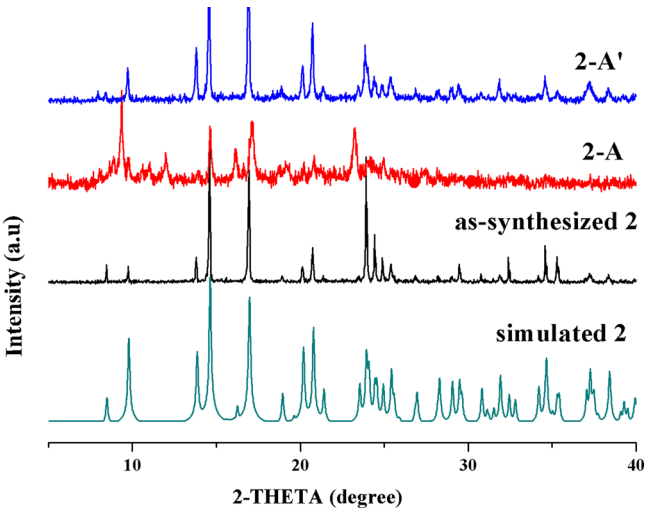

Figure 7. XRPD patterns: simulated from single-crystal X-ray data of **2**; as-synthesized **2**, the dehydrated form **2-A**; the rehydrated form **2-A′**.

$CuC_{16}H_{12}N_4O_4$: C, 49.55; H, 3.12; N, 14.45%. Found: C, 49.30; H, 3.16; N, 14.30%.) and XRPD results indicate that the anhydrous $[Cu(cna)_2(bpy)]_n$ (**2-A**) reveals no significant change of crystalline phase which the main peaks are duplicate to those of XRPD pattern of as-synthesized **2**. The new peaks appear at 9.37° and 23.26° are ascribed to the drastic change in the coordination environments around Cu(II) center during dehydration process. Moreover, the original crystalline phase $[Cu(cna)_2(bpy)(H_2O)_2]_n$ (**2-A′**) can be restored from **2-A** after rehydration process, confirmed by the coincidence in XRPD patterns and elemental analysis (Anal. Calcd $CuC_{16}H_{16}N_4O_6$: C, 45.34; H, 3.80; N, 13.22%. Found: C, 45.26; H, 3.69; N, 13.00%.). This result confirms the rigid supramolecular framework of **2** during thermal dehydration and rehydration processes. Furthermore, this behavior has been further verified by TGA, IR, and solid-state UV−vis diffuse reflectance spectra. The TGA profiles of **2** and **2-A′** (Figure 8) are identical showing the release of two coordination water molecules at the first step of weight loss (Anal. Calcd: 8.50% Found: 8.33% for **2-A′**), whereas the TGA profile of anhydrous form **2-A** shows no weight loss, remaining stable up to ∼107 °C, and then the structure gradually collapses. The UV−vis spectra clearly show that the parallel bands observed in **2** and **2-A′** implying the same Cu(II) environments (Figure S5), whereas the anhydrous **2-A** shows the blue-shifted absorption broadband with λ_{max} around ∼590 nm, giving the deep blue color. In fact these values of the transition energy are in the usual range for the pseudo-octahedral geometry of Cu(II) center.[60] In addition, these results agree with the reversible change in IR spectra for ν(O−H) of coordination water molecules around 3544−3200 cm^{-1} and the ν_s(OCO) of cyanoacetate at ∼1600 cm^{-1} and the fingerprint region below 818 cm^{-1} (Figure S6). All of the results prove the supramolecular robustness of **2**.

Interestingly, this phenomenon is not observed in the isomorphous analogues containing Co(II) (**2-Co**) and Ni(II)

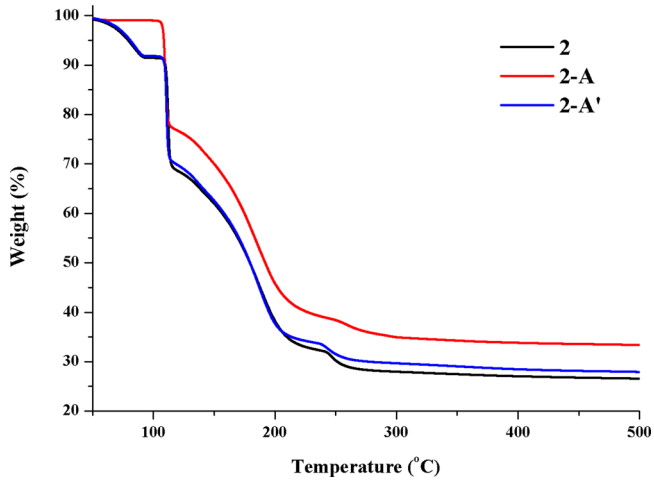

Figure 8. TGA curves of **2**, the dehydrated form **2-A**, and rehydrated form **2-A′**.

(**2-Ni**) centers. The crystal structures of **2-Co** and **2-Ni** are confirmed by XRD, IR spectra, TGA, and elemental analysis (see Figure S7−S9). The coincidence in XRPD patterns and IR spectra of **2**, **2-Co**, and **2-Ni** imply the identical crystalline structures, whereas the TGA profiles of **2-Co** and **2-Ni** reveal the releases of two coordination water molecules at the higher temperature range 85−120 °C for **2-Co** and 95−140 °C for **2-Ni**. Then, the structures continuously decompose with no observed stable anhydrous phases in TGA profiles. The dehydrated forms of **2-Co-A** and **2-Ni-A** were examined and obtained by heating the polycrystalline sample at 115 °C, 135 °C for 20 min for **2-Co** and **2-Ni**, respectively, and the colors changed from orange to brown for **2-Co-A**, blue to green for **2-Ni-A** (Figure S10). The XRPD results indicate that **2-Co-A** and **2-Ni-A** are amorphous forming by the collapse of supramolecular structure. Moreover, these anhydrous amorphous phases cannot be regenerated to the original crystal structure after immersion into water for 1 day (Figure S11 and S12).

The observation of the robust framework of **2** may be attributed to the cooperative effects between the diverse intermolecular interactions stabilizing noncovalent supramolecular motifs together with the Jahn−Teller distortion in Cu(II) d^9 system. The X-ray analysis of **2** revealed that two coordination water molecules in the role of H-donors display the individual intermolecular hydrogen bonds only through unbound oxygen atoms from terminal cyanoacetate as H-acceptors (Figure 4). Thus, upon eliminating the coordination water in **2**, these unbound carboxylic oxygen atoms possibly weakly interact with the vacant Cu(II) sites leading to the elongated octahedral geometry, as evidenced by electronic spectra of **2-A** (Figure S5). In addition, the coordination bridge via rigid bpy backbone plays a role for supporting the structural skeleton, as well as, the other noncovalent interactions especially the 1D hydrogen bonding array involving terminal cyano groups and C−H···π interactions together efficiently support the stabilization of overall supramolecular framework of **2-A** (Figure S13). Furthermore, the structural collapses of the anhydrous analogues **2-Co-A** and **2-Ni-A** point out that besides noncovalent interactions and coordination bridges, the Jahn−Teller effect in the Cu(II), d^9 system plays a significant role in stabilizing the distorted octahedral coordination sphere,[65−67] giving rise to the structural flexibility that is not found in **2-Co-A** and **2-Ni-A** analogues. Remarkably, the dehydration process in **2-A** can be reversed after

DOI: 10.1021/acs.cgd.5b00453
Cryst. Growth Des. 2015, 15, 3804−3812

immersing the dehydrated sample in water, regenerating the original crystalline phase, which is an indication of the robust but flexible supramolecular framework constructed by 1D polymeric chains in **2**.

Magnetic Measurements. The magnetic susceptibilities of powdered sample of **1** and **3** were measured between 2 and 300 K under a constant *dc* magnetic field of 0.1 T (Figures S14 and S15). At 300 K the $\chi_M T$ values are 0.45 and 0.41 cm^3 K mol^{-1} for **1** and **3**, respectively, which are typical of Cu(II) and above that expected for uncoupled Cu(II) centers (0.375 cm^3 K mol^{-1} for $g = 2$) because of spin−orbit coupling, i.e., $g > 2$. The $\chi_M T$ values of **1** slowly decrease, in a linear fashion, down to ∼15 K and then, more rapidly, reaching 0.33 cm^3 K mol^{-1} at 2 K. In contrast, the $\chi_M T$ values for **3** are practically constant until ∼10 K, and then the $\chi_M T$ values abruptly decrease to reach 0.19 cm^3 K mol^{-1} at 2 K. The corresponding plots of χ_M vs T for **1** and **3** show Curie-like behavior with a hint of a maximum in χ_M beginning below 2 K in **3**. The data are generally indicative of very weak antiferromagnetic coupling, this being responsible for the rapid decreases in $\chi_M T$ at very low temperatures,[18,49,68] although Zeeman level thermal depopulation effects may play a part in this region. There is no evidence in the temperature range studied for any long-range magnetic ordering.

In attempting to quantify the magnetic data, the 2D sheet motif of **1** ideally requires a two J model one for the *syn,anti*-$\eta^1{:}\eta^3{:}\mu_2$-cyanoacetate bridged chains, the other for the pyrazine bridged chains. Landee and Turnbull have recently reviewed low-dimensional Cu(II) molecular magnets[69] including related 2D rectangular sheets such as $[Cu(HCO_2)(pyz)(NO_3)]_n$ that showed a mixed antiferromagnetic (pyrazine bridge)/ferromagnetic (formate bridge) behavior and was fitted by Monte Carlo methods.[70] $[Cu(HCO_2)(pyz)(NO_3)]_n$ showed a broad maximum in $\chi_M T$ at 25.3 K, due to ferromagnetic exchange, and a maximum in χ_M at 6.5 K due to antiferromagnetic exchange. Clearly were do not observe such χ_M or $\chi_M T$ maxima in **1** so we conclude that antiferromagnetic exchange occurs along the cyanoacetate- and pyz-bridged chains, and is smaller in magnitude than in $[Cu(HCO_2)(pyz)(NO_3)]_n$. As in the case of 2D β-$[Cu(dca)_2(pyz)]_n$ where dca = $\mu_{1,5}$-NC(N)CN[71] we have used a model by Lines[72] for 2D systems with $S = 1/2$, based on that of Rushbrooke and Wood.[73] A good fit of the data was obtained (Figure S16) using a single J of −0.24 cm^{-1}, but the g value of 1.89 is lower than expected for Cu(II) and the $N\alpha$ (temperature independent susceptibility) of 400 × 10^{-6} cm^3 mol^{-1} is much higher than the normal 60 × 10^{-6} cm^3 mol^{-1}. The size of J is at the lower end of values found for *syn,anti*-$\eta^1{:}\eta^3{:}\mu_2$-carboxylate and pyrazine bridges. It is possible that there are traces of impurity in the sample of **1** that affect the $\chi_M T$ behavior and the fitting thereof.[69]

The $\chi_M T$ plot for **3** is indicative of very weak to zero exchange coupling, and this is not surprising in view of the large Cu···Cu separations and the poor superexchange pathways provided by the 1,2-di(4-pyridyl)ethylene linkers, along the ladder chains.

CONCLUSIONS

Five new coordination polymers constructed by self-assembly of the auxiliary *N,N′*-ditopic spacers and copper(II) cyanoacetates have been structurally characterized. Compounds **2**−**5** exhibit a polymeric chain structure, while **1** shows a 2D layer. This result demonstrated that the length of auxiliary spacers effectively influences the structural dimensionalities. The shortest pyrazine with Cu(II) cyanoacetate well provides the construction of 2D coordination polymer in **1**. Likewise, the structural diversity greatly results from the carboxylate groups in cyanoacetate that can coordinate with the Cu(II) center in various ways. The μ_2-1,3(*syn,anti*) bridging mode for **1**, **3**, and **5**, and μ_2-1,1 monatomic bridge in **4** are found, whereas cyanoacetate in **2** behaves as a terminal monodentate ligand. Besides the various coordination modes of carboxylates, the nitrile group in cyanoacetate has an influence on the established supramolecular interactions via either hydrogen bonding or N···π interactions, which mainly contributes to the stabilization of the overall supramolecular architecture. Particularly, compound **2** exhibits a robust supramolecular framework constructed by 1D polymeric chains during the thermal dehydration and rehydration processes that is not observed in the isomorphous series containing Co(II) and Ni(II) ions. This result demonstrates the significant role of Jahn−Teller distortions in the octahedral Cu(II) center accompanied by various intermolecular noncovalent interactions among interlaced polymeric chains for encouraging the design of a "soft" supramolecular framework with low dimensional building blocks.

ASSOCIATED CONTENT

Supporting Information

Figures of IR and UV−visible spectra, magnetic susceptibilities, XPRD patterns, and X-ray crystallographic information files (CIF) for **1**−**5**. The Supporting Information is available free of charge on the ACS Publications website at DOI: 10.1021/acs.cgd.5b00453. Crystallographic data were deposited with the following Cambridge Crystallographic Data Centre codes: CCDC 1053369−1053373 for **1**−**5** and CCDC 1408728 for **2-Co**.

AUTHOR INFORMATION

Corresponding Author

*E-mail: Jaursup@kku.ac.th; fax: +6643-202-373.

Notes

The authors declare no competing financial interest.

ACKNOWLEDGMENTS

Funding for this work is provided by The Thailand Research Fund: Grant No. TRG5780003 (for J.B.) and BRG5680009 (for S.Y.), the Higher Education Research Promotion and National Research University Project of Thailand, through the Advanced Functional Materials Cluster of Khon Kaen University, and the center of Excellence for Innovation in Chemistry (PERCH-CIC), Office of the Higher Education Commission, Ministry of Education, Thailand. K.S.M. thanks the Australian Research Council for a Discovery grant.

REFERENCES

(1) Cheetham, A. K.; Rao, C. N. R.; Feller, R. K. *Chem. Commun.* **2006**, 4780.
(2) Janiak, C. *Dalton Trans.* **2003**, 2781.
(3) Kitagawa, S.; Kitaura, R.; Noro, S.-i. *Angew. Chem., Int. Ed.* **2004**, *43*, 2334.
(4) Kuppler, R. J.; Timmons, D. J.; Fang, Q.-R.; Li, J.-R.; Makal, T. A.; Young, M. D.; Yuan, D.; Zhao, D.; Zhuang, W.; Zhou, H.-C. *Coord. Chem. Rev.* **2009**, *253*, 3042.
(5) Schneemann, A.; Bon, V.; Schwedler, I.; Senkovska, I.; Kaskel, S.; Fischer, R. A. *Chem. Soc. Rev.* **2014**, *43*, 6062.
(6) Stock, N.; Biswas, S. *Chem. Rev.* **2012**, *112*, 933.
(7) O'Keeffe, M.; Yaghi, O. M. *Chem. Rev.* **2012**, *112*, 675.
(8) Suh, M. P.; Park, H. J.; Prasad, T. K.; Lim, D.-W. *Chem. Rev.* **2012**, *112*, 782.
(9) Yoon, M.; Srirambalaji, R.; Kim, K. *Chem. Rev.* **2012**, *112*, 1196.

DOI: 10.1021/acs.cgd.5b00453
Cryst. Growth Des. 2015, 15, 3804−3812

(10) Carballo, R.; Castineiras, A.; Covelo, B.; Vazquez-Lopez, E. M. *Polyhedron* **2001**, *20*, 899.
(11) Hu, H.-L.; Suen, M.-C.; Yeh, C.-W.; Chen, J.-D. *Polyhedron* **2005**, *24*, 1497.
(12) Jassal, A. K.; Sharma, S.; Hundal, G.; Hundal, M. S. *Cryst. Growth Des.* **2015**, *15*, 79.
(13) Liu, Q.-Y.; Yuan, D.-Q.; Xu, L. *Cryst. Growth Des.* **2007**, *7*, 1832.
(14) Wang, H.; Zhang, D.; Sun, D.; Chen, Y.; Zhang, L.-F.; Tian, L.; Jiang, J.; Ni, Z.-H. *Cryst. Growth Des.* **2009**, *9*, 5273.
(15) Wang, X.-F.; Zhang, Y.-B.; Huang, H.; Zhang, J.-P.; Chen, X.-M. *Cryst. Growth Des.* **2008**, *8*, 4559.
(16) Zhu, H.-F.; Zhang, Z.-H.; Sun, W.-Y.; Okamura, T.-a.; Ueyama, N. *Cryst. Growth Des.* **2005**, *5*, 177.
(17) Mikuriya, M.; Yoshioka, D.; Handab, M. *Coord. Chem. Rev.* **2006**, *250*, 2194.
(18) Boonmak, J.; Youngme, S.; Chaichit, N.; Albada, G. A. v.; Reedijk, J. *Cryst. Growth Des.* **2009**, *9*, 3318.
(19) Boonmak, J.; Youngme, S.; Chotkhun, T.; Engkagul, C.; Chaichit, N.; Albada, G. A. v.; Reedijk, J. *Inorg. Chem. Commun.* **2008**, *11*, 1231.
(20) Kurmoo, M. *Chem. Soc. Rev.* **2009**, *38*, 1353.
(21) Wang, X.-Y.; Wang, Z.-M.; Gao, S. *Chem. Commun.* **2008**, 281.
(22) Sokolova, M. N.; Budantseva, N. A.; Fedoseev, A. M. *Russ. J. Coord. Chem.* **2011**, *37*, 478.
(23) Feng, X.; Shi, X.-G.; Ruan, F. *Z. Kristallogr. - New Cryst. Struct.* **2009**, *224*, 193.
(24) Feng, X.; Feng, T.-C.; Zhao, J.-S.; Shi, X.-G.; Ruan, F. *Z. Kristallogr. New Cryst. Struct.* **2009**, *224*, 541.
(25) Shova, S. G.; Simonov, Y. A.; Gdaniec, M.; Novitchi, G. V.; Lazarescu, A.; Turta, K. I. *Russ. J. Inorg. Chem.* **2002**, *47*, 847.
(26) Novitskii, G.; Shova, S.; Voronkova, V. K.; Korobchenko, L.; Gdanec, M.; Simonov, Y. A.; Turte, K. *Russ. J. Coord. Chem.* **2001**, *27*, 791.
(27) Nakamoto, T.; Hanaya, M.; Katada, M.; Endo, K.; Kitagawa, S.; Sano, H. *Inorg. Chem.* **1997**, *36*, 4347.
(28) Darensbourg, D. J.; Holtcamp, M. W.; Longridge, E. M.; Khandelwal, B.; Klausmeyer, K. K.; Reibenspies, J. H. *J. Am. Chem. Soc.* **1995**, *117*, 318.
(29) Wasson, J. R.; Shyr, C.-I.; Trapp, C. *Inorg. Chem.* **1968**, *7*, 469.
(30) Leong, W. L.; Vittal, J. J. *Chem. Rev.* **2011**, *111*, 688.
(31) Vittal, J. J. *Coord. Chem. Rev.* **2007**, *251*, 1781.
(32) Hu, S.; He, K.-H.; Zeng, M.-H.; Zou, H.-H.; Jiang, Y.-M. *Inorg. Chem.* **2008**, *47*, 5218.
(33) Yu, F.; Li, D.-D.; Cheng, L.; Yin, Z.; Zeng, M.-H.; Kurmoo, M. *Inorg. Chem.* **2015**, *54*, 1655.
(34) Lee, E. Y.; Suh, M. P. *Angew. Chem., Int. Ed.* **2004**, *43*, 2798.
(35) Cingolani, A.; Galli, S.; Masciocchi, N.; Pandolfo, L.; Pettinari, C.; Sironi, A. *J. Am. Chem. Soc.* **2005**, *127*, 6144.
(36) Piromchom, J.; Wannarit, N.; Boonmak, J.; Pakawatchai, C.; Youngme, S. *Inorg. Chem. Commun.* **2014**, *40*, 59−61.
(37) Kitagawa, S.; Uemura, K. *Chem. Soc. Rev.* **2005**, *34*, 109.
(38) Boonmak, J.; Nakano, M.; Chaichit, N.; Pakawatchai, C.; Youngme, S. *Dalton Trans.* **2010**, *39*, 8161.
(39) Hogan, G. A.; Rath, N. P.; Beatty, A. M. *Cryst. Growth Des.* **2011**, *11*, 3740.
(40) Kawano, M.; Fujita, M. *Coord. Chem. Rev.* **2007**, *251*, 2592.
(41) Parshamoni, S.; Sanda, S.; Jena, H. S.; Tomar, K.; Konar, S. *Cryst. Growth Des.* **2014**, *14*, 2022.
(42) Fan, L.; Zhang, X.; Sun, Z.; Zhang, W.; Ding, Y.; Fan, W.; Sun, L.; Zhao, X.; Lei, H. *Cryst. Growth Des.* **2013**, *13*, 2462.
(43) Niu, D.; Yang, J.; Guo, J.; Kan, W.-Q.; Song, S.-Y.; Du, P.; Ma, J.-F. *Cryst. Growth Des.* **2012**, *12*, 2397.
(44) Chang, Z.; Zhang, D.-S.; Chen, Q.; Li, R.-F.; Hu, T.-L.; Bu, X.-H. *Inorg. Chem.* **2011**, *50*, 7555.
(45) Drabent, K.; Ciunik, Z. *Cryst. Growth Des.* **2009**, *9*, 3367.
(46) Tian, A.-x.; Ying, J.; Peng, J.; Sha, J.-q.; Pang, H.-j.; Zhang, P.-p.; Chen, Y.; Zhu, M.; Su, Z.-m. *Cryst. Growth Des.* **2008**, *8*, 3717.
(47) Liu, G.-X.; Huang, Y.-Q.; Chu, Q.; Okamura, T.-a.; Sun, W.-Y.; Liang, H.; Ueyama, N. *Cryst. Growth Des.* **2008**, *8*, 3233.
(48) Brown, S.; Cao, J.; Musfeldt, J. L.; Conner, M. M.; McConnell, A. C.; Southerland, H. I.; Manson, J. L.; Schlueter, J. A.; Phillips, M. D.; Turnbull, M. M.; Landeel, C. P. *Inorg. Chem.* **2007**, *46*, 8577.
(49) Carballo, R.; Covelo, B.; Fallah, M. S. E.; Ribas, J.; Vazquez-Lopez, E. M. *Cryst. Growth Des.* **2007**, *7*, 1069.
(50) Phuengphai, P.; Youngme, S.; Mutikainen, I.; Gamez, P.; Reedijk, J. *Polyhedron* **2012**, *42*, 10.
(51) *SMART 5.6*; Bruker AXS Inc.: Madison, WI, 2000.
(52) *APEX2*; Bruker AXS Inc.: Madison, WI, 2014.
(53) *SAINT 4.0 Software Reference Manual*; Siemens Analytical X-Ray Systems Inc.: Madison, WI, 2000.
(54) Sheldrick, G. M. *SADABS, Program for Empirical Absorption correction of Area Detector Data*; University of Göttingen: Göttingen, Germany, 2000.
(55) Sheldrick, G. M. *Acta Crystallogr., Sect. A: Found. Crystallogr.* **2008**, *A64*, 112.
(56) Addison, A. W.; Rao, T. N.; Reedijk, J.; Van Rijn, J.; Verschoor, G. C. *J. Chem. Soc., Dalton Trans.* **1984**, 1349.
(57) Jasiewicz, B.; Warzajtis, B.; Rychlewska, U. *Polyhedron* **2011**, *30*, 1703.
(58) Mooibroek, T. J.; Gamez, P.; Reedijk, J. *CrystEngComm* **2008**, *10*, 1501.
(59) Chai, X.-C.; Sun, Y.-Q.; Lei, R.; Chen, Y.-P.; Zhang, S.; Cao, Y.-N.; Zhang, H.-H. *Cryst. Growth Des.* **2010**, *10*, 658.
(60) Tabbì, G.; Giuffrida, A.; Bonomo, R. P. *J. Inorg. Biochem.* **2013**, *128*, 137.
(61) Youngme, S.; Wannarit, N.; Remsungnen, T.; Chaichit, N.; Albada, G. A. v.; Reedijk, J. *Inorg. Chem. Commun.* **2008**, *11*, 179.
(62) Youngme, S.; Cheansirisomboon, A.; Danvirutai, C.; Pakawatchai, C.; Chaichit, N. *Inorg. Chem. Commun.* **2008**, *11*, 57.
(63) Youngme, S.; Chotkhun, T.; Leelasubcharoen, S.; Chaichit, N.; Pakawatchai, C.; Albada, G. A. v.; Reedijk, J. *Polyhedron* **2007**, *26*, 725.
(64) Lin, Z.; Han, D.; Li, S. *J. Therm. Anal. Calorim.* **2012**, *107*, 471.
(65) Kozlevcar, B.; Golobic, A.; Strauch, P. *Polyhedron* **2006**, *25*, 2824.
(66) Zabierowski, P.; Szklarzewicz, J.; Kurpiewska, K.; ski, K. L.; Nitek, W. *Polyhedron* **2013**, *49*, 74.
(67) Youngme, S.; Wannarit, N.; Pakawatchai, C.; Chaichit, N.; Somsook, E.; Turpeinen, U.; Mutikainen, I. *Polyhedron* **2007**, *26*, 1459.
(68) Phuengphai, P.; Youngme, S.; Pakawatchai, C.; Albada, G. A. v.; Quesada, M.; Reedijk, J. *Inorg. Chem. Commun.* **2006**, *9*, 147.
(69) Landee, C. P.; Turnbull, M. M. *Eur. J. Inorg. Chem.* **2013**, *2013*, 2266.
(70) Keith, B. C.; Landee, C. P.; Valleau, T.; Turnbull, M. M.; Harrison, N. *Phys. Rev. B: Condens. Matter Mater. Phys.* **2011**, *84*, 104442.
(71) Jensen, P.; Batten, S. R.; Fallon, G. D.; Hockless, D. C. R.; Moubaraki, B.; Murray, K. S.; Robson, R. *J. Solid State Chem.* **1999**, *145*, 387.
(72) Lines, M. E. *J. Phys. Chem. Solids* **1970**, *31*, 101.
(73) Rushbrooke, G. S.; Wood, P. J. *Mol. Phys.* **1958**, *1*, 257.

DOI: 10.1021/acs.cgd.5b00453
Cryst. Growth Des. 2015, 15, 3804−3812

Inorganica Chimica Acta 437 (2015) 11–15

Contents lists available at ScienceDirect

Inorganica Chimica Acta

journal homepage: www.elsevier.com/locate/ica

Synthesis, crystal structure and luminescent properties of three new zinc/cadmium coordination polymers containing cyanoacetate and 1,2-di(4-pyridyl)ethylene

Porntiva Suvanvapee, Jaursup Boonmak *, Sujittra Youngme

Materials Chemistry Research Center, Department of Chemistry and Center of Excellence for Innovation in Chemistry, Faculty of Science, Khon Kaen University, Khon Kaen 40002, Thailand

ARTICLE INFO

Article history:
Received 3 May 2015
Received in revised form 8 July 2015
Accepted 27 July 2015
Available online 17 August 2015

Keywords:
Coordination polymer
Crystal structure
Cyanoacetate
1,2-Di(4-pyridyl)ethylene
Luminescence

ABSTRACT

Three mixed-ligand coordination polymers based on cyanoacetate (cna) and 1,2-di(4-pyridyl)ethylene (dpe), namely $[M(cna)_2(dpe)]_n$ ($M = Zn^{II}$ (**1**), (**2**), and Cd^{II} (**3**)) were synthesised and structurally characterized. Compound **1** exhibits a 1D zigzag polymeric chain, while compounds **2** and **3** are isostructural exhibiting 1D-ladder chain structures built from double-μ_2-dpe connecting between $[M_2(\mu_{1,3}\text{-cna})_2(cna)_2]$ secondary building units. The adjacent polymeric chains of **1**–**3** are linked by various intermolecular weak hydrogen bonds and N···π and/or C–H···π interactions through cyanoacetate and dpe ligands, stabilizing overall 3D supramolecular networks. Furthermore, the divergence of structural motifs between **1** and isostructures **2** and **3** strongly influences on their solid-state photoluminescent properties at room temperature. Compound **1** exhibits intense photoluminescence, whereas this is quenched in compounds **2** and **3**.

1. Introduction

The synthesis and design of coordination polymers (CPs) have attracted great attention owing to their interesting topologies and their potential applications in catalysis, gas storage, magnetism and non-linear optical properties and so on [1–10]. However, from a crystal engineering viewpoint, how to construct the predictable networks with desired properties still remains a great challenge owing to the large number of intermolecular forces which are affected by many variable factors such as reaction stoichiometry, temperature, solvent, counterions and so on [1,6,11]. It is well-known that the most common synthetic method for the construction of novel CPs is the mixed-ligands strategy [2,12–15]. The combination of different ligands can effectively contribute a variety of structural frameworks with fascinating properties [2,12–14,16–19]. One of the most powerful ligand used for such strategy is carboxylate anions that can bind toward metal centers in various ways, such as terminal monodentate, chelating to one metal center, bridging bidentate in a *syn–syn*, *syn–anti*, and *anti–anti* configurations and multiple bridges, resulting in the formation of various new structural types of metal carboxylates [20–25]. On the other hand, many rod-like *N*,*N*′-ditopic organic co-ligands have been widely used as additional building blocks for the construction of several multidimensional CPs [2,26–28].

Coordination polymers constructed from d^{10} transition metal ions, particularly, abundant zinc(II) and cadmium(II) ions, together with luminescent organic ligands containing conjugated π systems and aromatic rings have been a growing interest because of their potential applications in chemical sensors and electroluminescent display [2,4,9,29–33]. In addition, the coordination environment and the arrangement of organic linkers within CPs can strongly affect the luminescent properties. Therefore, controlling molecular interactions is crucial to tuning the luminescent properties of CPs [9,16,17,29,32,34–39]. In this work, we choose a cyanoacetate anion (cna) and semi-flexible 1,2-di(4-pyridyl)ethylene (dpe) luminescent spacer incorporating zinc(II) and cadmium(II) ions to develop new luminescent coordination networks. The cyanoacetate ($NC_2H_2CO_2^-$) anion contains both nitrile (—C≡N) and carboxylic groups which not only well provides rich coordination sites but also effectively serves as intermolecular hydrogen-accepter sites, as well as fabricating the N···π interaction toward neighboring aromatic moieties [40–43]. These versatile connection sites allow cyanoacetate to be a good candidate for constructing 3D

* Corresponding author. Fax: +66 43 202 373.
E-mail address: Jaursup@kku.ac.th (J. Boonmak).

http://dx.doi.org/10.1016/j.ica.2015.07.045
0020-1693/

supramolecular structures. However, the mixed-ligands complexes containing cyanoacetate have been rarely reported [40–50]. Herein, three novel mixed-ligands coordination polymers, formulated as $[M(cna)_2(dpe)]_n$ (M = Zn^{II} (**1**), Zn^{II} (**2**), and Cd^{II} (**3**)) were successfully obtained. The syntheses, crystal structures and luminescent properties for **1**–**3** have been studied in this context.

2. Experimental

2.1. Materials and physical measurements

All chemical were obtained from commercial sources and were used without further purification. Elemental analyses (C, H, N) were carried out with a Perkin-Elmer PE 2400CHNS analyzer. FT-IR spectra were obtained in KBr disks on a Perkin-Elmer Spectrum One FT-IR spectrophotometer in 4000–450 cm^{-1} spectral range. The X-ray powder diffraction (XRPD) data were collected on a Bruker D8 ADVANCE diffractometer using monochromatic Cu Kα radiation, and the recording speed was 0.5 s/step over the 2θ range of 5–40° at room temperature. Photoluminescent spectra of the sample powders were performed on a Shimadzu RF-5301PC spectrofluorometer with the excitation at 285 nm in the wavelength range of 300–560 nm. The excitation and emission pass widths are 1.5 and 3.0 nm, respectively.

2.2. Synthesis

2.2.1. $[Zn(cna)_2(dpe)]_n$ (**1**) and (**2**)

The solution containing $Zn(O_2CCH_3)_2{\cdot}2H_2O$ (109 mg, 0.5 mmol) and cyanoacetic acid (85 mg, 1 mmol) in water and methanol (4 mL, 1:1 v/v) was mixed with 1,2-di(4-pyridyl)ethylene (90 mg, 0.5 mmol) in dimethylformamide (2 mL). This mixture solution was allowed to stand undisturbed at room temperature. After five days, deep yellow rhomboid-shaped crystals of **1** and small pale yellow crystals of **2** were obtained. These crystals were manually separated, washed with water and dried in air. Yield for **1**: 75 mg (36%) based on zinc salt. *Anal.* Calc. for $ZnC_{18}H_{14}N_4O_4$: C, 52.00; H, 3.39; N, 13.48. Found: C, 51.79; H, 3.21; N, 13.30%. IR (KBr, cm^{-1}): 3060w, 2918w, 2261m (ν(C≡N)), 1664s, 1623s (ν_{as}(OCO)), 1512w, 1401m, 1371m (ν_s(OCO)), 1269m, 1077w, 1027m, 844m, 733w, 612w, 561m. Yield for **2**: 125 mg (60%) based on zinc salt. *Anal.* Calc. for $ZnC_{18}H_{14}N_4O_4$: C, 52.00; H, 3.39; N, 13.48. Found: C, 51.23; H, 3.33; N, 13.23%. IR (KBr, cm^{-1}): 3066w, 2261m (ν(C≡N)), 1642s, 1612s (ν_{as}(OCO)), 1513m, 1423s, 1383s (ν_s(OCO)), 1263m, 1204m, 1074m, 1015m, 994m, 915m, 836m, 716w, 557s.

2.2.2. $[Cd(cna)_2(dpe)]_n$ (**3**)

The solution containing $Cd(NO_3)_2{\cdot}4H_2O$ (154 mg, 0.5 mmol) and cyanoacetic acid (85 mg, 1 mmol) in water (4 mL) was mixed with 1,2-di(4-pyridyl)ethylene (90 mg, 0.5 mmol) in dimethylformamide (2 mL). This mixture solution was allowed to stand undisturbed at room temperature, yielding pale yellow crystals of **3** after four days. Yield: 145 mg (63%) based on cadmium salt. *Anal.* Calc. for $CdC_{18}H_{14}N_4O_4$: C, 46.72; H, 3.05; N, 12.11. Found: C, 46.15; H, 2.92; N, 11.70%. IR (KBr, cm^{-1}): 2261m (ν(C≡N)), 1609s (ν_{as}(OCO)), 1502w, 1370s (ν_s(OCO)), 1270w, 1201w, 1081w, 1021m, 981m, 892w, 831m, 713w, 544(m).

2.3. X-ray crystallography

All reflection data **1**–**3** were collected on a Bruker D8 Quest PHOTON100 CMOS detector with graphite-monochromated Mo Kα radiation using the APEX2 program [51]. Raw data frame integration was performed with SAINT [51], which also applied correction for Lorentz and polarization effects. An empirical absorption correction by using the SADABS program [51] was applied. The structure was solved by direct methods and refined by full-matrix least-squares method on F^2 with anisotropic thermal parameters for all non-hydrogen atoms using the SHELXTL software package [52]. All hydrogen atoms were placed in calculated positions and refined isotropically. The details of crystal data, selected bond length and angles for compounds **1**–**3** are listed in Tables 1 and 2. The weak intermolecular hydrogen bonding for **1**–**3** are shown in Table 3.

Table 1
Crystallographic data for compounds **1**–**3**.

	1	**2**	**3**
Formula	$C_{18}H_{14}N_4O_4Zn$	$C_{18}H_{14}N_4O_4Zn$	$C_{18}H_{14}N_4O_4Cd$
Molecular weight	415.72	415.72	462.74
T (K)	293(2)	293(2)	293(2)
Crystal system	triclinic	triclinic	triclinic
Space group	$P\bar{1}$	$P\bar{1}$	$P\bar{1}$
a (Å)	9.1501(4)	7.7072(3)	8.0430(3)
b (Å)	10.7211(5)	10.5091(4)	10.7219(4)
c (Å)	11.3426(5)	11.7022(5)	11.5496(4)
α (°)	106.610(1)	70.292(1)	70.838(1)
β (°)	107.798(1)	86.023(1)	82.340(1)
γ (°)	109.208(1)	72.587(1)	69.025(1)
V (Å^3)	903.36(7)	850.89(6)	878.33(6)
Z	2	2	2
ρ_{calcd} (g cm^{-3})	1.528	1.623	1.750
μ (Mo Kα) (mm^{-1})	1.391	1.477	1.276
Data collected	3697	3249	4727
Unique data (R_{int})	3463(0.0150)	2771(0.0261)	4339(0.0169)
R_1[a]/wR_2[b] [$I > 2\sigma(I)$]	0.0253/ 0.0667	0.0424/ 0.1029	0.0248/ 0.0578
R_1[a]/wR_2[b] [all data]	0.0276/ 0.0680	0.0545/ 0.1081	0.0288/ 0.0594
Goodness-of-fit (GOF)	1.060	1.059	1.094
Maximum/minimum electron density (e Å^{-3})	0.320/−0.253	1.195/−0.504	0.562/−0.323

[a] $R = \sum||F_o| - |F_c||/\sum|F_o|$.
[b] $R_w = \{\sum[w(|F_o| - |F_c|)]^2/\sum[w|F_o|^2]\}^{1/2}$.

Table 2
Selected bond lengths/Å and angles/° for **1**–**3**.

1			
Zn–O1	1.9373(13)	Zn–O3	1.9899(13)
Zn–N2	2.0268(13)	Zn–N1	2.0381(13)
O1–Zn–O3	109.03(6)	O1–Zn–N2	111.99(6)
O3–Zn–N2	108.39(6)	O1–Zn–N1	97.13(6)
O3–Zn–N1	109.85(6)	N2–Zn–N1	119.76(5)
2			
Zn–O1	2.035(3)	Zn–O4	2.048(3)
Zn–O3	2.061(3)	Zn–N1	2.146(3)
Zn–N2	2.180(3)	O1–Zn–O4	97.28(13)
O1–Zn–O3	134.17(12)	O4–Zn–O3	128.53(13)
O1–Zn–N1	93.83(10)	O4–Zn–N1	88.77(11)
O3–Zn–N1	89.09(10)	O1–Zn–N2	89.45(10)
O4–Zn–N2	91.58(11)	O3–Zn–N2	88.07(10)
N1–Zn–N2	176.63(10)		
3			
Cd–N2	2.2938(15)	Cd–O3	2.3043(17)
Cd–O4	2.3059(15)	Cd–N1	2.3105(15)
Cd–O2	2.3595(16)	Cd–O1	2.4836(16)
N2–Cd–O3	87.00(6)	N2–Cd–O4	89.66(6)
O3–Cd–O4	127.54(8)	N2–Cd–N1	173.11(5)
O3–Cd–N1	87.76(6)	O4–Cd–N1	89.98(6)
N2–Cd–O2	96.81(6)	O3–Cd–O2	96.88(8)
O4–Cd–O2	135.45(6)	N1–Cd–O2	88.26(6)
N2–Cd–O1	86.75(6)	O3–Cd–O1	148.79(8)
O4–Cd–O1	82.97(6)	N1–Cd–O1	100.04(6)
O2–Cd–O1	53.68(5)		

Table 3
Intermolecular weak hydrogen bond lengths/Å angles/° in studied structures of **1**–**3**.

D–H···*A*	d(*D*–H)	d(H···*A*)	d(*D*···*A*)	<(DHA)
1[a]				
C4–H4···O4^{i}	0.93	2.40	3.313(2)	168
C6–H6···O4^{ii}	0.93	2.54	3.458(3)	170
C11–H11···N3^{iii}	0.93	2.54	3.194(4)	128
C17–H17A···O2^{iv}	0.97	2.35	3.256(3)	155
2[b]				
C6–H6···N3^{i}	0.93	2.61	3.490(7)	158
C7–H7···O2^{ii}	0.93	2.46	3.379(6)	170
C10–H10···O1^{iii}	0.93	2.54	3.239(5)	132
C17–H17B···O1^{iii}	0.97	2.70	3.539(3)	145
C17–H17A···N4^{iv}	0.97	2.49	3.310(9)	142
3[c]				
C6–H6···N3i	0.93	2.51	3.403(4)	160
C7–H7···O2^{ii}	0.93	2.67	3.579(6)	163
C11–H11···O1^{ii}	0.93	2.51	3.355(3)	146
C17–H17B···O1^{iii}	0.97	2.51	3.197(3)	136
C17–H17A···N4	0.97	2.65	3.346(9)	128

[a] Symmetry code for **1**: (i) = 1 − *x*, 2 − *y*, 1 − *z*; (ii) = −1 + *x*, *y*, *z*; (iii) = 1 + *x*, 1 + *y*, 1 + *z*; (iv) = 1 − *x*, 1 − *y*, −*z*.
[b] For **2**: (i) = −1 + *x*, 1 + *y*, *z*; (ii) = −*x*, 1 − *y*, −*z*; (iii) = 1 − *x*, 1 − *y*, −*z*; (iv) = −*x*, −*y*, 1 − *z*.
[c] For **3**: (i) = 1 − *x*, 1 − *y*, −*z*; (ii) = −1 + *x*, 1 + *y*, *z*; (iii) = −1 + *x*, *y*, *z*.

3. Results and discussion

3.1. Crystal structure

3.1.1. $[Zn(cna)_2(dpe)]_n$ (*1*)

Single-crystal structure analysis reveals that all compounds crystallize in the triclinic system, $P\bar{1}$ space group (Table 1). The asymmetric unit of $[Zn(cna)_2(dpe)]_n$ (**1**) is shown in Fig. 1a. Each Zn(II) ion is coordinated by two oxygen atoms from two different monodentate cyanoacetate anions and two nitrogen atoms from two 1,2-di(4-pyridyl)ethylene molecules, showing a distorted tetrahedral ZnN_2O_2 choromophore. The ZnN_2O_2 moiety shows coordination distances and angles in ranges of 1.937(1)–2.038 (1) Å and 109.03(6)–119.76(5)°, respectively (Table 2). The adjacent zinc ions are bridged *via* μ_2-dpe spacers along *a* axis generating 1D zigzag chain of **1** with the Zn···Zn separations of 13.233(6) and 13.452(5) Å (Fig. 1b). The two pyridine rings of bipyridyl moieties are not coplanar with the dihedral angle between the two planar pyridine rings of 13.59°. The conformation of μ_2-dpe molecule is *anti* with C—CH=CH—C torsion angle of 125.59°. In the packing motif, each zigzag polymeric chain of **1** is assembled by the intermolecular weak H-bonding interactions (Fig. 1c) relating terminal nitrile-N from cyanoacetate and pyridyl–H from μ_2-dpe spacer (C11H···N3), unbound oxygen atoms from cyanoacetate acting as H-acceptor and pyridyl–H (C4H···O4), as well as ethylene–H from μ_2-dpe acting as H-donors (C6H···O4) (Table 3). In addition, the interchain C2–H···π interaction is observed between the neighboring μ_2-dpe moieties in *ac* plane with the separation of 3.435 Å. Moreover, the pyridyl–N atom from μ_2-dpe can also interact with the adjacent dpe rings with $N_{pyridyl}$···centroid(dpe) distance of 3.595 Å (Fig. 1c). All interactions complete the overall 3D supramolecular motif of **1** with the closest interchain Zn···Zn separation of 5.509(5) Å.

3.1.2. $[Zn(cna)_2(dpe)]_n$ (*2*) and $[Cd(cna)_2(dpe)]_n$ (*3*)

Compounds **2** and **3** are isostructural exhibiting 1D ladder-like structures. For **2**, each Zn(II) ion is five-coordination showing a distorted trigonal bipyamidal ZnN_2O_3 chromophore with a $\tau = 0.71$ (Addison's parameter [53] $\tau = 0$ for square pyramid and $\tau = 1$ for trigonal bipyramid) (Fig. 2a). The equatorial trigonal plane around the zinc atom is composed of three oxygen atoms from three different cyanoacetates, indicated by the angles of O1–Zn1–O3, O1–Zn1–O4 and O4–Zn1–O3 being 134.17(12)°, 97.28(13)° and 128.53(13)°, respectively. The axial position is occupied by two nitrogen atoms from two different μ_2-dpe spacers with N1–Zn–N2 angle of 176.63(10)°. The average Zn–O and Zn–N distances

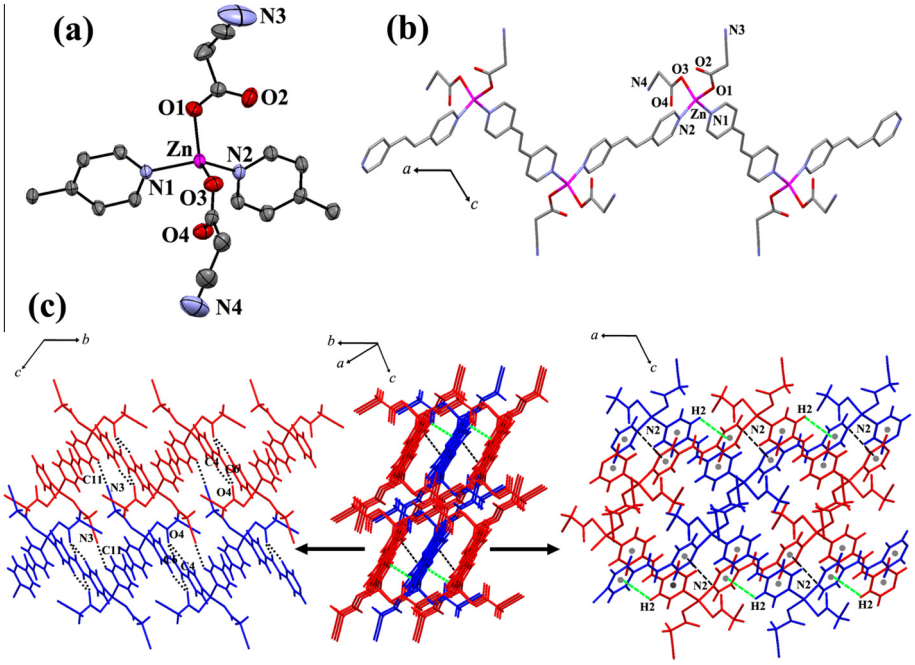

Fig. 1. (a) Asymmetric unit and atom labeling scheme of **1**. The ellipsoids are shown at 50% probability level. All hydrogen atoms are omitted for clarity. (b) 1D zigzag chain along *a* axis. (c) 3D packing diagram of **1** showing the assemblage of six polymeric chains *via* C–H···π (green broken lines) and N···π interactions (black broken lines). 2D sheet structure of **1** built from weak hydrogen bonding (black dotted lines) extending parallel to the *bc* plane (left). Another view in *ac* plane, 2D sheet structure formed by C–H···π (green broken lines) and $N_{pyridyl}$···π (black broken lines) interactions (right). (For interpretation of the references to color in this figure legend, the reader is referred to the web version of this article.)

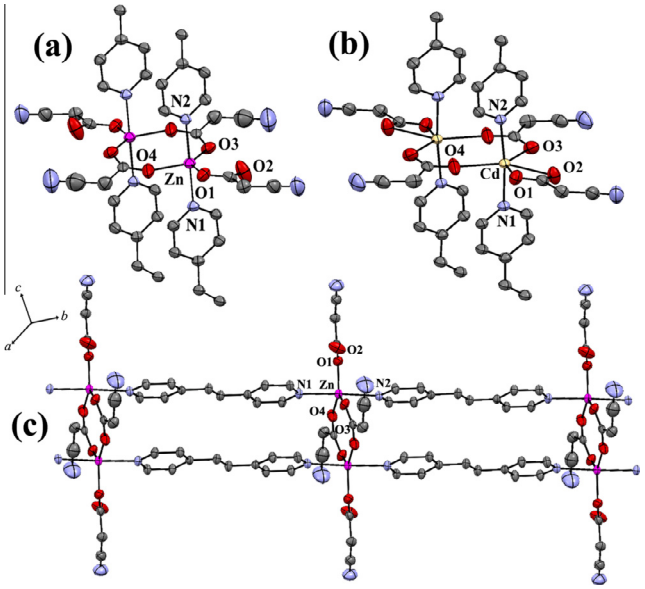

Fig. 2. Part of 1D ladder chain structures of **2**(a) and **3**(b) with used atom labeling. The ellipsoids are shown at 50% probability level. All hydrogen atoms are omitted for clarity. (c) 1D ladder-like structure of **2**.

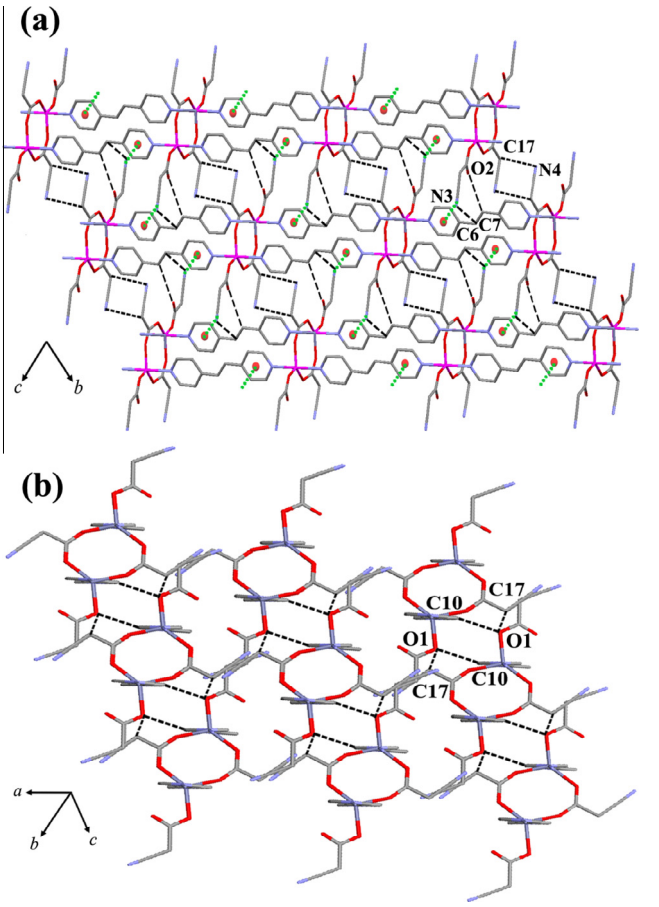

Fig. 3. (a) The packing diagram of ladder chains of **2** in *bc* plane showing weak hydrogen bonding (black broken lines) and $N_{nitrile}\cdots\pi$ interaction (green dotted lines). (b) Another view of 3D packing diagram showing weak hydrogen bonding through carboxylate oxygen from cyanoacetates. (For interpretation of the references to color in this figure legend, the reader is referred to the web version of this article.)

are 2.048(3) and 2.163(3) Å, respectively (Table 2). For compound **3**, each Cd(II) ion shows six-coordination formed by four carboxylate oxygen atoms from three different cyanoacetates and two nitrogen atoms from two μ_2-dpe molecules, generating a distorted octahedral CdN_2O_4 chromophore (Fig. 2b). The coordination distances around Cd(II) center are in the range of 2.294(2)–2.484 (2) Å (Table 2). The carboxylate bridges for μ_2-cna of **2** and **3** exhibit a double-*syn,anti*-η^1:η^3:μ_2 coordinative mode connecting between metal ions, giving rise to the dinuclear units with M···M separations of 3.397(5) and 4.013(2) Å for **2** and **3**, respectively. Additional cyanoacetate acts as terminal monodentate ligand for **2** and terminal chelating ligand for **3**. Moreover, the carboxyl-bridged dinuclear units are extended along the particular direction by paired μ_2-dpe spacers to create the infinite 1D ladder-like structures, as shown in Fig. 2c. The M···M separations across μ_2-dpe are 13.706(6) Å for **2** and 13.956(4) Å for **3**. The two pyridine rings of bipyridyl moieties are not coplanar with the dihedral angles between the two planar pyridine ring of 4.39° and 5.26° for **2** and **3**, respectively. The conformations of dpe molecules is *anti* with C—CH=CH—C torsion angles of 179.81° for **2** and 178.45° for **3**. The 3D packing structures of **2** and **3** are stabilized by various weak interchain H-bonding interactions (Fig. 3) involving terminal nitrile–N and oxygen atoms from cyanoacetates as H-acceptors and pyridyl, ethylene–H atoms from μ_2-dpe and alkyl–H atom from cyanoacetate as H-donors (Table 3). Furthermore, the nitrile–N from the terminal cyanoacetate can interact with the adjacent electron-deficient μ_2-dpe rings with N3···π distances of 3.382 and 3.388 Å for **2** and **3**, respectively, stabilizing the overall packing structures of **2** and **3**. The closest interchain M···M separations are 6.201(7) and 6.602(5) Å for **2** and **3**, respectively.

3.2. Photoluminescent properties

The phase purities of all compounds were confirmed by X-ray powder diffraction (Fig. S1), in which the experimental diffraction peaks are in good agreement with the pattern simulated from single-crystal data, implying the good phase purities of **1**–**3**.

The solid-state photoluminescent properties of **1**–**3** were investigated at ambient temperature. To compare the luminescent intensities, all emission spectra were determined with the same excitation wavelength (λ_{ex} = 285 nm) and the same spectral pass widths. As depicted in Fig. 4, compound **1** shows the intense emission band with maximum at 362 nm and shoulder bands near 380 and 450 nm, upon excitation at 285 nm. In contrast, the isostructures **2** and **3** show much weaker emission intensity with broad band with maxima around 470 nm. To understand the nature of emission bands, the luminescent spectrum of the free dpe ligand was also examined. The emission peaks of free dpe display the maximum in the 340–420 nm region and a broadband around 530 nm (λ_{ex} = 285 nm) [39,54], which may be assigned to intraligand π–π* and n–π* transitions [16,17,37,39]. Typically, in the compounds containing Zn(II)/Cd(II) ion with d^{10} configuration, there is no emission originates from the metal-to-ligand (MLCT) or ligand-to-metal charge transfer (LMCT), since the d^{10} metal ions are normally difficult to be oxidized or reduced [9,30,35,37]. Thus, the emission of **1**–**3** may be attributed to intraligand charge transition. Compared with the free dpe ligand, the emission patterns of **1**–**3** are quite similar to that of free dpe, implying the ligand-centered nature of the emission and display the blue-shifts which were attributed to coordination effects of dpe ligand to the metal centers [9,32,35,37]. The divergences of the emission spectra between **1** and isostructures **2** and **3** are attributed to the differences in coordination environments and the arrangement of π-conjugation between dpe moieties within supramolecular motifs [9,32].

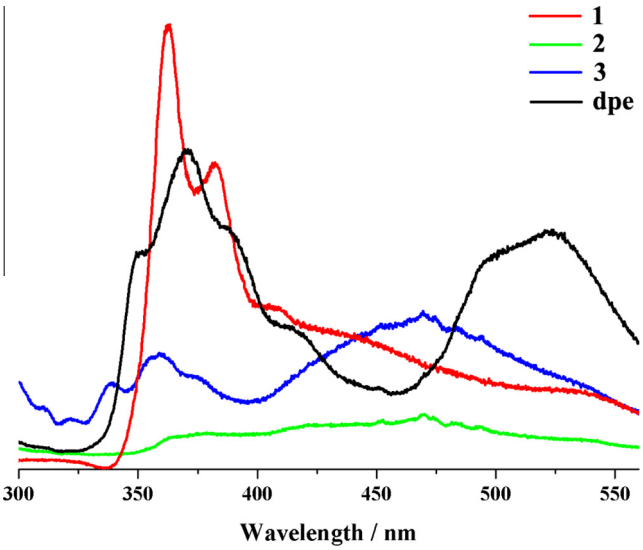

Fig. 4. The solid-state emission spectra of the free dpe and compounds **1**–**3** at room temperature.

4. Conclusion

In summary, three new 1D coordination polymers have been synthesised by self-assemblies of cyanoacetate with Zn(II)/Cd(II) ions and the 1,2-di(4-pyridyl)ethylene. Cyanoacetate well provides coordination site through carboxylate oxygen atoms, as well as, presents either various interchain H-bonding or N···π interactions through nitrile functional group, stabilizing whole 3D supramolecular frameworks. The result of photoluminescence for **1**–**3** in the solid state demonstrated that the orientation and the coordination environment of organic spacer within supramolecular frameworks powerfully affect the luminescent properties, and supports the idea that non-covalent supramolecular assemblies have great potential for utility in the chemistry of luminescent materials.

Acknowledgments

Funding for this work is provided by The Thailand Research Fund: Grant No. TRG5780003 (for Boonmak, J.) and BRG5680009 (for Youngme, S.), the Higher Education Research Promotion and National Research University Project of Thailand, through the Advanced Functional Materials Cluster of Khon Kaen University, and the center of Excellence for Innovation in Chemistry (PERCH–CIC), Office of the Higher Education Commission, Ministry of Education, Thailand.

Appendix A. Supplementary material

CCDC 1060710–1060712 contain the supplementary crystallographic data for **1**–**3**. These data can be obtained free of charge from The Cambridge Crystallographic Data Centre via http://www.ccdc.cam.ac.uk/data_request/cif. Supplementary data associated with this article can be found, in the online version, at http://dx.doi.org/10.1016/j.ica.2015.07.045.

References

[1] A.K. Cheetham, C.N.R. Rao, R.K. Feller, Chem. Commun. (2006) 4780.
[2] C. Janiak, Dalton Trans. (2003) 2781.
[3] S. Kitagawa, R. Kitaura, S.-I. Noro, Angew. Chem., Int. Ed. 43 (2004) 2334.
[4] R.J. Kuppler, D.J. Timmons, Q.-R. Fang, J.-R. Li, T.A. Makal, M.D. Young, D. Yuan, D. Zhao, W. Zhuang, H.-C. Zhou, Coord. Chem. Rev. 253 (2009) 3042.
[5] M. O'Keeffe, O.M. Yaghi, Chem. Rev. 112 (2012) 675.
[6] N. Stock, S. Biswas, Chem. Rev. 112 (2012) 933.
[7] M.P. Suh, H.J. Park, T.K. Prasad, D.-W. Lim, Chem. Rev. 112 (2012) 782.
[8] M. Yoon, R. Srirambalaji, K. Kim, Chem. Rev. 112 (2012) 1196.
[9] Y. Cui, Y. Yue, G. Qian, B. Chen, Chem. Rev. 112 (2012) 1126.
[10] Y.-W. Li, J.-R. Li, L.-F. Wang, B.-Y. Zhou, Q. Chena, X.-H. Bu, J. Mater. Chem. 1 (2014) 495.
[11] S.-I. Noro, S. Kitagawa, T. Akutagawa, T. Nakamura, Prog. Polym. Sci. 34 (2009) 240.
[12] G. Jiang, T. Wu, S.-T. Zheng, X. Zhao, Q. Lin, X. Bu, P. Feng, Cryst. Growth Des. 11 (2011) 3713.
[13] M. Du, X.-J. Jiang, X.-J. Zhao, Inorg. Chem. 46 (2011) 3984.
[14] H. Mao, C. Zhang, G. Li, H. Zhang, H. Hou, L. Li, Q. Wu, Y. Zhub, E. Wanga, Dalton Trans. (2004) 3918.
[15] D. Tian, Q. Chen, Y. Li, Y.-H. Zhang, Z. Chang, X.-H. Bu, Angew. Chem., Int. Ed. 53 (2014) 837.
[16] Y. Zhao, L.-L. He, H. Xu, X.-Y. Li, S.-Q. Zang, Inorg. Chim. Acta 404 (2013) 201.
[17] C.-C. Wang, C.-C. Yang, W.-C. Chung, G.-H. Lee, M.-L. Ho, Y.-C. Yu, M.-W. Chung, H.-S. Sheu, C.-H. Shih, K.-Y. Cheng, P.-J. Chang, P.-T. Chou, Chem. Eur. J. 17 (2011) 9232.
[18] R. Carballo, A. Castineiras, B. Covelo, E.M. Vazquez-Lopez, Polyhedron 20 (2001) 899.
[19] X.-Q. Liang, X.-H. Zhou, C. Chen, H.-P. Xiao, Y.-Z. Li, J.-L. Zuo, X.-Z. You, Cryst. Growth Des. 9 (2009) 1041.
[20] J. Boonmak, S. Youngme, T. Chotkhun, C. Engkagul, N. Chaichit, G.A.V. Albada, J. Reedijk Inorg. Chem. Commun. 11 (2008) 1231.
[21] H. Wang, D. Zhang, D. Sun, Y. Chen, L.-F. Zhang, L. Tian, J. Jiang, Z.-H. Ni, Cryst. Growth Des. 9 (2009) 5273.
[22] X.-F. Wang, Y.-B. Zhang, H. Huang, J.-P. Zhang, X.-M. Chen, Cryst. Growth Des. 8 (2008) 4559.
[23] J. Boonmak, S. Youngme, N. Chaichit, J. Reedijk Cryst. Growth Des. 9 (2009) 3318.
[24] P. Phuengphai, S. Youngme, N. Chaichit, J. Reedijk, Inorg. Chim. Acta 403 (2013) 35.
[25] Y. Kima, D.-Y. Jung, CrystEngComm 14 (2012) 4567.
[26] Z. Chang, D.-S. Zhang, Q. Chen, R.-F. Li, T.-L. Hu, X.-H. Bu, Inorg. Chem. 50 (2011) 7555.
[27] L. Fan, X. Zhang, Z. Sun, W. Zhang, Y. Ding, W. Fan, L. Sun, X. Zhao, H. Lei, Cryst. Growth Des. 13 (2013) 2462.
[28] G.-X. Liu, Y.-Q. Huang, Q. Chu, T.-A. Okamura, W.-Y. Sun, H. Liang, N. Ueyama, Cryst. Growth Des. 8 (2008) 3233.
[29] D. Bruhwiler, G. Calzaferri, T. Torres, J.H. Ramm, N. Gartmann, L.-Q. Dieu, I. Lopez-Duartec, M.V. Martinez-Dıaz, J. Mater. Chem. 19 (2009) 8040.
[30] Q. Zhang, F. Hu, Y. Zhang, W. Bi, D. Wang, D. Sun, Inorg. Chem. Commun. 24 (2012) 195.
[31] S. Jin, D. Wang, W. Chen, Inorg. Chem. Commun. 10 (2007) 685.
[32] X. Zhang, L. Hou, B. Liu, L. Cui, Y.-Y. Wang, B. Wu, Cryst. Growth Des. 13 (2013) 3177.
[33] B. Xu, J. Xie, H.-M. Hu, X.-L. Yang, F.-X. Dong, M.-L. Yang, G.-L. Xue, Cryst. Growth Des. 14 (2014) 1629.
[34] X.-L. Chen, Y.-L. Qiao, L.-J. Gao, H.-L. Cui, M.-L. Zhang, J.-F. Lv, X.-Y. Hou, Z. Anorg. Allg. Chem. 639 (2013) 403.
[35] G.-B. Yang, Z.-H. Sun, Inorg. Chem. Commun. 29 (2013) 94.
[36] X. Wang, C. Qin, E. Wang, Y. Li, N. Hao, C. Hu, L. Xu, Inorg. Chem. 43 (2004) 1850.
[37] R. Sen, D. Mal, P. Branda, R.A.S. Ferreira, Z. Lin, Cryst. Growth Des. 13 (2013) 5272.
[38] J. Ye, L. Zhao, R.F. Bogale, Y. Gao, X. Wang, X. Qian, S. Guo, J. Zhao, G. Ning, Chem. Eur. J. 21 (2015) 2029.
[39] J.-G. Kang, J.-S. Shin, D.-H. Cho, Y.-K. Jeong, C. Park, S.F. Soh, C.S. Lai, E.R.T. Tiekink, Cryst. Growth Des. 10 (2010) 1247.
[40] D.J. Darensbourg, E.V. Atnip, J.H. Reibenspies, Inorg. Chem. 31 (1992) 4475.
[41] T. Nakamoto, M. Hanaya, M. Katada, K. Endo, S. Kitagawa, H. Sano, Inorg. Chem. 36 (1997) 4347.
[42] G. Novitskii, S. Shova, V.K. Voronkova, L. Korobchenko, M. Gdanec, Y.A. Simonov, K. Turte, Russ. J. Coord. Chem. 27 (2001) 791.
[43] M.N. Sokolova, N.A. Budantseva, A.M. Fedoseev, Russ. J. Coord. Chem. 37 (2011) 478.
[44] D.J. Darensbourg, Inorg. Chem. 30 (1991) 358.
[45] D.J. Darensbourg, M.W. Holtcamp, E.M. Longridge, B. Khandelwal, K.K. Klausmeyer, J.H. Reibenspies, J. Am. Chem. Soc. 117 (1995) 318.
[46] D.J. Darensbourg, J.A. Joyce, C.J. Bischoff, J.H. Reibenspies, Inorg. Chem. 30 (1991) 1137.
[47] X. Feng, T.-C. FengII, J.-S. ZhaoIII, X.-G. ShiI, F. RuanI, Z. KristallogrI, NCS 224 (2009) 541.
[48] X. Feng, X.-G. Shi, F. Ruan, Z. Kristallogr, NCS 224 (2009) 193.
[49] S.G. Shova, Y.A. Simonov, M. Gdaniec, G.V. Novitchi, A. Lazarescu, K.I. Turta, Russ. J. Inorg. Chem. 47 (2002) 847.
[50] P. Startnowicz, Acta Crystallogr., Sect. C 49 (1993) 1621.
[51] APEX2 SAINT and SADABS, Bruker AXS Inc., Madison, WI, 2014.
[52] G.M. Sheldrick, Acta Crystallogr., Sect. A 64 (2008) 112.
[53] A.W. Addison, T.N. Rao, J. Reedijk, J. Van Rijn, G.C. Verschoor, J. Chem. Soc., Dalton Trans. (1984) 1349.
[54] W. Zhu, R. Zheng, X. Fu, H. Fu, Q. Shi, Y. Zhen, H. Dong, W. Hu, Angew. Chem., Int. Ed. 54 (2015) 6785.